Cooperative Communication In Near Field Magnetic Induction Communication Systems

A thesis submitted in fulfilment of the
requirements for the award of the degree

Doctor of Philosophy

from

UNIVERSITY OF TECHNOLOGY, SYDNEY

by

Mehrnoush Masihpour
January 2012

SCHOOL OF COMPUTING AND COMMUNICATIONS
CENTRE FOR REAL TIME INFORMATION NETWORKS

Abstract

Near-Field Magnetic Induction Communication (NFMIC) is a relatively new technology which has been proposed for short-range applications such as body-area networks. Since it uses a rapidly-decaying magnetic near-field instead of an electromagnetic wave as the signal transmission mechanism, it is ideal for situations in which limited transmission range is actually an advantage, such as where minimising inter-network interference or avoiding location disclosure are considered important.

To date, little work has been done on multihop techniques specifically designed for NFMIC systems. Most existing applications, such as Radio Frequency Identification (RFID) and Near Field Communication (NFC) are strictly point-to-point. However, when each network node only needs to transmit occasionally, multihop relaying techniques have the potential to significantly reduce power consumption and overall levels of magnetic field egress. Cooperative retransmission strategies, where network nodes that are neither a transmission source nor sink can participate in relaying of frames at the physical layer, have been proposed as a solution for range-extension of conventional electromagnetic/radiofrequency networks. This thesis aims to propose, analyse and simulate a variety of strategies for cooperative relaying which are appropriate for the specific needs of multihop NFMIC networks.

A link budget model for NFMIC is firstly developed and thoroughly analysed, for a variety of non-ideal channel conditions. Three relaying strategies are then proposed and evaluated using the link-budget model under a variety of channel conditions, varying from near-ideal to the pathological case, and a wide variety of source, des-

tination and relay node placement configurations. Simulation results are used to identify the key factors which govern the performance of each technique and the conditions under which throughput can be maximised. A new link metric, which accurately captures these factors, is proposed and its benefits demonstrated through simulation. Finally, a number of opportunities for future study are identified.

Statement of Originality

I certify that the work in this thesis has not previously been submitted for a degree nor has it been submitted as part of requirements for a degree except as fully acknowledged within the text.

I also certify that the thesis has been written by me. Any help that I have received in my research work and the preparation of the thesis itself has been acknowledged. In addition, I certify that all information sources and literature used are indicated in the thesis.

Signed

Mehrnoush Masihpour
January, 2012

Dedication and Acknowledgments

To my beloved husband and my special parents:

Walking with you, through the journey of life has given me strength. Without you, my life would fall apart.

Mehdi, you are everything for me, without your love and understanding I would not be able to make it.

Mom, you have given me so much, you taught me to be strong and to pursue my dreams and never give up.

Daddy, you always told me to "never surrender". I think I have learnt my lesson . . .

Acknowledgments:

This thesis would not have been fulfilled without the guidance and the help of several individuals who contributed and extended their valuable assistance in the preparation and completion of this study.

First and foremost I offer my sincerest gratitude to my principal supervisor, Dr Mehran Abolhasan, who has supported me throughout my thesis with his patience and knowledge whilst allowing me to work in my own way. His sage advice, and insightful criticisms helped the writing of this thesis in countless ways. I attribute the level of my PhD degree to his encouragement and effort and without him this thesis would not have been completed.

I am truly indebted and thankful to my previous principal supervisor and my external supervisor, Associate Professor Dr Johnson Agbinya, for his invaluable guidance and support throughout my studies. It has been an honour for me to work with him since the beginning of my research study. He patiently and continuously assisted me in my research. He has not been only a great advisor, but also an encouraging and motivating friend.

It gives me great pleasure in acknowledging the support and help of my co-supervisor Dr. Daniel Franklin, whose perpetual energy and enthusiasm in research had inspired me. Besides, he was always accessible and willing to help me. I would like to thank him for his immense contribution to this thesis and his wise advices. I was also delighted to work with my co-supervisor, Professor Robin Braun. His technical knowledge and world class research expertise have been a great help in this thesis.

I also wish to express sincere appreciation to the Faculty of Engineering and Information Technology (FEIT), University of Technology, Sydney (UTS), for their extended long-term support and especially to Professor Hung Nguyen and Professor Mary-Anne Williams for having offered me an International Research Scholarship (IRS). I would like to extend further my appreciation to the Vice Chancellor's Conference

Funding and FEIT Travel Funding committees for their generous financial support of my conference attendance. I also would like to thank Professor Bijan Samali for his continuous help and support throughout my candidature. His guidance always helped me to find the right way in different situations.

It is with immense appreciation that I acknowledge the support of Thales Australia for funding this project, particularly Mr. Arthur Ollett and Mr. Stephane Ibos for their valuable advices.

I would like to show my gratitude to Ms. Phyllis Agius and Mr. Craig Shuard, Research Administration Officers, for their dedicated assistance. They have helped me whenever I needed administrative and paper works assistance.

Moving toward more personal acknowledgments, I am indebted to my wonderful sisters, Farnoush and Golnoush and my closest friend Ms. Sara Aarabi for helping me get through the difficult times, and for all the emotional support, comradery, and caring they provided.

Last, but most important, is the dedication of this thesis to my dearest parents, Nasrolah Masihpour and Ghamar Didehban, and my unexampled husband, Mehdi Farahi. I give my deepest expression of love and appreciation for the encouragement that my beloved Mehdi gave, and the sacrifices he made during the study. I would like to thank him for his understanding, sharing and endless love, which has always been a great source of motivation, inspiration and energy for me.

It is difficult to find a sounding word to describe my love for my parents, who bore me, raised me, supported me, taught me, and loved me. I would like to thank them for all what they have given to me. Their encouragement has meant so much to me during the pursuit of my PhD degree and the completion of this thesis.

Contents

1 Introduction **1**

1.1 Thesis Background and Motivations 1

1.2 Thesis Objectives and Scope 3

1.3 Contributions of the Thesis 3

1.3.1 NFMIC Link Budget 3

1.3.2 The Magneto Inductive Waveguide 5

1.3.3 Multihop Relaying Strategies for NFMIC Networks 6

2 Literature Review **8**

2.1 Chapter Overview 8

2.2 Far-Field and Near-Field 9

2.2.1 Far-Field 9

2.2.2 Near-Field 11

2.3 Body Area Network and available short range communication technologies 14

2.3.1 Overview of Body Area Network 14

2.3.2 Short Range Communication Technologies 17

2.4 Magnetic Induction Communications in Near-Field 22

2.4.1 Magnetic Communication Bubble 27

2.5 Cooperative Communications 28

2.5.1 Cooperative Communications in RF 28
2.5.2 Cooperative Communication Usage Scenarios and the Impact of Different Environments 40
2.5.3 Cooperative Communications in NFMIC 42
2.5.4 Magneto Inductive Waveguide devices 45
2.6 Summary 51

3 NFMIC Link Budget 52
3.1 Chapter Overview 52
3.2 Link budget in electromagnetic RF-based communication systems . 53
3.2.1 Free Space Propagation 54
3.2.2 Stanford University Interim Model 56
3.3 NFMIC Link Budget 57
3.3.1 Ferrite Cored (Enhanced Magnetic Flux) - Line of Sight . . 59
3.3.2 Simulation Results 60
3.4 NFMIC Link Budget: AM1 Model and a Comparison between The Two AM Models 70
3.4.1 AM Model: 73
3.4.2 AM1 Model 74
3.4.3 Simulation Results 75
3.5 Summary 80

4 Magneto Inductive Waveguide Link Budget (Multi-node NFMI Communications) 81
4.1 Chapter Overview 81
4.2 Magneto-Inductive Waveguide Link Budget Model 82
4.2.1 One Section Peer to Peer: Line of Sight 85
4.2.2 Multi-Section Waveguide 86

4.2.3 Simulation Results 87
4.3 Magneto Inductive Waveguide Voltage Excitation Methods 92
4.3.1 Array Edge Excitation 94
4.3.2 Array Centre Excitation 96
4.3.3 Collinear Array Excitation 99
4.4 Summary 100

5 Multihop Relay Techniques for Communication Range Extension in NFMIC 102

5.1 Chapter Overview 102
5.2 NFMIC Cooperative Communications 103
5.2.1 Description of the System 103
5.2.2 NLoS NFMIC Multihop Relay Strategies 110
5.2.3 LoS NFMIC Multihop Relay Strategies 116
5.3 Relay selection based on separation distance 123
5.3.1 NLOS 124
5.3.2 LoS 133
5.4 Relay selection based on a new metric (*relay link indicator*) 137
5.4.1 NLoS 138
5.4.2 LoS 139
5.4.3 Simulation Results 141
5.4.4 Effect of different antenna displacement on the relay link indicator 146
5.5 Summary 149

6 Conclusion 150

6.1 Contributions 150
6.2 Future Work 154

Bibliography **157**

A NFMIC-GUI **167**

A.1 Overview 167

A.2 NFMIC-GUI 167

B Master/Assistant Relay Selection Based on Angle and Lateral Displacements **173**

B.1 Overview 173

B.2 Figures 174

C NFMIC Realistic Range and Interference Test **180**

C.1 Chapter Overview 180

C.2 Realistic Range of Magnetic Induction Communication Hardware . 180

C.2.1 Hardware Experiments 182

C.2.2 Detection Range 182

C.2.3 Detection Range Results 183

C.2.4 Interference Tests 183

C.2.5 Interference Tests Results 185

C.3 Summary 186

List of Figures

2.1 Near and Far Field of a Radio Frequency Identifier Reader (adapted from [1]) . . . 9

2.3 Near Field Path Loss [2] . . . 13

2.4 Inductive Transmitter and Receiver (adapted from [3]) . . . 23

2.5 Two parallel coils centred on an axis (adapted from [4]) . . . 23

2.6 Lumped Circuit Models of Parallel Inductive Coils (adapted from [4]) . . . 23

2.7 Inductive coils . . . 25

2.8 Tuned resonating circuits . . . 25

2.9 Overall view of a multi-hop relay cell . . . 31

2.10 Transparent relay frame structure [5] . . . 36

2.11 Non-Transparent Relay Frame Structure [5] . . . 38

2.12 Multihop Relay- Non-Transparent Relay Frame Structure [5] . . . 39

2.13 Magnetic waveguide and circuit model (adopted from [6]) . . . 44

2.14 Two-Port Devices with Simple Mirror (adopted from [7]) . . . 46

2.15 Three-Port Splitters (adopted from [7]) . . . 49

3.1 Free Space Propagation . . . 55

3.2 Distance versus receiving coil radius . . . 62

3.3 Distance versus transmitting coil radius . . . 63

3.4 Distance versus receiving coil radius for different magnetic permeabilities 64

3.5 Distance versus transmitting coil radius for different magnetic permeabilities 64

3.6 Distance versus transmitting and receiving coil magnetic permeability 66

3.7 Distance versus transmitter (receiver) Q-factor 67

3.8 Distance versus transmitter and receiver Q-factor 68

3.9 Distance versus transmission power 68

3.10 Distance versus receiver sensitivity 69

3.11 MI transceivers and the equivalent circuit model (adapted from [8] . 70

3.12 Communication range vs. transmitter coil radius at 13.56MHz . . . 76

3.13 Communication range vs. transmitter coil radius at 300MHz 76

3.14 Communication range vs. transmitter coil radius at 900MHz 77

3.15 Communication range vs. received power at 13.56MHz 77

3.16 Communication range vs. received power at 300MHz 78

3.17 Communication range vs. received power at 900MHz 78

3.18 Communication range vs. operating frequency 79

4.1 Distance vs. transmitting coil radius when $\beta >> 2$ 88

4.2 Distance vs. transmitting coil radius when $\beta << 2$ 88

4.3 Received power vs. transmitting coil radius when $\beta << 2$ and $N = 15$ 89

4.4 Received power vs. communication range when $\beta << 2$ and $N = 20$ 90

4.5 Distance Threshold vs. transmitting coil radius when $\beta = 2$ 90

4.6 Waveguide experiment configuration 92

5.1 ideal transmitting and receiving coil configuration and the circuit model (adapted from [9]) 105

5.2 Lateral Misalignment (adapted from [9]) 107

5.3 Angle Misalignment (adapted from [9]) 108

5.4 NLoS-MI Relay 110

5.5 NLoS- MAMI Relay1 113

5.6 NLoS- MAMI Relay2 115

5.7 LoS-MI Relay 117

5.8 LoS- MAMI Relay1 120

5.9 LoS- MAMI Relay2 121

5.10 NLOS-MI Relay-relay node at different distances 125

5.11 NLOS-MAMI Relay1-achieved range 125

5.12 NLOS-MAMI Relay2-achieved range 126

5.13 RSS and achieved distance-comparison between the three methods 126

5.14 achieved data rate-comparison between the three methods 127

5.15 NLOS-MI Relay-Optimum Q-factor 131

5.16 NLOS-MAMI Relay1-Optimum Q-factor 132

5.21 LOS-achieved data rates comparison between the three methods . . 136

5.22 NLOS-achieved received power in MI Relay 142

5.23 LOS-achieved data rates in MI Relay 142

5.24 NLOS-achieved received power in MAMI Relay1 143

5.25 NLOS-achieved received power in MAMI Relay2 143

5.26 NLOS-comparison between the three relaying methods 144

5.27 LOS-comparison between MAMI Relay1 and MAMI Relay2 . . . 144

5.28 Relay link indicator vs. distance 147

5.29 Relay link indicator vs. angle misalignment 147

5.30 Relay link indicator vs. lateral misalignment 148

A.1 Home Page 168

A.2 Air and Ferrite-cored coil comparison 169

A.3 Air and Ferrite-cored coil comparison and link budget calculations for various inputs 170

A.4 Received power calculations and graphs vs. antenna coil components 171

A.5 Q-factor, efficiency, received power and capacity calculation for a set of parameters 172

B.1 NLoS MAMI Relay1: achieved received signal against the relaying nodes lateral misalignment 174

B.2 NLoS MAMI Relay2: achieved received signal against the relaying nodes lateral misalignment 175

B.3 LoS MAMI Relay1: achieved data rates against the relaying nodes lateral misalignment 176

B.4 LoS MAMI Relay2: achieved data rates against the relaying nodes lateral misalignment 177

B.5 NLoS MAMI Relay1: achieved received signal against the relaying nodes angle misalignment 177

B.6 NLoS MAMI Relay2: achieved received signal against the relaying nodes angle misalignment 178

B.7 LoS MAMI Relay1: achieved data rates against the relaying nodes angle misalignment 178

B.8 LoS MAMI Relay2: achieved data rates against the relaying nodes angle misalignment 179

C.1 Radio Adaptor [10] 181

C.2 Speaker Microphone [10] 181

C.3 Near Field Magnetic Induction Communication 182

C.4 Body Area Network (adapted from [11]) 184

C.5 Effective Detection Range 184

List of Tables

2.1 RFID properties (adapted from [12]) 19

2.2 Short Range Communication Technologies 20

3.1 Simulation Design Parameters 61

3.2 Magnetic Permeability of different Materials 63

4.1 AEE and ACE received voltages (Note: N indicates Noise) 99

5.1 MAMI Relay1 and 2 comparison-Master/Assistant Selection 131

List of Abbreviations

3D	3 Dimensional
ACE	Array Centre Excitation
AEE	Array Edge Excitation
AF	Amplify and Forward
AM	Agbinya-Masihpour
AoA	Angle of Arrival
BAN	Body Area Network
BS	Base Station
CAE	Collinear Array Excitation
DF	Decode and Forward
DL	Downlink
DSSS	Direct-Sequence Spread Spectrum
EF	Estimation and Forward
EM	Electromagnetic
FFD	Full Function Device
HF	High Frequency
IrDa	Infrared Data Association
ISM	Industrial, Scientific and Medical
ICT	Information and Communication Technology
IEEE	Institute of Electrical and Electronics Engineers
IG-BAN	Interest Group-Body Area Network
ISO	International Organization for Standardization
LF	Low Frequency

LoS	Line of Sight
LT	Location Tracking
M/A	Master/Assistant
MAC	Medium Access Control
MAMI	Master/Assistant Magnetic Induction
MI	Magnetic Induction
MIC	Medical Information and Communication
MICT	Medical Information and Communication Technology
MMAC	Mobility adoptive collision free MAC
MR-BS	Multihop Relay-Base Station
MR-Cell	Multihop Relay-cell
MS-MAC	Mobility aware MAC for Sensor Networks
MST	Minimum Spanning Tree
NFMI	Near Field Magnetic Induction
NFMIC	Near Field Magnetic Induction Communications
NLoS	Non Line of Sight
NTP	Network Time Protocol
OFDM	Orthogonal Frequency Division Multiplexing
OFDMA	Orthogonal Frequency Division Multiple Access
PBS	Pairwise Broadcast Synchronization
PC	Personal Computer
PHY	Physical Layer
Q-Factor	Quality Factor
Ra	Relay Assistant
RBS	Reference Broadcast Synchronization
RF	Radio Frequency
RFID	Radio Frequency Identification
RFD	Reduced Function Device
Rm	Relay Master
RS	Relay Station

RSS	Received signal Strength
Rx	Receiver
SAR	Specific Absorption Rate
SINR	Signal to Interference Noise Ratio
SNR	Signal to Noise Ratio
SS	Subscriber's Station
S-TDMA	Self-Organized Time Division Multiple Access
SUI	Stanford University Interim
TC	Triangle Centroid
TDMA	Time Division Multiple Access
TDoA	Time Difference of Arrival
Tx	Transmitter
UHF	Ultra High Frequency
UL	Uplink
UMTS	Universal Mobile Telecommunications System
UWB	Ultra Wide Band
WLAN	Wireless Local Area Network
WPSM	Warfighter Physiologic Status Monitoring
WiMAX	Worldwide Interoperability for Microwave Access

Chapter 1

Introduction

1.1 Thesis Background and Motivations

Historically, the need for communication over long distances has motivated scholars in the field to focus mainly on the communication over large distances. In fact, since the invention of the telephone in 1876, the aim has been to increase the communication range. It took Alexander Graham Bell and his assistant Thomas Watson almost forty years to be able to establish communication between two different cities [13]. More recently, the need for communication of digital information such as voice, images and videos, over wireless has shifted the attention of many scholars toward communication over shorter distances; since greater capacity is achievable over shorter distances and at higher frequencies, where more spectrum is available to be allocated to bandwidth-hungry applications. In this context, short range communication technologies such as Bluetooth, ZigBee, WiFi, Ultra-Wideband (UWB) and Z-Wave have been standardised to address the need for wireless communication over short distances [14]. Most of these technologies use electromagnetic waves to transmit data over the wireless medium. However, a different form of short range communication technology known as *Near Field Magnetic Induction Communication* (NFMIC) has recently emerged and is seen as a possible solution to address many issues associated with other existing radio frequency communication technologies.

NFMIC is a promising solution for situations in which existing electromagnetic (EM) radio frequency-based (RF-based) communication systems fail to operate properly. NFMIC is a low power transmission technique, which uses near-field magnetic flux to transmit data instead of radiating electromagnetic waves [15]. One of the major benefits of magnetic waves over electromagnetic waves is that in NFMIC, the impact of the environment on the transmitted signal is quite different to its effect on electromagnetic RF-based systems. In fact, electromagnetic waves may be absorbed easily by the communication channel, particularly when soil, rocks or water exist in the channel. This is a major problem in RF-based communication systems, where information is modulated on radiated electromagnetic waves [8]. Although RF-based systems are suitable for long range communication, magnetic waves are more effective for data transmission over shorter distances. Since they are not strongly affected by the environment. This characteristic of magnetic induction (MI) communication makes it appropriate for using in underwater and underground communications, where EM waves are severely attenuated. Embedded medical devices may also benefit from NFMIC, since body tissue has less impact on transmitted MI-signals compared to RF-signals.

Although NFMIC has a number of advantages over EM RF-based communications, the effect of path loss in the system is much more critical. This is because the transmitted MI signal flux density decreases rapidly (faster than EM waves) as it travels through the channel. This results in very limited communication range, because the signal power decreases as distance increases in proportion to the sixth power of distance [16, 17].

There are currently few commercially available products built upon NFMI technology. FreeLinc recently released to market MI radios, which are capable of producing voice signal in a limited distance of about 1.45m [3].

While a number of studies has been conducted into mechanisms for extending the communication range of RF-based systems through cooperative retransmission [5, 18–20], only a limited amount of research has been done to evaluate performance

and apply this technique in NFMIC [6–8].

1.2 Thesis Objectives and Scope

Since the communication range of NFMIC systems is limited, the objective of this study is to apply the cooperative communication concept in NFMIC systems, in order to extend the communication range. This can potentially allow NFMIC to be applied where longer range is required, such as local area networks (LAN). However, the principal application of this thesis is to enhance the communication range and channel data rate in Body Area Networks (BAN).

Recently a new method has been proposed, known as the *magneto-inductive waveguide*, which forms the basis for this study [5, 18–20]. This thesis presents a proper signal propagation model for magnetic induction communications, proposes a number of multihop communication techniques applicable to a NFMIC, and throughly evaluates the performance of these mechanisms through analysis and simulations. The following section provides an overview of the main contributions of this thesis.

1.3 Contributions of the Thesis

1.3.1 NFMIC Link Budget

One of the fundamental requirements for modelling a communication network is the determination of an expression for link budget. The link budget should take into account the gains and losses of the transmitter and receiver, and the signal attenuation due to propagation. However, this concept has not been widely explored for NFMIC systems, and there is a need for a link budget model which is applicable to a NFMIC system. A link budget model for NFMIC is proposed in Chapter 3. Using this model, the achievable communication range based on the antenna characteristics is analysed.

Relevant Publications

- J. Agbinya and M. Masihpour, "Power equations and capacity performance of magnetic induction communication systems," *Wireless Personal Communications Journal*, pp. 115, 2010, 10.1007/s11277-011-0222-x.
Online. Available:
http://www.springerlink.com/ content/9k1154175n324328/

- J. Agbinya and M. Masihpour, "Near field magnetic induction communication link budget: Agbinya-masihpour model," in Broadband and Biomedical Communications, 2010 International Conference on, Dec.
Online. Available:
http://ieeexplore.ieee.org/stamp/stamp.jsp?arnumber=05723604

- J. Agbinya and M. Masihpour, "Magnetic induction channel models and link budgets: A comparison between two agbinya-masihpour models," in Communications and Electronics (ICCE), 2010 International Conference on, aug. 2010, pp. 400 405.
Online. Available:
http://ieeexplore.ieee.org/stamp/stamp.jsp?arnumber=05739497

- J. Agbinya and M. Masihpour, "Power equations and capacity performance of magnetic induction body area network nodes," in Broadband and Biomedical Communications,2010 International Conference on, Dec.
Online. Available:
http://ieeexplore.ieee.org/stamp/stamp.jsp?arnumber=05723607

- Mehrnoush Masihpour and Johnson I Agbinya; "NFMIC simulator"; in *"Principles of Inductive Near Field Communications for Internet of Things"* (ed. Agbinya JI); ISBN: 978-87- 92329-52-3 ,Rivers publishers, Denmark

- Johnson I Agbinya and Mehrnoush Masihpour; "Part III: WiMAX and LTE Link Budget"; in *"Planning and Optimisation of 3G and 4G Wireless Networks"* (ed. Agbinya JI), ISBN: 978-87-92329-24-0 2009 River Publishers, pp. 105 136

1.3.2 The Magneto Inductive Waveguide

In Chapter 4, the magneto inductive waveguide is studied, a link budget model for a waveguide communication system is proposed and its performance is extensively studied. It is shown that to maximise the performance of a waveguide transmission system, the voltage excitation method has an important role to play. Three methods of voltage excitation methods for a waveguide system are proposed and compared. It is also shown that a linear waveguide model is not directly applicable to a BAN and that there is a need to develop multihop communication techniques applicable to a BAN in a 3D environment.

Relevant Publications

- M. Masihpour and J. Agbinya, "Cooperative relay in near field magnetic induction: A new technology for embedded medical communication systems," in Broadband and Biomedical Communications, 2010 International Conference on, Dec.[Online. Available:]
http://ieeexplore.ieee.org/xpls/abs$_all.jsp?arnumber = 5723612$

- J. Agbinya and M. Masihpour, "Excitation methods for magneto inductive waveguide communication systems," in Broadband and Biomedical Communications ,2010 International Conference on, Dec.
Online. Available:
http://ieeexplore.ieee.org/stamp/stamp.jsp?arnumber=05723606

- Mehrnoush Masihpour and Johnson I Agbinya; "Magneto Induction Link Budget"; in *"Principles of Inductive Near Field Communications for Internet of Things"* (ed. Agbinya JI); ISBN: 978-87-92329-52-3, Rivers publishers, Denmark

- Mehrnoush Masihpour and Johnson I Agbinya; "Magneto Inductive Waveguide Devices"; in *"Principles of Inductive Near Field Communications for*

Internet of Things" (ed. Agbinya JI),ISBN: 978-87-92329-52-3, Rivers publishers, Denmark

1.3.3 Multihop Relaying Strategies for NFMIC Networks

In Chapter 5, three multihop relaying techniques are proposed that model communication in an imperfect 3D environment, where undesirable and inevitable antenna displacements exist. The proposed techniques use idle devices in the network to assist in the communication from a source to a destination, in order to either increase the communication range or the channel data rate. The methods are evaluated and compared for two different cases: firstly where a direct line of sight exists between the source and the destination, and secondly when the target receiver is out of the direct range of the original source. The methods are analysed for relay selection based on a number of different metrics, namely separation distance, angular displacement and lateral displacement. Finally, a more appropriate relay node selection metric is proposed: the *relay link indicator*. It is shown that the relay link indicator is a superior metric for relay node selection is NFMIC compared to the other mentioned three metrics.

Relevant Publications

Accepted journal paper:

- Mehrnoush Masihpour, Mehran Abolhasan, Daniel Franklin "NFMIC Cooperative Communication Methods for Body Area Networks", Journal of Networks, 2012

Submitted Journal Paper:

- Mehrnoush Masihpour, Daniel Franklin, Mehran Abolhasan, "Multihop Relay Techniques for Communication Range Extension in Near Field Magnetic Induction Communication Systems", IEEE Transactions on Wireless Communications, 2012

Other Publications:

- Mehrnoush Masihpour, Johnson Agbinya and Mehran Abolhasan; "Energy scavenging for magnetically coupled communication devices" ; in *"Energy Scavenging and Optimization Techniques for Mobile Devices"*(ed. Hrishikesh Vanketash and Gabriel-Miro Muntean), CRC press, 2012, U.S.

- Mehrnoush Masihpour and Johnson I Agbinya; "Wireless Power Transfer"; in *"Principles of Inductive Near Field Communications for Internet of Things"* (ed. Agbinya JI), ISBN: 978-87-92329-52-3, Rivers publishers, 2012, Denmark

- Mehrnoush Masihpour and Johnson I Agbinya; "Part I: Overview of WiMAX cellular technology"; in *"Planning and Optimisation of 3G and 4G Wireless Networks"* (ed. Agbinya JI), ISBN: 978-87-92329-24-0 2009 River Publishers, pp. 33 66

- Mehrnoush Masihpour and Johnson I Agbinya; "Part II: Planning and Dimensioning of WiMAX and LTE Networks"; in *"Planning and Optimisation of 3G and 4G Wireless Networks"* (ed. Agbinya JI), ISBN: 978-87-92329-24-0 2009 River Publishers, pp. 33 66

Chapter 2

Literature Review

2.1 Chapter Overview

The objective of this chapter is to provide a comprehensive literature review on the topics directly related to the subject of this thesis. The topics discussed include an overview of the far-field and near-field communications regions and the specific characteristics of each region. Different short range communication techniques in the near-field region is discussed and compared. However, since the main focus of this thesis is on near-field magnetic induction communications, a detailed overview of the technology and potential applications is given.

The objective of this thesis is to study the NFMI cooperative communication for BANs; therefore potential benefits of NFMIC to BANs and also the shortcomings of the technology are examined followed by a discussion of the principle of cooperative communication in both RF and NFMI communication systems. Relevant studies on NFMI cooperative communications are evaluated and discussed.

The chapter concludes that, firstly there is a need to determine a proper link budget model for NFMIC, and secondly that the existing techniques for NFMIC range extension are not directly applicable to a BAN and that there is a need to develop cooperative communication models to enhance the communication range and the total performance of NFMIC systems.

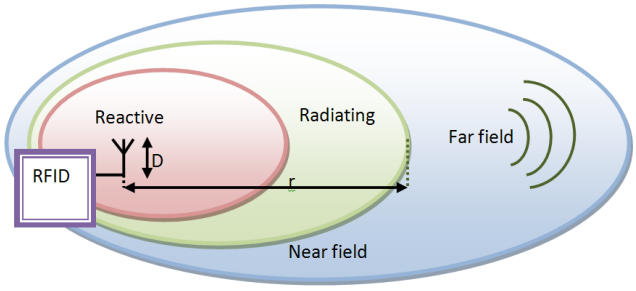

Figure 2.1 Near and Far Field of a Radio Frequency Identifier Reader (adapted from [1])

2.2 Far-Field and Near-Field

2.2.1 Far-Field

While far field refers to the region around a radiating antenna in which EM waves are radiated into space, the term near field describes a region close to the transmitting antenna in which non-radiating magnetic waves exist. In fact, both near field and far field exist around any radiation source [21]. The boundary between near field and far field is not fixed and it changes with the operating frequency. It also depends on the error rate that an application can tolerate [21]. In current literature there are at least three different definitions of these two terms [13]. The boundary between near and far field may be defined using transmission range, wave impedance or phase variation of radiation. For instance, in radio communications, the communication range is of prime importance while for antenna designers, the radiation phase perspective is more appropriate. Wave impedance is the dominant consideration for shielding of radiation [13].

Figure 2.1 illustrates how the area around an antenna is divided into different regions. The two main regions are near-field and far-field. In the far-field region, a combination of electric and magnetic waves is propagated as electromagnetic waves. Figure 2.2 shows the different components of an electromagnetic wave. As may be seen from the figure, an electromagnetic wave consists of an electric field and a magnetic field, which are perpendicular to each other and also to the direction of propagation.

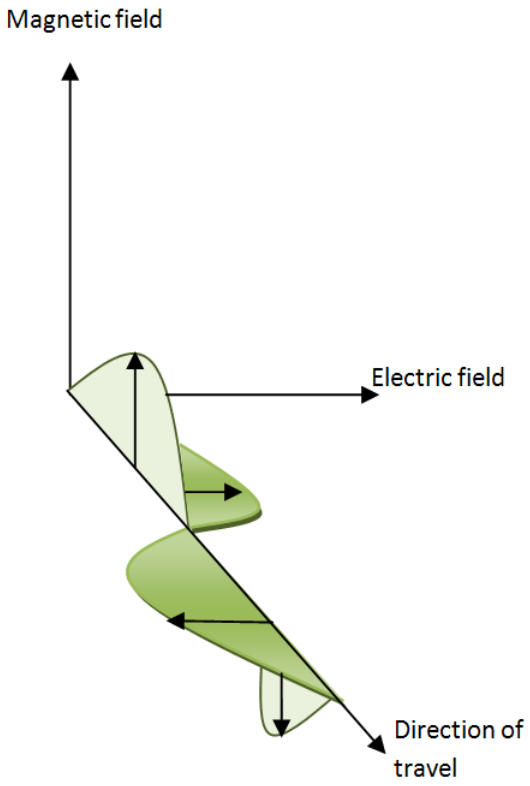

Figure 2.2 Propagating Electromagnetic Electric and Magnetic Fields (adapted from [1])

By contrast near-field consists of two regions: reactive and radiative. In the radiating region, the angular field distribution depends on distance, while in the reactive zone energy is stored and not radiated [1].

According to the literature, the boundary between far field and near field is not a specific point. Therefore, the boundary between these two regions needs to be determined based on the specific application. For a small electric antenna, it is conventionally defined that the reactive near field boundary (the maximum allowable range in near field) is [13]:

$$r_{max} = \frac{\lambda}{2\pi} \tag{2.1}$$

where λ is wavelength. For larger antennas, where antenna size is much larger than wavelength, this boundary may be defined as [22]:

$$r_{max} = 0.62\sqrt{\frac{D^3}{\lambda}} \tag{2.2}$$

where D is the largest dimension of antenna (see Figure 2.1) [22]. Conventionally, wireless communications occur in the far-field region, where information is transferred through the radiation of electromagnetic waves. While radiating EM waves in far-field sufficiently addresses the need for communications over larger distances, it may not be the best possible solution for short range communications. When communications over very short distances are required, often it is difficult to limit the EM transmitted signal to within close proximity of the transmitter. In this context, NFMIC has been seen as an efficient technique for limited range communications. The main principle of NFMIC is to modulate the magnetic field at the transmitting device and demodulate it at the receiver [23]. Section 2.4 discusses main concepts of an NFMIC system in detail.

2.2.2 Near-Field

The basic principle of near field communication (NFC) is to bring devices close together to be able to establish secure communication and transmit data at high data rates [24]. For example, two NFC-enabled devices such as a mobile phone and a computer can be brought in close proximity to be able to transfer data directly and wirelessly between a computer and a mobile phone [24]. The photos on a digital camera can be displayed on a TV directly using the NFC-enabled devices [24]. The NFC-forum was established by NXP semiconductor, Nokia and Sony in 2004 and is a non-profit industry association to advance the use of NFC short-range wireless interaction in consumer electronics, mobile devices and PCs [25]. According to the NFC forum [25]:

> "products with built-in NFC will dramatically simplify the way consumer devices interact with one another, helping people speed connections, receive and share information and even make fast and secure payments."

Communication in the near-field can occur through the use of electric-field or magnetic-field. Electric and magnetic waves have different behaviour in the near-field region. Therefore, different link equations are required to model the signal propagation in each case [26]. One of the main differences is that there is a need for specific antenna types for data transmission using each field type. Electric field transmission requires an electric antenna such as a dipole or whip while magnetic field needs a magnetic antenna such as a loop or loopstick antenna [26]. The link equation describes the received signal power at the receiving antenna and it is proportional to the square of time average of electric field intensity **E**, which indicates the force experienced by a stationary positive unit point particle at a specific position within the field:

$$P_R(\mathbf{E}) \propto \left\langle |\mathbf{E}|^2 \right\rangle \propto \left(\frac{1}{(\beta r)^2} - \frac{1}{(\beta r)^4} + \frac{1}{(\beta r)^6} \right) \tag{2.3}$$

where $\beta = \frac{2\pi}{\lambda}$ [13, 26]. Therefore, the power equation in near-field is [13, 26]:

$$P_L(r, f) = \frac{P_R(\mathbf{E})}{P_T} = \frac{G_T G_R}{4} \left(\frac{1}{(\beta r)^2} - \frac{1}{(\beta r)^4} + \frac{1}{(\beta r)^6} \right) \tag{2.4}$$

The received magnetic-field signal power at the receiver from a co-polarised transmitting antenna is also proportional to the square of the time average of magnetic field intensity, **H**, which refers to the ability of a magnetic field to exert on moving electric charges and is as follows [13, 26]:

$$P_R(\mathbf{H}) \propto \left\langle |\mathbf{H}|^2 \right\rangle \propto \left(\frac{1}{(\beta r)^2} + \frac{1}{(\beta r)^4} \right) \tag{2.5}$$

Therefore path loss equation for the link may be expressed as [13]:

$$P_L(r, f) = \frac{P_R(\mathbf{H})}{P_T} = \frac{G_T G_R}{4} \left(\frac{1}{(\beta r)^2} + \frac{1}{(\beta r)^4} \right) \tag{2.6}$$

This equation models the received signal from two unlike antennas (electric to magnetic and magnetic to electric).

It can be seen from Figure 2.3 that when the communication range is smaller than 0.1λ ($r < 0.1\lambda$), the transmitted signal decays at a rate equal to +60 dB per decade

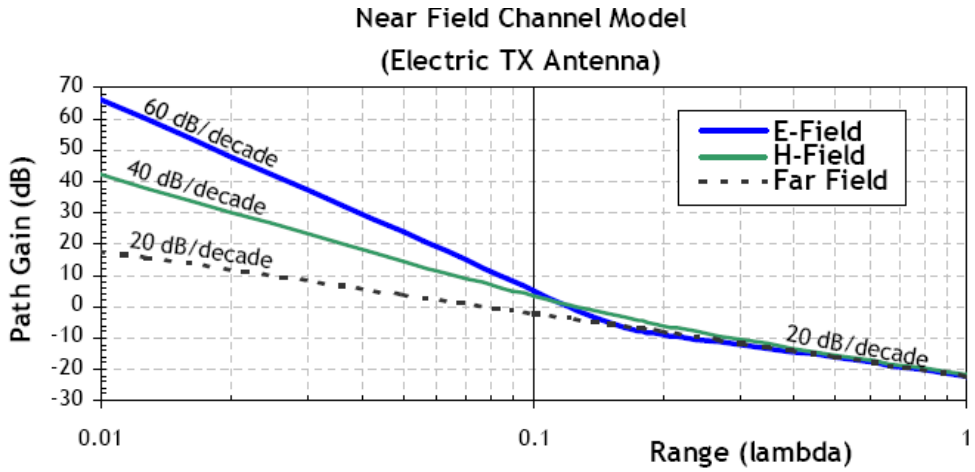

Figure 2.3 Near Field Path Loss [2]

of distance. Above the intermediate range (i.e. $r > 0.1\lambda$), the decay in received signal or path loss is about -20 dB per decade of distance [2, 26].

From Equation 2.6, when $\beta r = 1;\ r = \frac{\lambda}{2\pi}$, near field path loss approximates to

$$P_L(r, f) \approx \frac{G_T G_R}{4} \tag{2.7}$$

Thus the path loss for a typical near-field channel is approximately -60 dB. A normal approximation for matched antennas (electric to electric or magnetic to magnetic) is [13]:

$$P_L = 10\log_{10}(P_L(r, f)) = -6 + 20\log_{10}(G)\ \ dB \tag{2.8}$$

When unlike antennas are used (electric to magnetic, magnetic to electric and $\beta r = 1;\ r = \frac{\lambda}{2\pi}$), near field path loss approximates to [13]:

$$P_L = 10\log_{10}(P_L(r, f)) = -3 + 10\log_{10}(G_T G_R)\ \ ;(dB) \tag{2.9}$$

There are a number of short-range communication technologies which use the electromagnetic RF in near-field to communicate information. Technologies such as Bluetooth, UWB, ZigBee and RFID are some examples of communications being performed in the near-field using electric waves [27]. In the following section, each technology is briefly described and their performance is compared. However, since

this thesis aims to study NFMIC as a short range communication method for BAN, first an overview of BAN and its requirements is given.

2.3 Body Area Network and available short range communication technologies

2.3.1 Overview of Body Area Network

The BAN interest group (IG-BAN) was first approved as a study group by the IEEE 802 Executive committee in November 2006, six month after it was started as an interest group at a meeting in Jacksonville, USA [28]. BAN aims to provide reliable, short range (2-5m) and low power communications in close proximity to the human body. BAN can be classified in two categories: *on-body* (wearable) and *in-body* (implant) [28, 29]. On-body BAN refers to a network of smart intelligent devices carried by a person or located closely on the person's body, while in-body BAN consists of devices implanted inside the human body [28, 29]. BAN devices are often required to sense and gather information from a human body or from the ambient environment. Therefore, a BAN can be seen as a special type of a sensor network, although it has a number of features which distinguish it from a typical sensor network [29]. For example, all the devices within a BAN are considered equally important and there are no redundant nodes [29]. Since the communications in BAN occurs in or around a human body, the transmitted signal suffers form high attenuation due to the signal absorption by the body tissues. On the other hand, transmission power has to be extremely low to prevent interference with the other existing communication systems and to avoid tissue damages from RF heating [29]. The specifications of a BAN highly depends on the usage scenario, however, there are some common requirements that must be addressed in many personal area communications such as very low power consumption, high reliability and security, safety for human body and compatibility with body energy harvesting. A BAN may have variety of usage scenarios. Some of the most important usage models are as follows:

Medical and health care: A BAN can be used for different purposes at hospitals such as automatic medical diagnosis, treatment and dosing to improve the quality of treatment and management efficiency in hospitals [28–30]. It is also useful for remote patient monitoring. In Medical ICT (MICT), the main purpose of using a BAN is to collect the vital information regarding a patient's condition such as blood pressure, body temperature, glucose level, heartbeat and brain or cardiac signals and transmit the data to a command unit (action unit) or a central controller, which can be a smart device located in hospital and controlled by a doctor or nurse. It also may be a digital device controlled by the patients themselves [28–30]. BAN devices used for medical purposes are often in the form of implants and need to be located inside the human body. In such an environment, the transmitted EM signal is highly attenuated by the body tissue since communication channel is in fact the human body and contains body tissues and water. To increase the received signal strength, one approach is to increase the transmission power. However, this increases in power consumption, results in an increase in the level of interference with the other existing communication devices and may be hazardous to the body. Another approach is to use multihop communications to increase the reliability of communication while the transmission power is maintained at a minimum level. In Chapter 5, different multihop communication techniques for BANs are proposed and evaluated.

Assisting people with disabilities: In this usage model, BAN devices may be used for object detection such as detecting stairs and vacant seat in trains also to provide guidance for routing and positioning [28]. As an example, a BAN can be used to assist a speech-impaired person [28], in which sensors may be located on the person's fingers to collect information such as the movement of fingers and relative position of fingers in respect to each other and also to the hand and communicate the gathered information to a central node to be further interpreted as vocal language [28]. Using a BAN to assist elderly or people with disabilities can significantly improve their quality of life and also may decrease the cost and need for human resources, to aid people with disabilities.

Entertainment: A BAN may be used by a person for entertainment purposes such as gaming, music and video playing and so on [28, 30]. The typical devices in such networks are mobile phones, laptop computers, music players and headsets [30]. This usage scenario requires the highest data rate among all the applications discussed here, since the real time video streams require data rates in range of 384 kbit/s up to 20 Mbit/s [30]. Since the cost and power consumption needs to be minimised, it is very challenging to achieve required data rates for this category of BAN application.

Personal fitness monitoring: This application requires data rates range between 128 kbit/s to 384 kbit/s [30]. BAN for fitness monitoring typically consists of a music player and some sensors collecting the information relevant to the exercise, such as sensors to monitor heart rate, speed, body temperature, oxygen level and rate of glucose consumption [30]. The collected information may be further sent through a gateway, to a central data base or to a coach, monitoring the athlete [30]. This can highly improve the training of professional athletes.

Public Safety: A BAN may be used by firefighters, police, ambulance officers, emergency service or military personel for public safety purposes. Vital information from individuals and the ambient environment may be collected in order to detect an emergency situations which may require quick actions from outside [30]. Information such as the level of toxic gas in the air and the temperature can be collected and the sensor may warn the person or the action unit [29, 30]. One example of BAN usage model in military is a U.S Army program known as *warfighter physiological status monitoring* (WPSM) [31]. This programs aims to address two issues. Firstly, to reduce injuries caused by environmental factors such as high temperature and altitude sickness [31]. Authors of [31] discuss that having access to WPSA data enables the commanders at different levels to effectively have access to their troops and enhance their performance. According to [31], the second purpose of WPSM program is to increase the chance of survival for casualties. WPSM information can help the combat medic to quickly access the wounded person.

In general, WPSM comprise of three main units: firstly a group of BAN sensors,

which collect the vital data; secondly, a decision support software; and finally a database management system [31]. The function of decision support software is to interpret data collected by the BAN sensors in order to automatically conclude whether the person is dead, alive or injured and to make an recommendation decision based on the situation [31]. The database management system consists of the information required for decision-making such as the identification of important physiological parameters and prediction of the clinical outcome [31].

2.3.2 Short Range Communication Technologies

A BAN may use a variety of technologies for communication between the sensor nodes. While one technique can be advantageous for a specific application, it may be unsuitable for another. However, it should address the fundamental requirements of a BAN: low transmission power, minimal interference level, low cost, simplicity, high security and reliability as well as small size [28]. Some of the commonly used short range technologies include:

Specific low level Radio: It operates in the 430 MHz frequency band and has a very low data rate of 2.4 kbit/s. Although this technology has very low power consumption and power emission, it is generally not suitable for BAN due to very low data rates [28].

Bluetooth (IEEE 802.15.1): Bluetooth technology has been used for voice and data transmission [32]. It operates in the busy 2.45 GHz ISM band. To minimise interference with other applications using the same operating frequency such as microwave ovens or cordless phones, Bluetooth uses a frequency hopping scheme [33]. In fact, by avoiding occupied frequencies in the hopping sequence, it also reduces interference with other applications. Frequency hopping occurs by rapidly switching a carrier between a set of frequency channels in a known sequence. Although Bluetooth is widely adopted by end users and vendors, it has major security issues which need to be addressed [33]. Security problem is mainly due to poor implementation of Bluetooth architecture on devices [33] leading to high profile Bluetooth hacks [33].

Bluetooth provides a communication range from 10 m to 100 m depending on the Bluetooth device class [32]. A peak data rate of 3 Mbit/s may be achieved through a Bluetooth connection [32]. Bluetooth has very high emission power and power consumption among other technologies discussed here [28].

Ultra-wideband (UWB): UWB is another short range and low power (1 mW/Mbps) communication technology, which provides high data rates (up to 480 Mbit/s) by using large bandwidth [27, 32, 34, 35]. However, at a distance of 10 m, the data rate reduces to 110 Mbps [32]. UWB is capable of operating at frequencies in the range between 3.1 GHz and 10.6 GHz, therefore, a large bandwidth can be allocated to applications demanding high data rates [35]. UWB may be used in five different categories of applications: Multimedia communication, radar applications, biomedical monitoring, sensor networking and location and tracking (LT) [34]. LT refers to the collection of location information from the signals traveling between different nodes [34]. However, UWB transmission losses by the human body are very significant [28]. Therefore, using UWB in implantable BAN is a very challenging task.

ZigBee: The main objective of ZigBee is to provide low cost, low power and low data rate communications [36]. Similar to Bluetooth, ZigBee uses the 2.4 GHz ISM band, therefore, ZigBee devices may interfere with each other and also with other existing communication devices [32, 36, 37] . At this frequency, it achieves a data rate of 250 kbps [32]. There are 16 channels within 2.4 GHz band, which are available to ZigBee devices [37]. ZigBee devices may be connected together through direct sequence spread spectrum (DSSS) [37]. A ZigBee network consists of at least one full function device (FFD), which acts as a coordinator within the network as well as one or more reduced function device (RFD). They can be connected together through a point-to-point, star or mesh topology [37]. The main target application of ZigBee is remote control monitoring and data acquisition in industrial, domestic and infrastructure applications, where low data rates, low power and ease of use is desirable [27, 32]. It is able to achieve a communication range 10 m to 100 m [32].

Table 2.1 RFID properties (adapted from [12])

Property	**LF (125 kHz)**	**HF (13.56 MHz)**	**UHF (915/2450 MHz)**
Read Range	Low (< 24 Inch)	Moderate (<1.2 m)	high(<5 m)
DataRate	slow	Moderate	Fast
Read through the glass,cloths,wood,etc.	yes	yes	yes
Power consumption	Low	Moderate	High

However, the low data rate, maximum 250 kb/s, is a limiting factor for ZigBee being used in a BAN.

RFID (Radio Frequency IF dentification): RFID technology defines more than 140 different ISO standards for a broad range of applications [32]. It may operate at frequencies from less than 100 MHz, more than 100 MHz and in UHF band (868 MHz to 954 MHz). The transmitter and receiver need to be located within a few meter of each other in order to be able to communicate [32]. This system consists of a reader and a tag from which the reader can extract information. The tag is capable of operating in two different modes [12, 32]; passive and active modes. For a passive tag there is no need for a battery or an internal power source. In this case the reader powers the tag through electromagnetic induction, which actuates it and allows the reader to pull the information from the tag [12]. However, active tags have their own source of power which enables the tags to communicate with the reader over longer distances. The need for a power source in active tags results in higher cost and periodic battery replacement [12]. Since RFID devices operate at a diverse range of frequencies, there is a correspondingly variety of characteristics such as data rates, penetration to objects, communication range and the power consumption [12]. Table 2.1 compares different characteristics of RFIDs operating at different frequencies [12]. RFID technology is mainly used for object tracking and automatic identification and data capture.

Table 2.2 summarizes the characteristics of different popular short range commu-

Table 2.2 Short Range Communication Technologies

Technology	**Operating Frequency**	**Peak Data Rate**	**Comm. Range**	**Comments**
Bluetooth	2.45 GHz	3 Mbit/s	10 m to 100 m	Security issues
Ultra-wide band (UWB)	Range: 3.1 and 10.6 GHz	480 Mbit/s	-	High signal absorption rate by body tissues
Specific Low Level Radio	430 MHz	2400 bit/s	-	Very low data rate
ZigBee	2.4 GHz	250 kbit/s	10 to 100 m	Low data rate
Radio frequency identification (RFID)	less and more than 100 MHz in UHF band (868 to 954 MHz)	Depends on frequency	Up to 5 m	Automatic identification and data capture applications

nication techniques. As may be seen from the table, each technology posses certain benefits and drawbacks. For example, Bluetooth sufferes from security issues. Moreover, Bluetooth power consumption is high. Use of Zigbee is limited to the applications requiring low data rates. However, while RFID and UWB are more efficient techniques for use in applications where short range and high data rates are required, they suffer from the signal absorption by the channel where it contains water, organic matters and body tissues. It also suffers from interference from other existing technologies since most existing wireless communications occur through the radiation of EM waves. Moreover, they may be more prone to signal diffraction and scattering where the communication occurs in or on person's body.

NFMIC offers advantages over the conventional EM-RF communications when it is used for short proximity communications. Magnetic induction may provide better signal quality since its behavior is much more predictable than RF [3, 38–40]. RF communications often suffer from frequency spectrum contention, reflection, shadowing and fading resulting from the surrounding environment and the presence of

objects such as vehicles, buildings and the human body. By contrast, NFMIC is mainly affected by the magnetic permeability of channel and is more robust to reflection, shadowing and diffraction.

To improve the quality of RF signals in order to achieve adequate reliability, higher transmission power is required. However, increasing the transmission power leads to some issues such as interference, inter-system frequency contention and higher power consumption. By contrast, NFMIC not only achieves reliability but also reduces the required power consumption. Increasing the transmission power to achieve higher signal to noise ratio also results in potential security risks. By increasing the power, the chance of the signal being detected by unauthorised parties increases. However, MI waves mitigate such problems inherently without the need for expensive and complex security algorithms and techniques. MI signals attenuate with the sixth power of distance, or about 60 dB per decade of distance [3, 14, 41]. Although this property of MI makes it unsuitable for transmission over long distances, it allows secure communication over short range. It also results in less interference with other communication systems and reduces frequency spectrum contention [3, 38–42].

Due to its low power consumption, reliability and the inherent difficulty of long-range detection, NFMIC is widely regarded as a good solution for short range military applications [3, 43]. NFMIC also can be used in wide range of non-military applications such as contactless payment cards, medical implants and monitoring devices, entertainment applications on mobile phones and personal wireless electronics and so on. NFMIC is also a promising solution for underwater and underground communications in which RF communications is difficult, inefficient or impossible [6, 44, 45]. While EM waves are severely attenuated by soil, water, body tissues and rocks, MI waves are capable of penetrating more deeply in such environments [6, 44, 45]. These benefits are countered by the limited data rates achievable through MI communications systems. This, together with the limited communications range, may render MI communications unsuitable in applications where longer range or higher capacity is required, such as video communications within a person's

communication region (*communication bubble*) or inter vehicle communications.

The following section provides a discussion of the theoretical basis of magnetic induction communications in near-field.

2.4 Magnetic Induction Communications in Near-Field

NFC occurs through a basic physical principle. A simple peer-to-peer magnetic induction communication system consists of a transmitting and a receiving coil, which act as antennas in the system. The coils are included in resonant circuits in series (Figure 2.6) or parallel. The total impedance of the circuit is given by:

$$Z(j\omega) = R + j(X_L - X_C)\,(\Omega) \tag{2.10}$$

where:

$$X_L = \omega L = 2\pi f L\ (\Omega) \quad \text{and} \quad X_C = \frac{1}{\omega C} = \frac{1}{2\pi f C} \tag{2.11}$$

In Equation 2.11, X_L and X_C are the inductive and capacitive reactance of the inductor and capacitor respectively and ω is angular frequency in radians per second ($C_1 = C_2 = C$ and $L_1 = L_2 = L$). Resistance R represents the sum of ohmic source resistance of the transmitting circuit (i.e. $R = R_s + R_{L1} = R_L + R_{L2}$), and any parasitic resistances of inductor and capacitors.

When inductive and capacitive reactance are equal, then the impedance of circuit is purely resistive. This condition ($X_L = X_C$) is known as *resonant*. When the resonant condition ($X_C = X_L$) is satisfied, the circuits are resonating at an angular frequency equal to $\omega_0 = {}^{1}\!\Big/\!\sqrt{LC}$. L and C are the self inductance of the coils and capacitance respectively. One of the most important performance indicators of MI system is the quality factor (*Q-factor*), which indicates how efficiently inductors and capacitors transfer the energy from a source to a destination. The quality factor can be determined by using the expression below and is dimensionless (i.e. it has no unit) [13]:

$$Q = \frac{Energy\ stored\ in\ the\ circuit\ per\ cycle}{Energy\ dissipated\ by\ the\ circuit\ per\ cycle} = \frac{Reactance}{Resistance} \tag{2.12}$$

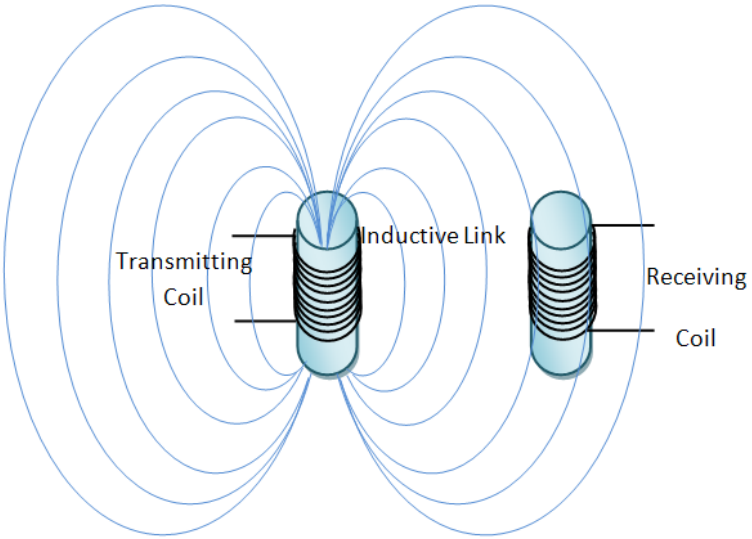

Figure 2.4 Inductive Transmitter and Receiver (adapted from [3])

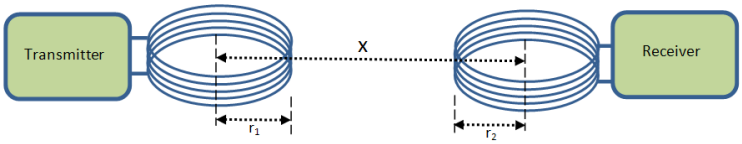

Figure 2.5 Two parallel coils centred on an axis (adapted from [4])

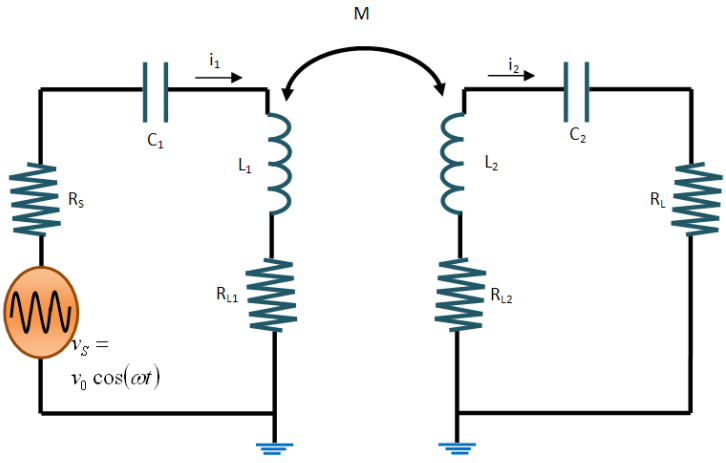

Figure 2.6 Lumped Circuit Models of Parallel Inductive Coils (adapted from [4])

Hence, based on resonant frequency, inductive and capacitive parameters of the resonating circuits, quality factors can be estimated using the following equation [13].

$$Q = \frac{\omega_0 L}{R} = \frac{1}{R\omega_0 C} \tag{2.13}$$

At resonance, maximum voltage is induced in the resonating inductors and is [13]:

$$V_0 = \frac{jX_L}{R} V_{in} = jQV_{in} \tag{2.14}$$

Equation 2.14 implies that inductors with higher Q-factor provide larger voltages in the output. In fact what happens in a peer-to-peer NFMIC system is that the voltage source at the transmitting circuit creates a current in that circuit. The voltage and current in the transmitter induce a current at the receiving circuit through the magnetic coupling between the transmitting and receiving coils. Data is modulated on the magnetic flux created by the transmitting coil and the receiver is able to receive the signal and demodulate it as long as it is within the created magnetic field. To evaluate how effective the mutual coupling is, the coupling coefficient (k) needs to be determined. Coupling coefficient is a function of the mutual inductance (M) and the self inductance of transmitting (L_1) and receiving (L_2) coils. It can be estimated using the following expression [16].

$$k = \frac{M}{\sqrt{L_1 L_2}} \tag{2.15}$$

According to Kirchoff's voltage law, voltages measured at the two inductive circuits (Figure 2.7) are:

$$V_1 = j\omega L_1 I_1 + j\omega M I_2 \tag{2.16}$$

$$V_2 = j\omega M I_1 + j\omega L_2 I_2 \tag{2.17}$$

Where I_1 is the current flowing in the first circuit and I_2 is the current in the secondary circuit (receiver).

To tune the circuits, coils are loaded with capacitors and resistors (Figure 2.8) [13]. Therefore, based on Kirchoff's voltage law, voltage and current across transmitting and receiving circuits are as shown in Equation 2.18 and 2.19 [13].

$$V_1 = \left[R_1 + j\omega L_1 + (1/j\omega C_1)\right] I_1 + j\omega M I_2 \tag{2.18}$$

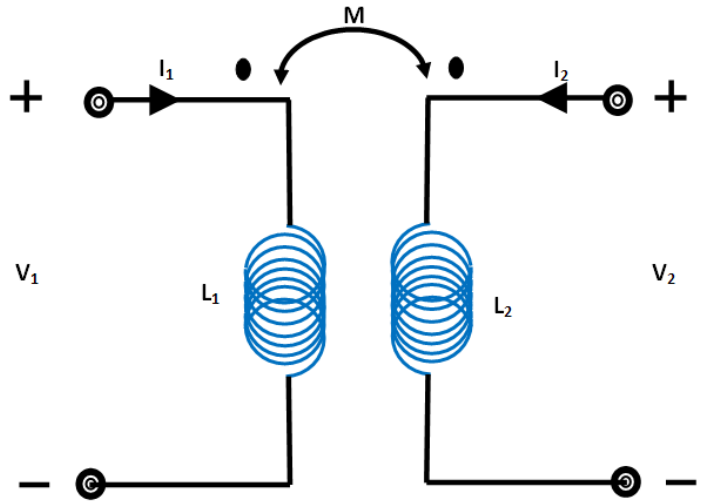

Figure 2.7 Inductive coils

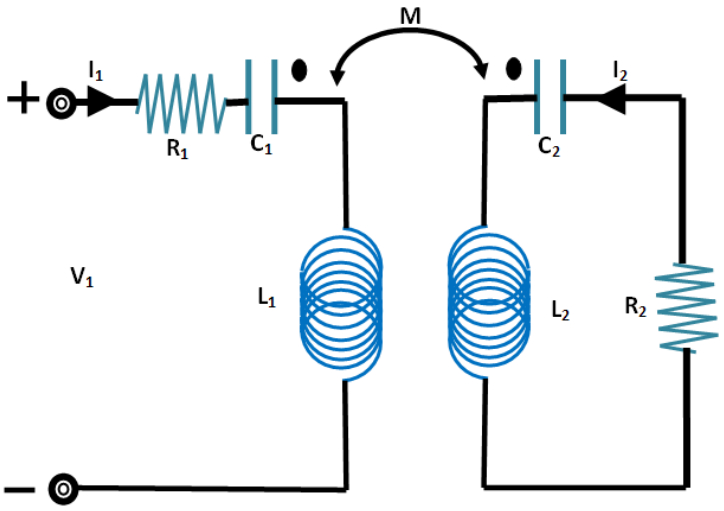

Figure 2.8 Tuned resonating circuits

$$0 = j\omega M I_1 + [R_2 + j\omega L_2 + (1/j\omega C_2)]\, I_2 \tag{2.19}$$

When the circuits resonate at the same frequency, the following relationship between circuit parameters is maintained [13]:

$$I_1 = \frac{V_1}{R_1} \tag{2.20}$$

$$P_1 = \frac{0.5|V_1|^2}{R_1} \tag{2.21}$$

$$I_2 = \frac{-j\omega M I_1}{R_2} = \frac{-j\omega M V_1}{R_1 R_2} \tag{2.22}$$

$$P_2 = \frac{\omega^2 M^2 |V_1|^2 R_2}{2(R_1 R_2)^2} \tag{2.23}$$

where P_1 and P_2 are transmission and the received power respectively. Therefore, the power transfer function becomes [13, 16, 17]:

$$\frac{P_2}{P_1} = \frac{\omega^2 M^2 R_1 R_2}{(R_1 R_2)^2} = \frac{\omega^2 k^2 L_1 L_2}{R_1 R_2} = k^2 Q_1 Q_2 \tag{2.24}$$

Equation 2.24 is fundamental for performance evaluation of an NFMIC system. If the Q-factor and coupling coefficient of the system are known, a power transfer function can be estimated, which consequently may be used for capacity and communication range estimation and network design. However, the coupling coefficient can also be expressed as a function of the radius of transmitting and receiving coils as well as separation distance between them [13, 15]:

$$k(x) = \frac{r_1^2 r_2^2}{\sqrt{r_1 r_2}\left(\sqrt{x^2 + r_1^2}\right)^3} \tag{2.25}$$

The coil efficiency determines how effective the resonating circuits are in transferring the power from a source to a sink [15]. The efficiency of transmitter (η_T) is a function of the source resistance (R_S) and the resistance of transmitting coil (R_{LT}), and the efficiency of receiver (η_R) is a function of load resistance (R_L) and receiving coil resistance (R_{LR}) [15].

$$\eta_T = \frac{R_S}{R_{LT} + R_S}; \;\; \eta_R = \frac{R_L}{R_{LR} + R_L} \tag{2.26}$$

As mentioned in [15], quality factor of transceivers also may be defined as:

$$Q_T = \frac{\omega_0 L_T}{R_{LT} + R_S}; \;\; Q_R = \frac{\omega_0 L_R}{R_{LR} + R_L} \tag{2.27}$$

Quality factors, efficiencies and coupling coefficients determine the performance of the whole magnetic induction system, in terms of the capacity, received signal power and communication range.

2.4.1 Magnetic Communication Bubble

NFMIC has been seen as a promising solution for a secure communication. In such systems communication usually occurs in a person's so-called *communication bubble* [15]. Although there is little information in current literature, precise analysis of a magnetic communication bubble has been done in [15]. According to Agbinya et al, the communication bubble edge is not the same as near and far field boundary. In fact, the boundary of a communication bubble depends on the sensitivity of receiver. The radius of a bubble is a distance d where received signal power is equal to the sensitivity of the receiver. For example if receiver is highly sensitive then bubble size is larger than when receiver sensitivity is lower [15]. However, the size of a bubble may also be determined based on the required capacity within the communication bubble. According to the well known Shannon-Hartley theorem, the capacity of a magnetic bubble at the edge of bubble where signal to noise ratio (*SNR*) approaches the threshold of detection, is [15]:

$$C = B_f f_0 \log_2 \left(1 + \frac{P_{rd}(\omega = \omega_0)}{N}\right) = B_f f_0 \log_2 2 = B_f f_0 \tag{2.28}$$

In this equation, f_0 is the centre frequency and B_f (the 3 dB fractional bandwidth) is defined as:

$$B_f = \frac{B}{f_0} = \frac{\sqrt{-\left(Q_T^2 + Q_R^2\right)^2 + \sqrt{\left(Q_T^2 + Q_R^2\right)^2 + 4.\left(Q_T^2.Q_R^2\right)}}}{\sqrt{2} Q_T Q_R} \tag{2.29}$$

If $Q_T = Q_R = Q$, Equation 2.29 simplifies to $B_f = 0.664/Q$ and results in a capacity at the edge of bubble of [15]:

$$C = B_f f_0 = \frac{0.664 f_0}{Q} \tag{2.30}$$

Equation 2.30 implies that a higher quality factor does not automatically lead to higher capacity. To evaluate performance of a magnetic bubble, a new metric has been proposed by Agbinya et al in [15]. The metric is called a *distance bubble factor* (σ) and is a function of quality factors of coils as well as efficiencies and coil radii:

$$\sigma = P_T Q_1 Q_2 \eta_1 \eta_2 r_1^3 r_2^3 \tag{2.31}$$

Therefore, according to [15], received power may be expressed as:

$$P_R\left(\omega=\omega_0\right)=P_T Q_T Q_R \eta_T \eta_R \frac{r_R^3 r_T^3}{\left(x^2+r_T^2\right)^3} \cong \frac{\sigma}{x^6};\ \ r_T << x \tag{2.32}$$

Equation 2.32 implies that MI received signal power decays with the sixth power of distance. This means that by increasing the communication range, received signal power decreases faster than in EM case. Very high path loss is a major problem in NFMIC systems. Therefore, NFMIC cannot be used in applications where longer communication ranges with high data rates are required. This thesis aims to enhance NFMIC range by exploiting cooperative communications. The following section provides an overview of cooperative communications in both RF and NFMI communication systems.

2.5 Cooperative Communications

2.5.1 Cooperative Communications in RF

According to a number of studies, it is clear that the number of applications and users for wireless broadband communication is growing rapidly [5, 18–20]. It has been predicted that 48% of broadband subscribers will use wireless systems by 2012 [18]. Therefore, to address the subscriber's requirements of reliable, fast and cheap wireless transmission of data such as voice, video and text, a large amount of spectrum bandwidth is required. However, the availability of frequency spectrum is limited. Consequently, in many situations, multiple users and/or networks need to share the same spectrum, leading to increased generation of interference, due to the overlapped signals. Commonly used strategies which try to avoid this limitation, include frequency reuse and a progressive reduction of cell size in cellular systems such as in UMTS and WiMAX. However, having smaller cells to achieve higher capacity and greater frequency reuse requires a higher number of base stations, since each cell requires its own base station. Consequently, deployment and maintenance of such networks is expensive for the operators and service providers, which leads to higher costs per subscriber.

To improve the achievable communication range and to enhance the capacity without increasing transmission power or reducing receiver sensitivity, multihop relaying has been developed for wireless communication system such as cellular networks [46–50], UWB [51], ZigBee [52], IEEE 80.2.11 and many more [53–55]. In general, multihop relaying refers to a communication method in which data is routed to the destination through one or more intermediate nodes or so-called *relay stations* (RS). RSs are capable of performing some functions normally carried out by the main base station. Multihop relaying can achieve higher capacity or provide extended coverage and consequently higher reliability and throughput with lower cost and less complexity compared to conventional star-topology communication systems. In other words, instead of using a large number of base stations, one or more semi-base station components may be used to assist the main base station (BS) to relay user data between a base station and user station. Since a RS is less complex compared to a BS, it is less costly for operators and consequently for subscribers. In this section, multihop relaying in EM RF-based system is discussed.

A number of different types of multihop networks have been proposed. The first is multihop infrastructure-based systems [5, 18–20, 46], which consist of one or more fixed relaying stations that are used along with the main base station to relay the data between a source (which could be a BS, user station or another RS) and a destination (BS, user station or another RS) [5,18–20]. This type of multihop relay is appropriate for long range cellular networks to cover dead spots (areas that are out of direct communication range of a base station) or to enhance network capacity in highly crowded areas such as cities, shopping malls and amusement parks.

2.5.1.1 Multihop Infrastructure-Based Systems in Cellular Networks

In cellular networks, *multihop-relay cell* (MR-cell) refers to a cell consisting of both BS and RSs, and the BS serving such a cell is referred to as multihop relay base station (MR-BS). Figure 2.9 illustrates an MR-Cell. In fact, the MR-BS is designed to support relaying and is responsible for bandwidth requests of RS and subscriber stations (SS) as well as channel assignment for each communication [5, 18–20]. One

or more RS(s) is also employed within MR-cell to relay data between MR-BS and SS without the need for extra frequency channels. Therefore, it may decrease the cost of installation and operation since the need for wire lines or dedicated wireless backhaul is mitigated. Within an MR-cell, data between SS and BS can be either communicated through a RS or through a direct link between the MR-BS and SS [18]. The link between SS and RS or MR-BS (direct link) is often referred to as an access link, and the link between BS and RS or between RSs is known as a relay link or backhaul link [18]. The relay link can operate on time division duplex (TDD) or frequency division duplex (FDD). Transmission may be performed in full duplex or half duplex modes. In full duplex mode, a RS can transmit and receive simultaneously using different frequencies, while in half duplex mode RS is designed to either receive, transmit or remain idle at any times.

On the access link, the SS transmits data on uplink (UL) to the RS or MR-BS and receives data from MR-BS or RS on down link (DL). This implies that the SS transmits on the UL, and the BS transmits on DL, however, an RS needs to transmit on both UL to MR-BS and DL to SS. There are two different operating modes, in-band and out-of-band, which are chosen depending on how carrier frequency is used on access and relay links [20]. If the access and relay link both use the same frequency, it is referred to as in-band relaying, while the out-of-band relaying mode uses different frequencies for the access link and relay link.

2.5.1.2 Multihop ad-hoc and Multihop-Hybrid Networks

Multihop ad hoc is another multihop method which is suitable for both short range and long range communications [46, 49, 53, 56, 57]. In multihop ad hoc, there is no need for fixed infrastructure. A number of electronic devices such as mobile phones and laptop computers can be connected in a peer-to-peer fashion and relay the transmitted data from a source node to other nodes until the destination is reached. Multihop ad hoc can be used for inter and intra vehicle communications, personal area networks, local area networks, underground communications as well as communications in the battlefield. Multihop ad hoc is also helpful in case of natural disasters

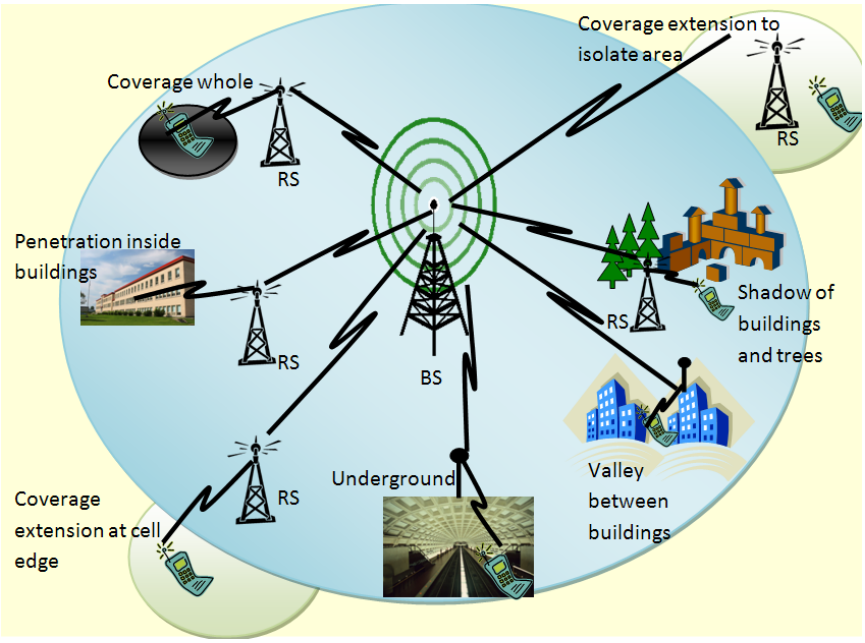

Figure 2.9 Overall view of a multi-hop relay cell

such as floods and storms, where the infrastructure may be damaged or destroyed as a result of the disaster [46, 49, 53, 56, 57]. In such scenarios, multihop ad hoc can be deployed for communication in disaster area for disaster recovery and management purposes.

If multihop ad hoc is used in combination with fixed infrastructure networks, it is known as multihop hybrid [49, 58]. In such systems, traffic can be relayed by other devices to allow communication with a user far away from the source and without the need to communicate directly with a fixed base station. This may be useful in busy and populated areas, where the base station is heavily loaded by data traffic. It can also enhance system coverage when a user is located outside the coverage range of a base station (for example, in dead spots). In this thesis, the multihop ad hoc technique is adopted since it is the most suitable for short range communication systems and body area networks in particular.

Ad hoc networks are classified into two categories, based on the architecture of the network; *centralised* (cluster-based) and *decentralised* (distributed) networks

[46, 54]. A centralised network consists of a number of nodes and only one cluster head, which is periodically elected by the other nodes in the mobile ad hoc network. The cluster head is in possession of all of the information about the entire network and is required to be located in the best position among all other nodes [54]. For instance, the node with the largest number of neighbors can be elected as a cluster head [54]. By contrast, in distributed ad hoc networks, all nodes have the same amount of information about the network.

While centralised networks have complex architecture and limited flexibility, distributed networks are simpler to implement [54]. However, distributed networks suffer from larger end-to-end delay and higher rates of packet collision. Distributed networks are less prone to network failure, because if a node malfunctions there are connections to other nodes which can provide alternate paths to a destination [54]. Therefore, distributed networks are suitable for multihop communications. Since they are more robust to network failure, decentralised multihop ad hoc networks work well for military communications and disaster recovery applications, since robustness is a critical factor in such scenarios [54].

Another factor that makes distributed networks more suitable for military applications is their lower transmission power requirements. Since each node is not required to transmit the traffic through a central controller, transmission power can be lower at each node. Each node can communicate with a destination through its neighbors; therefore, communication is performed via multiple shorter links instead of one link with higher transmission power. High transmission power in military communications may result in security risks through location disclosure [54]. Thus low transmission power is highly desirable for military communications.

Multihop ad hoc has been considered for range extension and increased robustness in different short range communications systems such as wireless local area networks (WLANs) [46], ZigBee [52] and UWB [51]. In [52], the authors have developed a ZigBee prototype system for home security. Authors of [52] claim that it can theoretically achieve an unlimited coverage range. However, this claim may not be

achieved in practice. Achieving a large coverage area through conventional point to pont connections for such applications requires long range devices, which are often expensive and power-hungry [52].

In UWB networks, the coverage range is also limited and high data rates may not be achievable through a conventional single hop method. In [51], a simulation environment is proposed which can simulate an OFDM-based UWB multihop network (including both physical and medium access control (MAC) layers). Using this simulation environment, the authors have evaluated the performance of a multihop relay UWB network to determine whether it improves system performance measures such as end to end delay and packet loss [51]. It is concluded that the IEEE 802.15.3 TDMA MAC layer can perform adequately in multihop UWB networks if proper scheduling and routing methods are precisely defined and implemented. However, further study is required into more efficient scheduling schemes such as Self-organized Time Division Multiple access (S-TDMA), to maximise the capacity and frequency reuse in such communication systems [51].

However, studying multihop relay networks from different perspectives leads to different relaying categories. RS may operate in three different modes according to how the received signal is processed: either amplify and forward (AF), decode or forward (DF) and estimation and forward (EF) [19]. In AF mode, RS receives the signal, amplifies it and retransmits the signal to another node, which can be a SS, BS or another RS, while in DF mode, a RS decodes the received signal and again encodes it before retransmission to the next hop. In EF mode, RSs monitor the channel condition periodically and retransmits the signal using either AF or DF techniques depending on the channel condition.

In the context of topology, a relaying network may follow either a tree or a mesh structure [18]. In a tree structure there are up to two paths: a direct link between SS and MR-BS and an indirect path via an RS. In this topology, a signal can be relayed more than two hops along the communication path by different RSs, each one supervised by MR-BS. Alternatively, another possible topology is the multihop

mesh network. In this case, RSs can communicate with each other and do not follow a tiering structure as tree topology does; therefore there may exists more than two paths between SS and MR-BS which results in more robustness and reliability in the network [18].

RS may also perform in two different modes referred to as transparent and non-transparent mode based on the transmission of control information by RS [5, 20]. In fact this means that if the RS is allowed to transmit preamble and control information at the beginning of frame, it operates in a non-transparent mode. However, its control information may differ from MR-BS. In transparent mode, the RS does not transmit its own control data when relaying. Whereas non-transparent mode in transparent mode SS is aware of the existence of the RS. According to deployment scenario and the need for more capacity or coverage, one of these modes can be employed. Transparent mode is suitable for capacity improvement, while non-transparent relaying meet the needs when coverage enhancement is the main requirement [5, 20].

2.5.1.3 Transparent Relaying Mode

As mentioned earlier, transparent relaying mode is suitable when there is a need for capacity enhancement. In this case, one or more RS capable of operating in transparent mode are employed within a MR-cell alongside a MR-BS to relay data between MR-BS and SS [5, 20]. A transparent RS does not transmit its own control information, rather it sends data from MR-BS to SS and the SS is capable of decoding the control information from MR-BS. For deployment of such a network using transparent RSs, MR-BS and SS need to be in communication range of each other, because MR-BS needs to transmit control information and synchronisation messages to the SS directly. Moreover, performing the ranging process and security association and connection needs to be performed between MR-BS and SS via a direct link, since RSs should not be aware of these processes and have no access to keys or connection identifier [20]. Although the SS is within communication range of the MR-BS, multihop relays allow more throughput and data rates per subscriber.

In transparent relaying networks, MR-BS only uses the centralised scheduling mode, which means the MR-BS is responsible for scheduling and management of resource usage and determination of direct or indirect communication with the SS as well as determination of the modulation and coding scheme [20]. However, indirect communication (i.e. communication through a RS), is restricted to only two hops between MR-BS and SS, which means only one RS is used to relay the transmitted data in each indirect communication.

Assuming two-hop communication between SS and MR-BS, the frame is bisected into downlink and uplink sub-frames, where each sub-frame is itself divided into two sections: the access zone and the relay zone [5, 20]. However a small portion of the frame is dedicated to separate the UL and DL sub-frames known as *transition time*. Transition time is needed to allow for UL and DL to switch. In the DL access zone, the MR-BS transmits data directly to an SS, or to a transparent RS to be relayed to the SS. In the DL relay zone, the RS transmits data received from MR-BS in the DL access zone to the SS. This sub-section of the frame is used only when the communication is required to be assisted by a transparent RS, and otherwise it will be unused. An SS transmits its data to the associated RS, or directly to MR-BS on the UL access zone, while if data is required to be relayed by a transparent RS, it transmits data from SS to MR-BS on UL relay zone. Figure 2.10 shows a transparent relay frame structure [5, 20].

2.5.1.4 Non-Transparent Relaying Mode

In transparent relaying mode, MR-BS and RS associated with it use the same carrier frequency, which is known as in-band data transmission [20]. A transparent RS, which is selected by the MR-BS, performs unicast data transmission to a specific SS and is mainly deployed to operate on decode and forward (DF) mode. RS requires decoding data because the MAC layer needs the header and sub-header information to be able to perform its tasks; however the physical layer is unable to distinguish the difference between header's data and payload. A transparent RS demodulates and deinterleaves received signal. After that, it remodulates and re-interleaves the signal

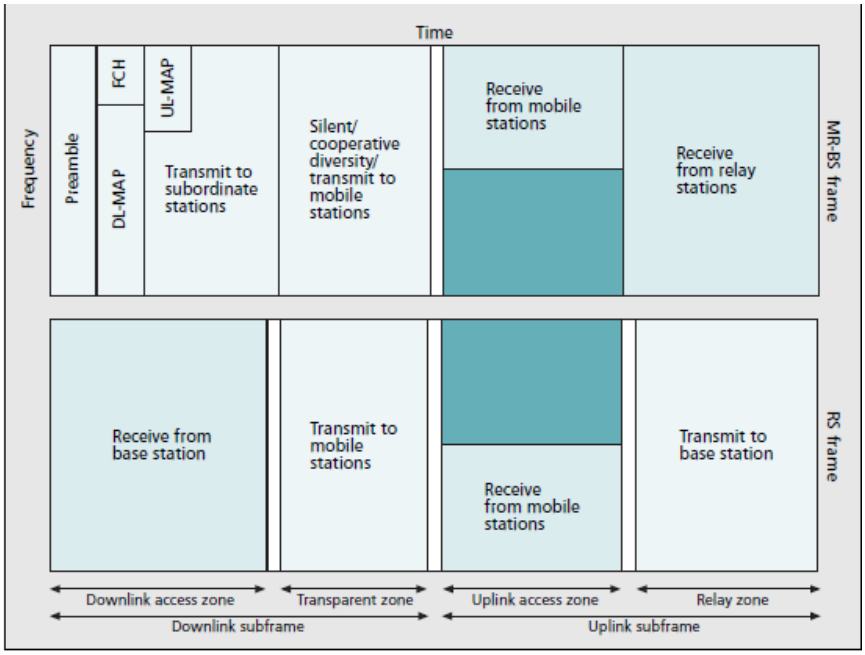

Figure 2.10 Transparent relay frame structure [5]

and transmits it to required station.

A mobile SS may change its location frequently, therefore, the channel conditions may change. Depending on the quality of the communication channel, a MR-BS may chose another RS to assist the communication; however if SS leaves MR cell for another cell, handover occurs between BSs, which is similar to traditional handover in cellular networks [5, 20].

Although transparent relaying may improve the capacity of a wireless network, it has some associated drawbacks. Preamble data is sent by MR-BS, which contains information about the channel to be used for the channel condition estimation. The problem is that SS may be expecting a communication link between BS and SS, but data transmission is in fact between RS and SS. Thanks to *orthogonal frequency division multiple access* (OFDMA) technology, this problem is somewhat relaxed by using the OFDMA sub-channel pilot symbols. However, this correction has an associated performance loss. Another problem is that SS expects to obtain a frequency offset from the BS, while communication is actually between RS and SS. To imitate

this offset, the RS needs to modify its signal before transmission to the SS.

Whereas for a transparent RS, the SS is aware of the existence of the RS, a non-transparent RS is perceived as a base station by the SS [5, 20]. This means that the existence of a non-transparent RS is unknown to a SS. In comparison with transparent mode, non-transparent mode is more complex and costly, because it needs to have more features of a BS compared to transparent mode. A non-transparent RS is incapable of decoding control information from MR-BS, hence, it needs to add its control information at the beginning of frame [5, 20]. This implies that the contents of frame control headers, DL and UL map are different for the RS and MR-BS. For communication to be achieved using an RS, the SS does not need to be within the range of MR-BS. Therefore, it may significantly improve the coverage range of a BS and expand the cell size. Since in non-transparent relaying mode, the RS is designed to transmit synchronisation and control information to the SS, the SS is not required to be in direct communication range of MR-BS.

Although transparent relaying is strictly for centralised scheduling modes, non-transparent relaying is capable of operating in both centralised and distributed modes. Distributed scheduling means that the MR-BS and non-transparent RS can both perform bandwidth allocation to the stations that they serve [5, 20]. However, in centralised scheduling, the MR-BS decides on bandwidth allocation and bandwidth management for all links throughout the network; in this case bandwidth requests from the SS must reach the MR-BS first. This implies that the SS needs to be in MR-BS range, and the RS is used for capacity enhancement by improving the received signal strength.

Another difference between these two relaying modes is that non-transparent RSs and MR-BSs may operate either on the same or different carrier frequencies (i.e. so-called in-band and out-of-band modes). Also, in networks with non-transparent RSs, multihop relaying is possible. This means that more than two hops between MR-BS and SS may exist. For simplicity, to explain the frame structure of a non-transparent relay, a two-hop relay frame is discussed here.

Similar to the transparent relaying frame structure, the non-transparent relaying frame is divided into two parts, UL and DL, and each sub-frame is divided into two parts of access zone and relay zone. The DL relay zone is associated with data transmission from the MR-BS to the RS, while the DL access zone is concerned with transmission of data from the MR-BS to SS or from the RS to SS. Data is transmitted from the SS to MR-BS or RS during the UL access zone sub-frame, while data is transmitted from a RS to the MR-BS using UL relay zone sub-frame [5]. Figure 2.11 shows the frame structure for MR-BS and non-transparent RS. As can be seen, the MR-BS and RS both transmit their own control information, UL and DL map and preamble followed by the payload [5]. In this scenario, a SS can be synchronised with RS, which is already synchronised with the MR-BS. Therefore, there is no need for the SS to synchronise directly with MR-BS.

As mentioned previously, non-transparent relaying mode is capable of multihop transmission, and data between a MR-BS and SS may be relayed by more than one RS. This results in greater robustness, reliability and network performance. To achieve

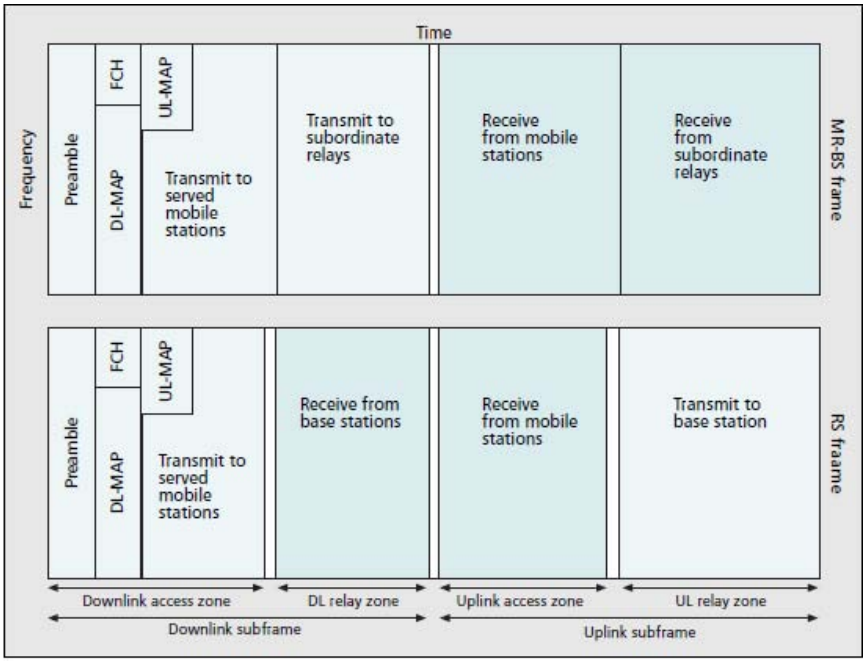

Figure 2.11 Non-Transparent Relay Frame Structure [5]

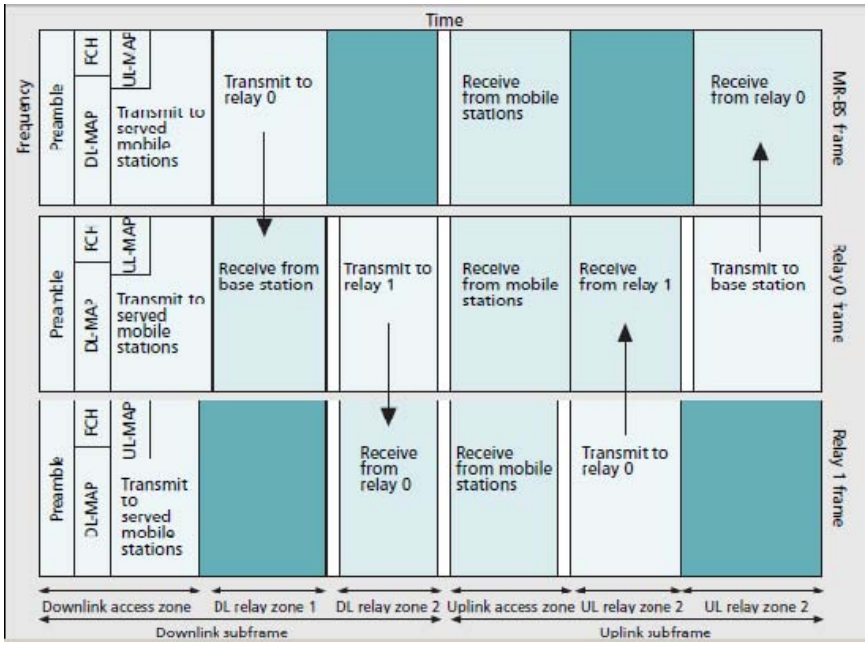

Figure 2.12 Multihop Relay- Non-Transparent Relay Frame Structure [5]

multihop relaying using non-transparent RSs, one approach is to extend the frame to include another zone, known as the multihop relaying zone. Figure 2.12 illustrates the frame structure of a simple three-hop non-transparent relaying mode for a MR-BS and two RSs [5]. In this scenario, the MR-BS transmits data to the first RS on the DL relay zone of the first RS (RS1). At this point, the DL relay zone corresponding to the second RS (RS2) is empty at the MR-BS frame. RS1 receives data on its DL relay zone1. After that it transmits the data to RS2 on its DL relay zone2 and RS2 receives data in DL relay zone2. Finally data is transmitted to the SS by RS2. On UL, RS2 receives data from SS through its UL access zone and transmission to RS1 occurs on the UL relay zone1. RS1 receives data from the RS2 and transmits it to MR-BS using its UL relay zone2. Finally, the MR-BS receives SS' data, relayed by RS1 and RS2, on the UL relay zone2 of its frame.

Although there are a number of advantages using non-transparent RSs within the network, there are some disadvantages associated with them as well. RS deployment is much more complex and expensive than transparent RSs. Moreover, power control

and frequency reuse is very critical. Also, interference may occur, particularly during the transmission of preamble and control information, since RS and MR-BS may transmit their data simultaneously on the same frequency channel [5].

2.5.2 Cooperative Communication Usage Scenarios and the Impact of Different Environments

Different environments as well as different usage scenarios have important impacts on the planning and design of wireless networks. Different environment in terms of outdoor and indoor, densely or sparsely populated areas, environments with dense or sparse vegetation, flat or hilly areas and users with different levels of mobility and data type should be taken into account when planning for cooperative communication networks. In this section, a brief overview of different scenarios in which the relaying concept may improve RF-based communication performance is discussed.

One of the scenarios in which RSs may be used to improve coverage area is in suburban areas, where population is low and clusters of users are scattered within environments such as schools, shopping areas and hospitals [5, 19]. In other words, groups of users are located far from each other. In this case, investment to deploy a network with adequate coverage, which requires dedicated bandwidth and a multitude of BSs, is unjustified because of the high cost of backhaul. Therefore, using RSs instead of expensive and complex BSs is a good solution for providing coverage enhancement in rural areas at low cost of deployment and maintenance. In such networks, one MR-BS is used alongside a number of fixed RSs to form a macro MR-cell.

There are often blind spots or so-called *coverage holes* within a building when doors, walls and furniture act as obstacles and prohibit the signal from traveling through the entire building [5,19]. To improve coverage within buildings, there is a need for more BSs, which leads to higher cost of deployment. To enhance in-door coverage while keeping costs low, fixed RS may be used to address the problem of coverage holes. Moreover, fixed RSs may be located outside buildings, for example on roof tops with a direct LoS with MR-BS to provide higher capacity and throughput inside the

building. RSs may also be deployed in tunnels to cover an underground environment. In this case, the RS is located outside the tunnel, where it is able to communicate with the MR-BS and finally provide coverage inside the tunnel where direct LoS between BS an SS does not exist [5, 19].

Cooperative communications may also be used in the case of an emergency or disaster, when infrastructure networks are damaged and there is a demand for communications to assist the disaster management and recovery process. In this situation, a fast, reliable and cost effective wireless network is required [5, 19, 20]. Using BSs is costly and complex, while using nomadic RSs instead is highly efficient in terms of cost, time, complexity, power consumption, reliability and feasibility. There is another scenario in which nomadic RSs are capable of offering efficient coverage and capacity. During event such as sport matches, fairs and festivals when high capacity is needed for a short period of time, nomadic RSs can be used within MR-cell to provide the required capacity. They also can be used for extra coverage where fixed and infrastructure networks are unable to address the need of coverage in areas such as the edge of cell.

The most complex form of a RS is a mobile RS, which are used mainly in vehicular networks to offer higher throughput and data rates for users inside a vehicle [5]. In this scenario there are a number of users using nomadic devices (such as a laptop computers) inside a high speed vehicle (such as a train), and these users require services such as Internet access. To improve the reliability of network and also to increase throughput and capacity, RSs are located outside the vehicle, particularly on roof tops to provide users with fixed access to backhaul. The mobile RS communicates with MR-BS and relays user data between the user devices and main base station. This results in a higher signal to noise ratio at the cell edge and consequently higher data rates and reliability may be achieved.

Another case where RSs are useful is in the initial deployment of a wireless network; when cost is much more important than capacity since the number of users is low [20]. Therefore, an MR-BS may be used in conjunction with a number of RSs to

deliver additional coverage. However, the RSs may be replaced by BSs when the number of subscribers is increased and more capacity is required.

2.5.3 Cooperative Communications in NFMIC

Although extensive studies have been conducted in cooperative RF communication systems, this concept has not been extensively investigated for NFMIC. As mentioned earlier, NFMIC is limited to very short communication distances. The main relaying method proposed for cooperative relaying in NFMIC has been the *magneto inductive waveguide* model. Different range extension techniques used in RF communications may be used in NFMIC to overcome the limited communication range. However, since the nature of the communication in NFMIC differs from RF communications, it is important to study the range extension methods which are most applicable to NFMIC. In this regard, this thesis studies multihop methods to be applied in a NFMIC system. This section provides an overview of NFMIC multihop relaying and related work.

The magneto-inductive waveguide method has been studied as a possible solution for multihop communications in NFMIC [6, 7, 44, 45, 59–66]. A magneto-inductive waveguide communication system consists of a number of NFMIC nodes. One or more nodes are located between the source and destination. A transmitter sends the data to a receiver through multihop relaying. Each node receives the data from its nearest neighbor on one side and transmits to the next neighbor on its other side via magnetic field coupling. Multihopping is performed until the data is delivered to its final destination. A typical waveguide system model can be seen in Figure 2.13. In this model, all cooperative nodes are passively powered and there is no need for an individual power source at each relaying node. When current in circuit n is induced due to mutual inductive coupling with the adjacent coils $n+1$ and $n-1$, the current-impedance relationship between them holds as [8]:

$$ZI_n + X\left(I_{n+1} + I_{n-1}\right) = 0 \tag{2.33}$$

In Equation 2.33, $Z = j(\omega L - 1/\omega c)$ is loop impedance, $X = j\omega M$ is the impedance

of coupling and $I_n = I.e^{-jkxn}$ is the current flowing in the nth circuit. x denotes the separation distance between adjacent coils.

Sun and Akyildiz in [6, 8] proposed a complex path loss model which relates the transmitted power and received power to system parameters such as permeability of medium, per unit resistance of wire used to create transmitting and receiving coils, number of turns of the coils, their radii, operating frequency and the communication range. Based on their model, for point-to-point communication, the power transfer function is as given by Equation 2.34.

$$\frac{P_R}{P_T} \approx \frac{\omega^2 \mu^2 N_T N_R r_T^3 r_R^3 \sin^2\alpha}{8d^6} . \frac{1}{4R_0\left(2R_0 + \frac{1}{2}j\omega\mu N_T\right)} \tag{2.34}$$

In this equation, R_0 is the per unit resistance of wire wound around the magnetic former, and d is distance between source and the final receiver. N_T, N_R, r_T and r_R are the number of turns of transmitting and receiving coils and the radius of transmitter and receiver coils respectively. α is axial misalignment angle between transmitter and receiver. ω is the angular frequency and μ is relative permeability of material used at core of the transmitting coils. By assuming a low resistance loop, and when high frequency and large number of turns are used $(R_0 << \omega\mu N_T)$, the power transfer function reduces to [6]:

$$\frac{P_R}{P_T} \approx \frac{\omega\mu N_R r_T^3 r_R^3 \sin^2\alpha}{16R_0 d^6} \tag{2.35}$$

Recently in [6, 44, 45], magneto-inductive waveguide communication has been studied for underground communications, where RF systems perform poorly due to the adverse channel conditions. In such an environment, the communication channel consists of rock and soil, possibly containing water and organic matter. Underground RF communications suffer from three major problems: high path loss, large antenna size and dynamic and unpredictable channel condition. The authors of [6, 44, 45] suggest that by using NFMIC, the problems of large antenna size and dynamic channel condition may be mitigated. MI waves are not affected by humidity, soil and rock since they all have nearly the same magnetic permeability as air [6,44,45]. However, the high path loss is still a problem and leads to limited coverage.

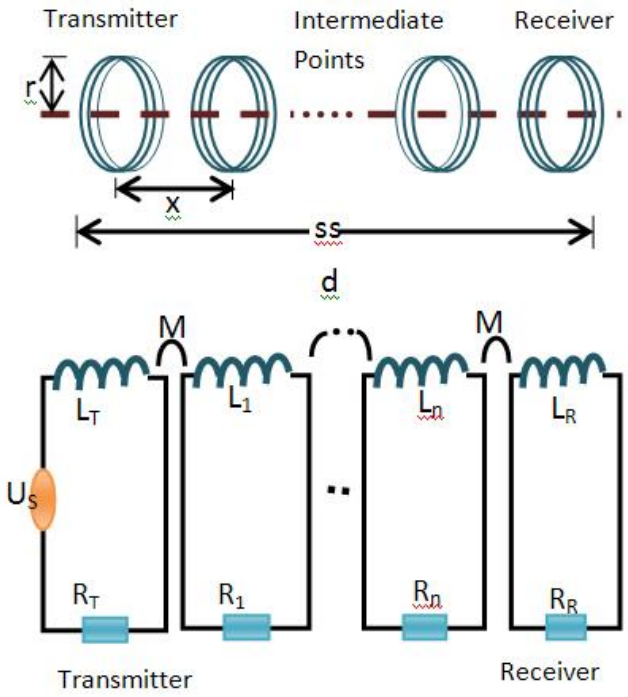

Figure 2.13 Magnetic waveguide and circuit model (adopted from [6])

To overcome the limited range, the authors in [6, 44] have investigated how a magneto inductive waveguide may be used to extend the communication distance. The performance of magneto-inductive model is compared with the conventional peer-to-peer MI and also EM communication techniques [6, 44]. The authors conclude that by implementing a waveguide system, lower path loss can be achieved regardless of the level of water content in the soil [6, 44].

In [45], Triangle Centroid (TC) deployment algorithms for underground MI sensor networks are proposed. In this algorithm, a Voronoi diagram is used to partition the network into non-overlapping triangular cells and a three pointed star topology in each triangular cell is used to obtain a *k-connected* network $(k > 3)$ [45]. The authors show that this algorithm is more robust to network failure than the Minimum Spanning Tree (MST) algorithm, which is only *1-connected*. However, The MST algorithm connects the entire network together with the optimum number of relaying nodes. In the MST algorithm, a node has only a single connection, therefore the

network is not robust to a node failure [45]. Although this work is well suited for underground communications, it is not realistic for a body area network. In a body area network, nodes may be randomly located and might frequently change their location. Therefore, in this thesis different multihop methods in a three dimensional environment are proposed which are more applicable to a body area network (this concept is studied extensively in Chapter 5).

2.5.4 Magneto Inductive Waveguide devices

In the previous section, the basic concepts of a magneto inductive waveguide system has been introduced. However, unlike Sun and Akyildiz [6, 8, 44, 45], Syms and Shamonina [7] have studied magneto inductive waveguide systems to exploit the effect of power reflection in the transmission line to create different magneto-inductive devices. If the waveguide transmission line is not terminated properly, there exists a power reflection from each receiver back to the transmitting nodes. From a telecommunication perspective, inappropriate termination of the communication link results in undesirable effects which may degrade the total performance of the network. More detail is provided in Chapter 4. Several magneto-inductive devices are discussed by Syms et al in [7] including two-port and three port devices. In the following section a magneto-inductive mirror and three-port splitters are discussed.

2.5.4.1 Two-Port Devices

Two-port devices include MI mirrors and their extension, Fabry-Perot, Bragg grating, tapers and couplers [7]. This section describes MI mirror as an example of a two-port MI device.

Magneto-Inductive Mirror

One of the most important applications of optics is the creation of mirrors. In optics, a mirror results in an image of an object due to reflection. A mirror effect is caused by a discontinuity in the medium through which light propagates causing the light to bend backwards and be received at a source. This creates an illusion of seeing the

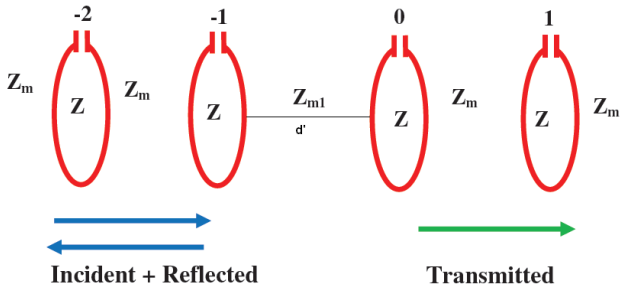

Figure 2.14 Two-Port Devices with Simple Mirror (adopted from [7])

object in a mirror at a distance. A similar effect exists in magnetic communications. A magneto-inductive mirror is caused by an electrical discontinuity or abrupt change in impedance. This causes currents to be reflected back from the discontinuity into the circuit.

A MI mirror is formed by connecting two sections of an MI waveguide. Each section supports a forward wave. The loop impedance and coupling are as in the traditional waveguide. However a section of the waveguide is coupled by $Z_{m1} = j\omega M_1$, where M_1 is the modified mutual inductance. The modified mutual inductance is achieved by varying the loop separation, locating the first coil from the source at a distance $\acute{d}$ different to the d used for the second section (Figure 2.14). The currents in the coils are taken as I_n, where n is the loop number. Due to the modified coupling, reflected waves are induced in the section with the modification.

This analysis focuses on nearest neighbor coupling and recursively extends the concept to the overall structure. The nearest neighbor I/Z relationship at loop n is [7]:

$$ZI_n + Z_m \left(I_{n-1} + I_{n+1}\right) = 0 \tag{2.36}$$

where $Z = R + j\omega L + 1/j\omega C$. An abruptly terminated MI waveguide would have zero reflection if the last element is terminated with a characteristic impedance [67] such that,

$$\left(R + j\omega L + 1/j\omega C + Z_0\right) I_n + Z_m I_{n-1} = 0 \tag{2.37}$$

Combining Equations 2.36 and 2.37:

$$Z_0 I_n = Z_m I_{n-1} = j\omega M I_{n-1} \tag{2.38}$$

Assuming a current wave $I_n = I_0 . \exp(-jkna)$ [7], then

$$Z_0 = j\omega M . \exp(-jka) \tag{2.39}$$

where, $r_T = r_R = a$.At the junction the following equations hold and need to be solved [7].

$$\begin{aligned} ZI_{-1} + Z_{m1} I_0 + Z_m I_{-2} = 0 \\ ZI_0 + Z_m I_1 + Z_{m1} I_{-1} = 0 \end{aligned} \tag{2.40}$$

Due to the discontinuity in the input line (a change in the mutual inductance impedance from Z_m to Z_{m1}), a reflected wave is created. The section of the waveguide with incident (I) and reflected waves (R) is referred to as the input line, and the one with only the transmitted wave (T) as the output. The MI model should naturally account for conservation of energy. The input energy is distributed into different components including the radiated power. In a high loss model it is critical to minimise the radiated power in order to contain and conserve the required communication power within a defined 'bubble' of interest. From a theoretical point of view, since the characteristic impedance of an MI wave is $Z_0 = j\omega M . \exp(-jka)$ [59], the power in the wave can be computed. The voltage across the characteristic impedance is $V_0 = I . Z_0$. The power carried by the wave is then given by the expression:

$$P = \tfrac{1}{2}\mathrm{Re}al\left[V_0 I^*\right] = \tfrac{1}{2}\mathrm{Re}\left[Z_0 I \times I^*\right]$$

$$= \frac{\mathrm{Re}al\left[j\omega M.I^2 \exp(-jka)\right]}{2} = \frac{\mathrm{Re}al\left[\omega M.I^2 \exp\left(-j\left(ka-\frac{\pi}{2}\right)\right)\right]}{2}$$

$$= \frac{\mathrm{Re}al\left[\omega M.I^2\left(\cos\left(ka-\frac{\pi}{2}\right)-j\sin\left(ka-\frac{\pi}{2}\right)\right)\right]}{2} \tag{2.41}$$

$$= \frac{\omega M.I^2 \cos\left(ka-\frac{\pi}{2}\right)}{2}$$

$$= \frac{\omega M.I^2 \sin(ka)}{2}$$

This power is proportional to the mutual inductance between two coils, the current carried by the transmitting coil and the phase shift per section (ka); where a is the radius of the coils. The value of k is traditionally complex to account for ohmic losses and as such this power is also a function of the ohmic losses.

2.5.4.2 Three-Port Devices

MI can also be used to create three-port devices. The theoretical discussion in [7] relates to the theory of similar optical devices. The three-port device discussed in this section is a general three-port splitter.

General Three-Port Splitters

An MI splitter is used to split an input power and transmit it through multiple channels towards different receivers. In the example given here, the three ports are oriented at 120° apart (Figure 2.15). Four equations are needed for the three waveguides with indexes i =1, 2 and 3 and one extra equation for the voltages in the loop identified with the index 0. The mutual inductances and currents in the three waveguides are given by the relations $Z_{mi} = j\omega M_i I_{i,n}; \quad i = 1,\ \ 2,\ \ 3$ [7]. Kirchoff's voltage equations for the 3-port splitter are [7]:

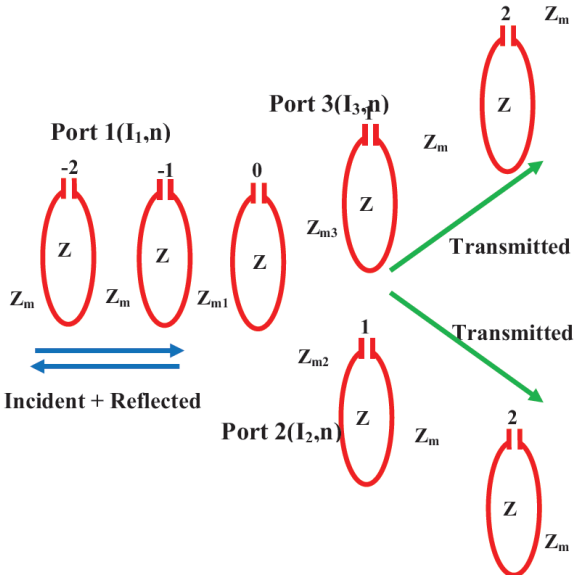

Figure 2.15 Three-Port Splitters (adopted from [7])

$$
\begin{aligned}
Z_{m1}I_0 + ZI_{1,-1} + Z_mI_{1,-2} &= 0 \\
ZI_0 + Z_{m1}I_{1-1} + Z_{m2}I_{2,1} + Z_{m2}I_{3,1} &= 0 \\
Z_{m2}I_0 + ZI_{2,1} + Z_mI_{2,2} &= 0 \\
Z_{m3}I_0 + ZI_{3,1} + Z_mI_{3,2} &= 0
\end{aligned}
\tag{2.42}
$$

The current I_0 is unknown. The current in the input waveguide is assumed to consist of both an incident and reflected wave and the currents in the output waveguide are the transmitted currents [7]. Therefore,

$$
\begin{aligned}
I_{1,n} &= I\exp\left(-jkna\right) + \mathrm{Re}exp\left(+jkna\right); \quad && n \leq -1 \\
I_{2,n} &= T_2\exp\left(-jkna\right); && n \geq 1 \\
I_{3,n} &= T_3\exp\left(-jkna\right); && n \geq 1
\end{aligned}
\tag{2.43}
$$

To derive the expressions for the transmission and reflection coefficients and also the reflected power and transmitted power coefficients, the methods used in the previous sections are adopted with the definition that $\mu_i = Z_{mi}/Z_m$; where i=1, 2, 3. This leads to the following relationships [7]:

$$\Re = \frac{R_{FP}}{I} = \frac{(1-\mu_1^2)\exp(jka) + (1-\mu_2^2-\mu_3^2)\exp(-jka)}{(\mu_1^2+\mu_2^2+\mu_3^2-1)\exp(-jka) - \exp(jka)} \tag{2.44}$$

$$\mathrm{I}_0 = \frac{I_0}{I} = \frac{\mu_1(\exp(-jka) - \exp(jka))}{(\mu_1^2+\mu_2^2+\mu_3^2-1)\exp(-jka) - \exp(jka)} \tag{2.45}$$

$$\Im_2 = \frac{T_2}{I} = \frac{\mu_1\mu_2(\exp(-jka) - \exp(jka))}{(\mu_1^2+\mu_2^2+\mu_3^2-1)\exp(-jka) - \exp(jka)} \tag{2.46}$$

$$\Im_3 = \frac{T_3}{I} = \frac{\mu_1\mu_3(\exp(-jka) - \exp(jka))}{(\mu_1^2+\mu_2^2+\mu_3^2-1)\exp(-jka) - \exp(jka)} \tag{2.47}$$

The power reflection and transmission coefficients for the splitter are [7]:

$$|\Re|^2 = \frac{\left[(\mu_1^2-1)^2 + (\mu_2^2+\mu_3^2-1)^2\right] - 2(1-\mu_1^2)(\mu_2^2+\mu_3^2-1)\cos(2ka)}{\left[1+(\mu_1^2+\mu_2^2+\mu_3^2-1)^2\right] - 2(\mu_1^2+\mu_2^2+\mu_3^2-1)\cos(2ka)} \tag{2.48}$$

$$|\Im_2|^2 = \frac{2\mu_1^2\mu_2^2\{1-\cos(2ka)\}}{\left[1+(\mu_1^2+\mu_2^2+\mu_3^2-1)^2\right] - 2(\mu_1^2+\mu_2^2+\mu_3^2-1)\cos(2ka)} \tag{2.49}$$

$$|\Im_3|^2 = \frac{2\mu_1^2\mu_3^2\{1-\cos(2ka)\}}{\left[1+(\mu_1^2+\mu_2^2+\mu_3^2-1)^2\right] - 2(\mu_1^2+\mu_2^2+\mu_3^2-1)\cos(2ka)} \tag{2.50}$$

It can be shown by adding these equations together that [7]:

$$|\Re|^2 + |\Im_2|^2 + |\Im_3|^2 = 1 \tag{2.51}$$

In other words, the input power is distributed into the three components consisting of a reflected power and two transmitted power components.

2.6 Summary

In this chapter an extensive literature review has been done to provide an insight into the characteristics of both the far field and near field communication regions mainly in terms of path loss. Then, an overview of BANs is provides to study the requirements of BANs, as a potential application of NFMIC. It is discussed that NFMIC may be beneficial for BAN over other communication techniques. This is done through a comparison between different short range communications with NFMIC. The fundamental theory of NFMIC is discussed and it is concluded that the effect of path loss is very critical in NFMIC, and there is a need for techniques to extend the communication range of NFMIC, in order to be used in applications where longer range is required. In this context, it is discussed that cooperative relaying may be a possible solution. Then, an overview of cooperative communication for both RF and NFMI communications is given. Magneto inductive waveguide method is discussed as a conventional and basic cooperative communication method in NFMIC. It is concluded that the conventional waveguide method may not be directly applicable to BANs, and proper NFMIC cooperative relaying techniques are required to extend the communication range and improve the data rates in NFMIC systems. It is also discussed that the first step to achieve a proper NFMIC cooperative relaying method is to determine the link budget in a NFMIC system.

Chapter 3

NFMIC Link Budget

3.1 Chapter Overview

This chapter proposes a link budget model for a peer to peer NFMIC system. In this context, first a brief overview is given on the concept of link budget. However, since to the best of our knowledge, there have not been a link budget model applicable to NFMIC, this concept is firstly discussed for RF communications to provide an insight into the topic.

In this chapter, *Agbinya-Masihpour*(AM) link budget model is proposed and studied through the theoretical analysis and Matlab simulations. AM link budget model is studied for two approaches: when the antenna coil wound around a ferrite core and also when they are air-cored. It is shown that using highly permeable material at the core of transmitting coils can highly improve the achieved communication rage. Then, based on the work done by [6, 8], another link budget model is developed and is compared with AM model both theoretically and by simulations.

3.2 Link budget in electromagnetic RF-based communication systems

In any communication systems, one of the fundamental concepts is to determine the link budget. Link budget refers to the difference between transmitted and received signal power [68, 69]. It specifies how power at transmitter is allocated along the communication chain to receiver. The reason for having a link budget is that signal loses some of its power as it travels through a wireless channel (i.e. path Loss) due to undesirable environmental and signal propagation effects such as fading, diffraction, reflection and scattering [68, 70, 71]. Therefore it is critical to determine the signal strength at receiver to be able to estimate other factors effecting network design and planning. Link budget has been explored extensively for traditional terrestrial RF-based electromagnetic wave communications. There are a number of channel models available for planning the wireless network in different environmental types; such as urban, suburban and rural areas, flat or hilly terrains and dense or scattered vegetation areas; because transmitted signal experiences different path losses in different environments.

RF-based EM communication channel models have taken into account different environmental characteristics and basically are the function of transmitter and receiver antenna gains, transmission power and all the possible losses. RF-based communication channel models have been studied from different perspectives, for example when direct LoS exists or not, or if detailed and precisely gathered data is needed (deterministic models), or modeling may rely on measured mean path losses for different environmental types (empirical models) [68–70].

Some of the channel models concerning RF-communication link budget are firstly the *Free Space* model, suitable when direct LoS exists between transmitter and receiver and uses *Friis* equation [69]. Secondly *two-ray* model, which concerns with communications where there are a direct LoS and a reflected path between transmitter and receiver [68]. *Hata-Okamura* model is valid in 150 MHz to 1500 MHz frequency

range and is suitable for distances more than 1 Km; however, modified form of this model known as *COST 231* has extended the frequency range to 2 GHz [68, 71]. In COST 231 model, similar to *Stanford University Interim (SUI)* and *Erceg* model, environment is categorized into three types with specific characteristics [70]. SUI and Erceg Model, which are particularly suitable for WiMAX, are available at frequency band of 3.5 GHz and 1.9 GHz respectively [68–70]. *Walficsh-Ikegami* is another model, recommended by WiMAX forum and proper for channel modeling at 800 MHz to 2000 MHz frequency range. This model can distinguish between the LoS and NLoS for WiMAX communications [68]. In this section, Free Space and SUI models will be briefly discussed to provide an insight into the link budget concept in RF-based systems.

3.2.1 Free Space Propagation

The medium separating receiver from transmitter plays an important role in the propagation of transmitted signal. Free space propagation is usually modeled with the Friis formula [69]:

$$P_r = P_t \frac{G_t G_r \lambda^2}{(4\pi d)^2} \tag{3.1}$$

Where P_r, P_t, G_r and G_t are received signal power, transmission power, receiver and transmitter antenna gains respectively. λ is the frequency wavelength. It is assumed in this expression that radiation is into a spherical space of radius d surrounding the antenna. The medium between transmitter and receiver is often a dielectric, air, a piece of wire, fiber or some liquid including water. Medium varies from application to application and from terrain to terrain. Medium between transmitter and receiver introduces a propagation loss as shown in Figure 3.1. Propagation loss is modeled using expression [69]:

$$L_p = 10xLog\left(\frac{4\pi d}{\lambda}\right)^2 \tag{3.2}$$

Propagation-exponent (x) is a function of terrain characteristics between transmitter and receiver and has values in the range 2 to 5 in urban areas (in free space $x = 2$).

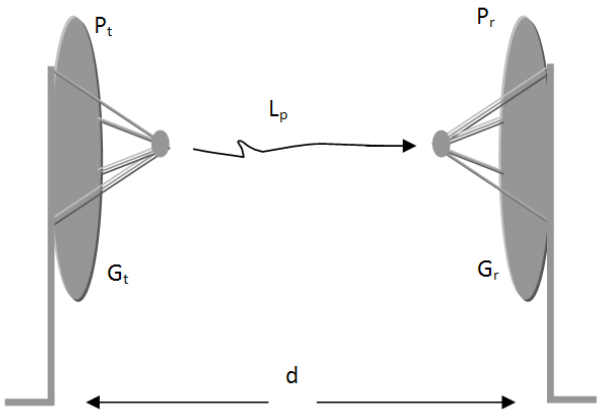

Figure 3.1 Free Space Propagation

The propagation loss is often expressed in decibels and is [69]:

$$L_p = 32.44 + 20Log\,(f) + 20Log\ (d) \tag{3.3}$$

Frequency (f) is measured in MHz and distance (d) in kilometres. Equation 3.3 implies that by using higher carrier frequencies, the free space loss will be higher. For instance, if two receivers have the same sensitivity, using carrier frequency 450 MHz, cell radius will be 7.78 times longer than when 3.5 GHz carrier frequency is used [72].

3.2.1.1 Free Space Link Budget

Determination of propagation losses is useful for the estimation of link budget. Link budget indicates the maximum allowable path loss per link. The maximum allowable path loss sets a limit on maximum cell size.

The plane earth model is more appropriate for cellular communications. The model ignores the curvature of the earth's surface and considers a two-path model of direct LoS and a ground reflected paths. In this model the heights of the transmitting and receiving antenna feature prominently in the propagation loss expression. Provided the heights of the antennas are less than the separation between the transmitter and

receiver (h_b and h_r), the propagation loss expression may be shown as [68]:

$$L_p = -10\log_{10}G_t - 10\log_{10}G_r - 20Log\,h_b - 20Log\,h_r + 40Log\,d \quad ;(dB) \quad (3.4)$$

3.2.2 Stanford University Interim Model

To estimate path loss using SUI model, environment is categorized in three different groups with different characteristics, known as A, B, and C [70]. A shows the hilly environment and moderate to very dense vegetation, which results in highest path loss. B refers to a hilly environment but rare vegetation or high vegetation but flat terrain. Finally C is referred to a flat area with rare vegetation, which leads to the lowest path loss.

SUI model is a suitable channel model for WiMAX implementation at 3.5 GHz, which can support for cell radius in range of 0.1 km and 8 km, and also base station antenna height between 10 m and 80 m and receiver antenna height in range of 2 m and 10 m [70]. In SUI model, path loss is calculated using equation:

$$L_p = A + 10\gamma\log_{10}\left({}^{d}/_{d_0}\right) + X_f + X_h + s\,;\ \text{for}\, d > d_0 \quad (3.5)$$

In this expression, d_0 =100 m is the reference distance and d is the distance between transmitter and receiver. s is a standard deviation which is a random variable. X_f is a correction term for frequency above 2 GHz and X_h is a correction term for transmitter antenna height [70].

$$X_f = 6.0\log_{10}\left({}^{f}/_{2000}\right) \quad (3.6)$$

$$X_h = -10.8\log_{10}\left({}^{h_r}/_{2000}\right)\,;\ \text{for A and B environment} \quad (3.7)$$

$$X_h = -20.0\log_{10}\left({}^{h_r}/_{2000}\right)\,;\ \text{for C environment} \quad (3.8)$$

f is the operating frequency and h_r is height of receiving antenna. However, in Equation 3.5, A is estimated using [70]:

$$A = 20\log_{10}\left(\frac{4\pi d_0}{\lambda}\right) \tag{3.9}$$

where λ is wavelength in meters. In Equation 3.5, γ is the path loss exponent, which may have different values between 2 and 5 for different environment types. It also depends on the height of base station antenna (h_b) and three constants parameters of a, b and c which vary with different type of environment categorized as A, B and C [70].

$$\gamma = a - bh_b + \frac{c}{h_b} \tag{3.10}$$

The path loss exponent in urban area where LoS exists is 2, while it is between 3 and 5 in urban area and NLoS. Finally the path loss exponent is more than 5 if signal propagation occurs in an indoor environment [68,70]. SUI model is used for WiMAX network planning in rural, urban and suburban areas.

3.3 NFMIC Link Budget

Although there are a number of studies on the concept of link budget for EM-based communication systems, there is no model directly applicable to the magnetic induction communications, because the impact of environment on magnetic waves is not identical to that of electromagnetic waves. Therefore, this study proposes a channel model for a point-to-point NFMIC link. The model is termed as *Agbinya-Masihpour* (AM) NFMIC channel model [73]. In this model, the link budget for an MI communication system is approached from two perspectives. Firstly when transmitting and receiving antennas are air-cored and secondly when they have ferrite cores to enhance magnetic fluxes. This section discusses the situation where direct LoS exists and antenna coils are cored with air or ferrite. It is further shown how ferrite core improves the link quality as well as achieved communication distance. Given a magnetic transmitter (T) and receiver (R) separated by distance d (Figure 2.5), the

power equation is [15] (see Chapter 2 for detail):

$$P_R = P_T \eta_T \eta_R Q_T Q_R k^2 (d) \tag{3.11}$$

$$P_R = P_T Q_T Q_R \eta_T \eta_R \frac{r_T^3 r_R^3}{\left(r_T^2 + d^2\right)^3} \tag{3.12}$$

where Q_T and Q_R are the quality factors of transmitter and receiver respectively, and η_T and η_R are the efficiencies of transmitting and receiving antennas, P_T denotes the transmission power and P_R is the received signal power; r_T (cm) and r_R (cm) denote transmitter and receiver coil radii respectively. Equation 3.12 may be expressed as:

$$(d^2 + r_T^2)^3 = \frac{P_T Q_T Q_R \eta_T \eta_R r_T^3 r_R^3}{P_R} \tag{3.13}$$

Furthermore let,

$$Q = 10 \cdot \log (Q_T Q_R) \tag{3.14}$$

$$\eta = 10 \cdot \log (\eta_T \cdot \eta_R) \tag{3.15}$$

$$P = (P_T - P_R;) \, (\mathrm{dBm}) \tag{3.16}$$

By substituting the above expressions in Equation 3.13, it may be shown as,

$$10. \log \left(d^6 \left(1 + \frac{r_T^2}{d^2} \right)^3 \right) = P + Q + \eta + 30. \log(r_T r_R) \tag{3.17}$$

Further it may be simplified as,

$$\log d = \frac{P + Q + \eta + 30. \log (r_T r_R) - 30. \log \left(1 + \frac{r_T^2}{d^2} \right)}{60} \tag{3.18}$$

The factor of 60 in Equation 3.18 indicates that in MI communications, inductive power decays to the sixth power of distance. Therefore the link budget equation becomes:

$$d = 10^{\frac{P+Q+\eta+30. \log\left(r_T r_R\right) - 30 \log\left(1+\frac{r_T^2}{d^2}\right)}{60}} \tag{3.19}$$

There are terms in Equation 3.19 which contribute significantly to the determination of communication distance and those that have insignificant effect on d. In the next

equation, those factors are separated. Therefore, let

$$d = 10^{\frac{P+Q+\eta}{60}}.10^{-\frac{1}{2}\left[\log(r_T r_R)-\log\left(1+\frac{r_T^2}{d^2}\right)\right]} \tag{3.20}$$

Alternatively this expression can be written as:

$$d = d'.\Delta d \tag{3.21}$$

Where:

$$d' = 10^{\frac{P+Q+\eta+30\log(r_T r_R))}{60}} \tag{3.22}$$

and the correction term is:

$$\Delta d = 10^{-\frac{1}{2}\left[\log\left(1+\frac{r_T^2}{d'^2}\right)\right]} \tag{3.23}$$

Since in reality the separation distance is far larger than the radius of transmitting antenna coil, hence the numerical value of Δd approaches unity. Therefore it can be neglected to simplify further analysis. Thus, the link budget equation may be expressed as:

$$d \approx d' = 10^{\frac{P+Q+\eta+30\log(r_T r_R)}{60}} \tag{3.24}$$

It is shown also using Matlab simulations that Δd has insignificant impact on achievable communication range (the results are shown in Section 3.3.2). However, this equation has not yet taken into account the relative magnetic permeability of the core material that is used to enhance magnetic field.

3.3.1 Ferrite Cored (Enhanced Magnetic Flux) - Line of Sight

Magnetic flux density (B) at the point d in a near field region is enhanced by the relative permeability of core material on which antenna coil is wound. The magnetic flux density is estimated using the following expression [13].

$$B = \frac{\mu_r\,\mu_0\,I.N.r_T^2}{2d^3} \tag{3.25}$$

Where μ_r is the relative permeability of ferrite core ($\mu_r = {\mu_{material}}/{\mu_0}$), I is loop current, N is the number of turns of coil and r_T is the radius of transmitting coil.

Assuming that receiver also uses a ferrite core former of relative permeability μ_R. Hence both transmitted and received fluxes are amplified by a factor equal to the relative permeability of each core. Thus inductive antennas have gains equal to their relative permeability of ferrite cores. Using ferrite core ensures that the coil of smaller radii can be used to form the NFMIC antennas. Following the same formulation previously discussed, the link budget equation for ferrite-cored antennas becomes:

$$d = 10^{\frac{P+Q+\eta+\mu+30.\log(r_T r_R)-30\log\left(1+\frac{r_T^2}{d^2}\right)}{60}} \tag{3.26}$$

Where:

$$\mu = 10 \cdot \log\left(\mu_T \cdot \mu_R\right) \tag{3.27}$$

This equation includes two new factors for the gains of antennas. Therefore, the transmission range will be enhanced by $10^{\frac{\log(\mu_T \cdot \mu_R)-\log\left(\mu_0^2\right)}{6}}$ times, where magnetic permeability of core of transmitter and receiver are μ_T and μ_R respectively. Simulation result also has shown the impact of ferrite core on achieved communication range and it is shown ferrite with different magnetic permeability can improve the communication range.

3.3.2 Simulation Results

The link budget model is simulated, using Matlab, where it is shown the relationship between the achieved communication range and different design parameters. The two discussed approaches (i.e. air-cored and ferrite-cored transceivers) are also shown and compared. The difference between these two cases is that the core material of coils has different magnetic permeabilities. The relative permeability of air is $4\pi \times 10^{-7}$H.m^{-1}, while the relative permeability of ferrite is greater than unity. For example high magnetic permeable material such as ferrite or manganese zinc has relative permeability of 640. This implies that by using ferrite with higher magnetic permeability longer transmission range can be achieved.

In the simulation, the transmission power is set to 200 μW (-7 dBm), which is sufficient power for short range communications such as in a sensor network. The re-

Table 3.1 Simulation Design Parameters

Parameter	**value**	**unit**
coil radius	0.5	cm
the length of coil	0.8	cm
number of turns	10	cm
load and source resistance	50	Ω
per unit resistance of copper wire	2.16	Ω
operating frequency	13.56	MHz
transmission power	-7	dBm
receiver sensitivity	-50	dBm
efficiency	98	%
magnetic permeability (ferrite or mangenese zinc)	0.0008	H.m^{-1}
magnetic permeability of air	$4\pi \times 10^{-7}$	H.m^{-1}

ceiver sensitivity is 10 nW (-50 dBm). The transmitting and receiving antennas are small coils with radius 5 mm and length 8 mm and the number of turns is 10. Since it is common to form magnetic coils with copper wire, it is also assumed in this study that copper wire are used in the antenna coils. The resistance of copper wire per unit of length is $R_0 = 2.16\ (\Omega)$ [6]. According to [6], this results in the self resistance of inductors to be $2\pi N r R_0\ (\Omega)$, where r is the coil radius and N is the number of turns. However the load and source resistance values are set to 50 Ω since it is a practical value for voice and data communications over short distances. This leads to the total efficiency of 98% (see Equation 2.26). The operating frequency is set to 13.56 MHz, since this frequency is designated ISM frequencies and also it ensures that the communication is well within the near field region. The wavelength of 13.56 MHz is 22 m, which implies that the near field and farfield boundary is approximately 3.5 m. For a BAN, the required communication range is often less than this amount, hence 13.56 MHz meets the criterion. Considering ferrite or mangenese zinc, the magnetic permeability is 0.0008 H.m^{-1} (relative permeability is 640). The design parameters are summerized in Table 3.1.

3.3.2.1 Distance versus transmitting and receiving coil radius

Equation 3.26 implies that achievable communication range increases as transmitter or receiver coil radius increases. This tendency can also be seen from Figure 3.2 and 3.3, which show the distance as a function of the transmitter (Figure 3.3) and receiver (Figure 3.2) coil radius. It is shown here that by using larger coils communication range can be extended. As mentioned earlier, transmission range easily can be enhanced by using ferrite material at the core of coils. Comparing dashed line (ferrite-cored) and the blue line (air-cored) in Figures 3.2 and 3.3 shows that transmission range is increased dramatically by using the ferrite with permeability of 0.0008H.m^{-1} at the core of both receiver and transmitter coils. Figures 3.4 and 3.5 show achieved communication range against receiver and transmitter coil radii respectively for different magnetic permeabilities. Table 3.2 shows corresponding material with the chosen values for simulations here.

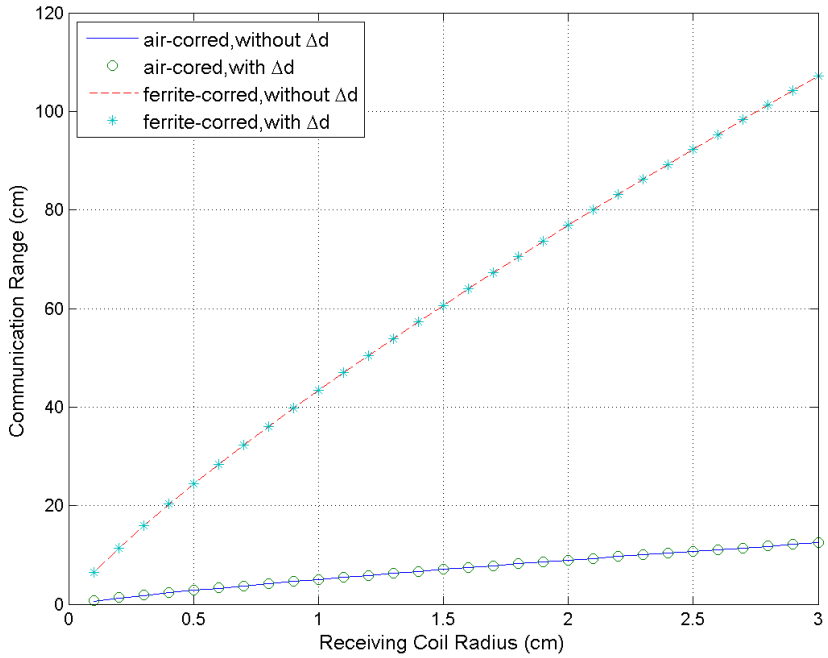

Figure 3.2 Distance versus receiving coil radius

Table 3.2 Magnetic Permeability of different Materials

Material	**magnetic permeability**
Aluminum	1.25×10^{-6} H.m^{-1}
Nickel	1.25×10^{-4} H.m^{-1}
Ferrite (manganese zinc)	$> 8 \times 10^{-4}$ H.m^{-1}
Electrical steel	5×10^{-3} H.m^{-1}
Permalloy	10^{-2}H.m^{-1}
Mu-metal	2.5×10^{-2}H.m^{-1}

Figures 3.4 and 3.5 show how to achieve a desired communication distance for the given coils with radius r range from 1 mm to 3 cm and based on the value of magnetic permeability. It can be seen here that the communication distance increases without the need for larger coils if high magnetic permeability material is used at the core. For example 50 cm communication distance is achieved by using a receiving coil of radius 1 cm if the magnetic permeability is 0.0008 H.m^{-1}. However, by using air-

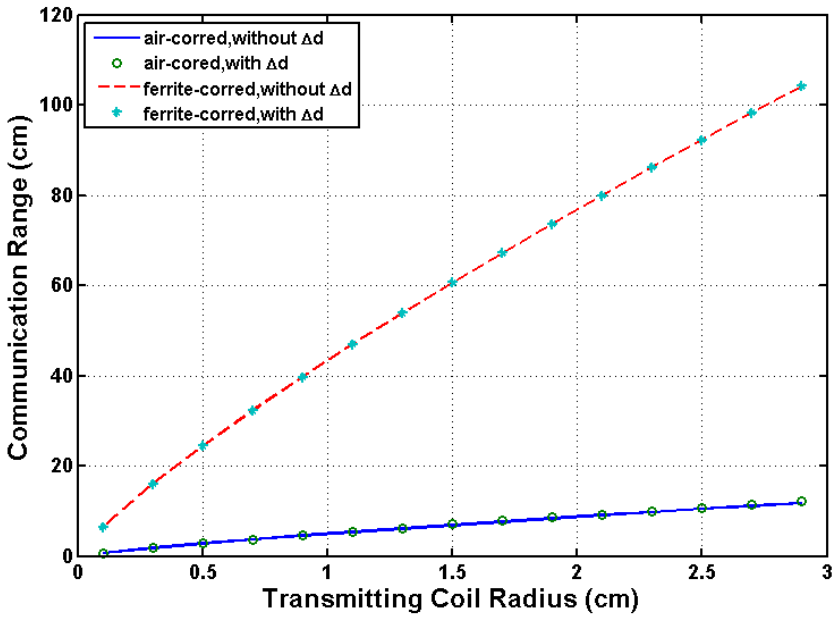

Figure 3.3 Distance versus transmitting coil radius

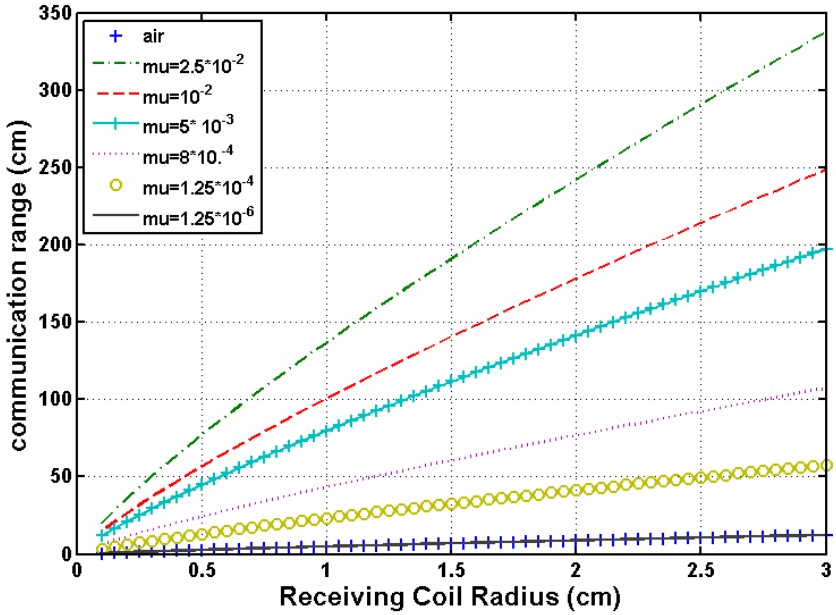

Figure 3.4 Distance versus receiving coil radius for different magnetic permeabilities

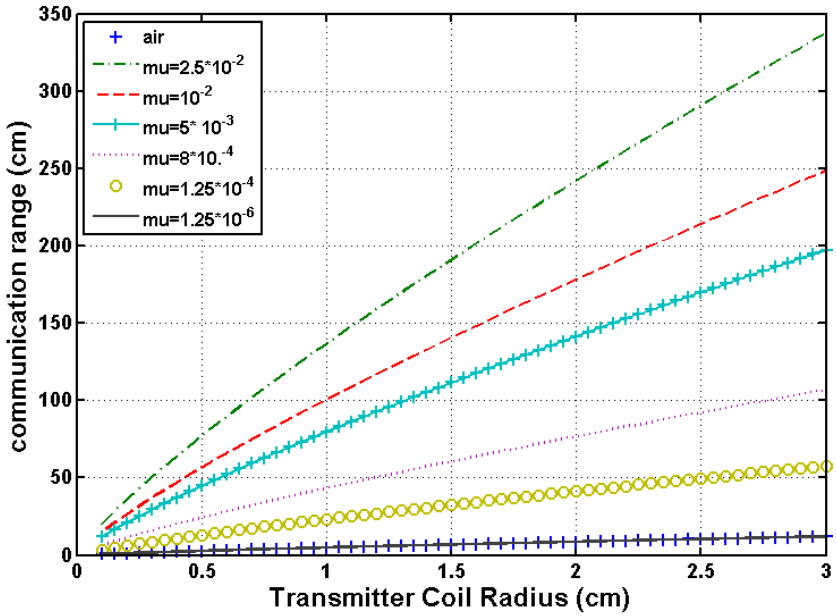

Figure 3.5 Distance versus transmitting coil radius for different magnetic permeabilities

cored coils (radius=1 cm) the achieved communication range reduces to only 6 cm (Figure 3.4). Similarly, Figure 3.5 advises the transmitting coil size for a required communication range at receiver.

For example in short range communications such as deployment of a personal area networks, if communication range of about 30 cm is required, to obtain desired coverage range using a transmitter with radius of 0.5 cm, ferrite at the core of both transmitter and receiver coil should have permeability of 0.0008 H.m^{-1}. However, only half this range is achieved through using large transmitting coil of radius 3 cm if the coils are air-cored (Figure 3.5). This means smaller antennas may be used to facilitate the same transmission range by employing ferrite materials with higher permeability. In other words, longer distances can be achieved with the same antenna size but higher permeability at the core of coil. This well facilitates the important requirement of BAN devices in which the smaller antennas need to be implemented.

As mentioned in Section 3.3, Equation 3.20 can be written as Equation 3.24, which means Δd has been eliminated from Equation 3.20. It was discussed that since Δd is far smaller than the value of d', therefore, it can be neglected for the simplicity of calculations. The simulation results also indicates that distance difference between the two cases of considering or neglecting Δd, is a very small value and neglecting of Δd has little effect on transmission range. As can be seen from Figure 3.2 and 3.3, the two graphs showing the two cases of including and neglecting Δd in the Equation 3.20 tend to overlap, which means the difference is close to zero and hence negligible. As distance increases (for example using ferrite-cored coils), the impact of Δd becomes smaller.

3.3.2.2 Distance versus transmitting and receiving antenna coils permeability

The magnetic permeability of material used at the core of a coil strengthens magnetic flux density. Consequently it can enhance the communication range by approximately $10^{\frac{\log(\mu_T \cdot \mu_R) - \log\left(\mu_0^2\right)}{6}}$ times. According to Figure 3.2, achieved range is 2.8 cm using air-cored coils with radius 5 mm, while this value is 24 cm using ferrite-cored

coils. This implies that the communication distance is enhanced 8.57 times. Since the permeability of transmitting and receiving coils are set to 0.0008 H.m^{-1}, therefore the numerical value of $10^{\frac{\log(\mu_T \cdot \mu_R) - \log\left(\mu_0^2\right)}{6}}$ is 8.6, which is very close to 8.57. For any given coil size using ferrite core, the distance is enhanced by about 8.6 times in the simulations. For instance, when the radius is 1 cm, the communication range is enhance from 5 cm to 43.37 cm and when the radius is 1.5 cm, it is improved from 7 cm to 60.63 cm.

Figure 3.6 shows the achieved range against the magnetic permeability. Dotted line shows how distance is enhanced by using ferrite at the core of both transmitting and receiving antennas (i.e. using identical ferrite material at both transmitter and receiver), while the plus-line shows the scenario when only one of the coils are ferrite-cored. The graph suggests that to enhance the communication range it is optimum to use both ferrite-cored coils at the transmitter and receiver. Also can be seen here that by neglecting Δd, the achieved distance is almost equal to the case when it is included.

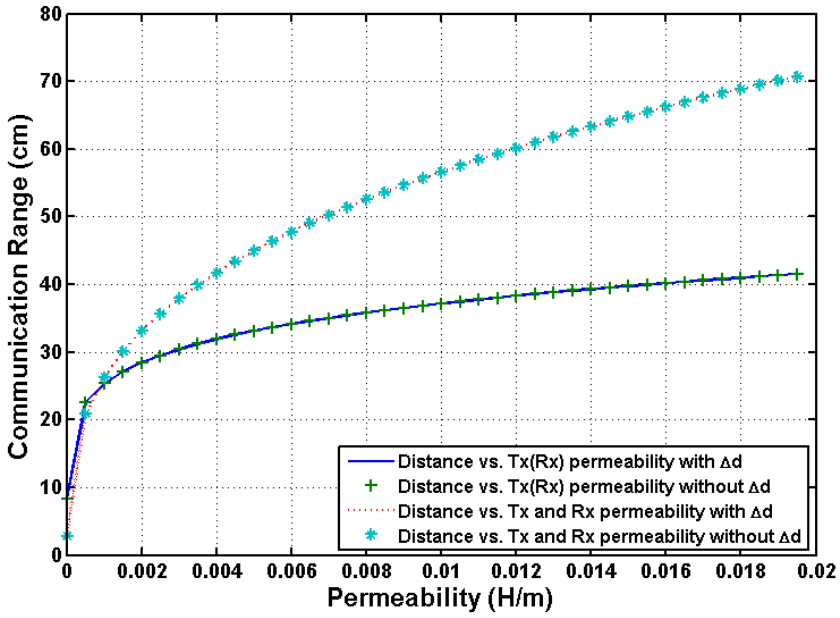

Figure 3.6 Distance versus transmitting and receiving coil magnetic permeability

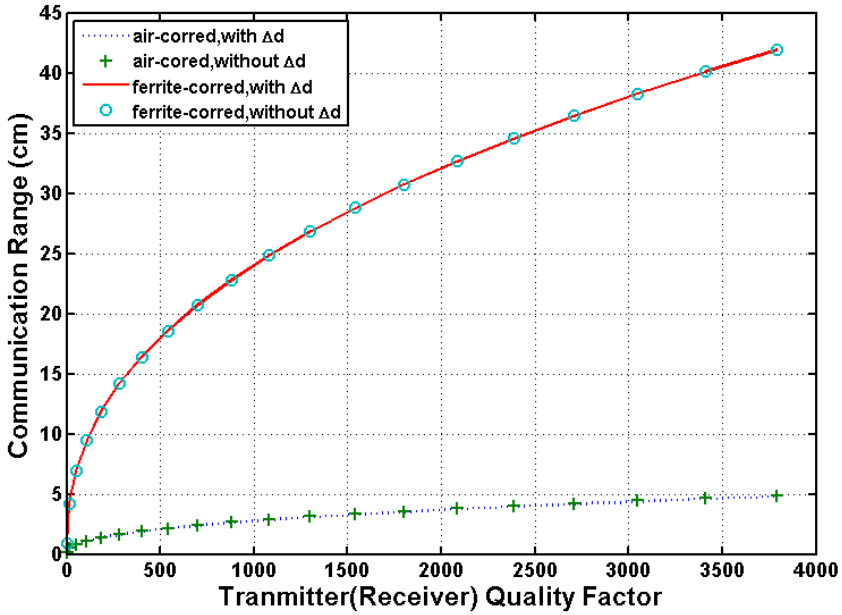

Figure 3.7 Distance versus transmitter (receiver) Q-factor

3.3.2.3 Distance versus transmitter and receiver Q-factor

Figure 3.7 shows how transmission range changes with different values of transmitter or receiver Q-factor for both air-cored and ferrite-cored (with permeability of 0.0008H.m^{-1}) coil . Communication range d has identical trend against both transmitter and receiver coil quality factor. In other words, if one of antenna coils has a specific value for Q-factor, as the Q-factor of coil at the other side increases, transmission range will increase at the same rate. Figure 3.8 shows the achieved transmission range as the Q-factor of the transmitter and receiver (identical Q-factors) changes for air and ferrite-cored coils. It can be seen from simulation result that typically, longer communication distance can be achieved by increasing Q-factor of the coil at receiver, transmitter or both. Although higher quality factor leads to longer communication range, it does not automatically improves the channel data rates (see Equation 2.28 and 2.30). This concept is discussed in detail and validated by simulations in Chapter 5 .

3.3.2.4 Distance versus transmission and received power

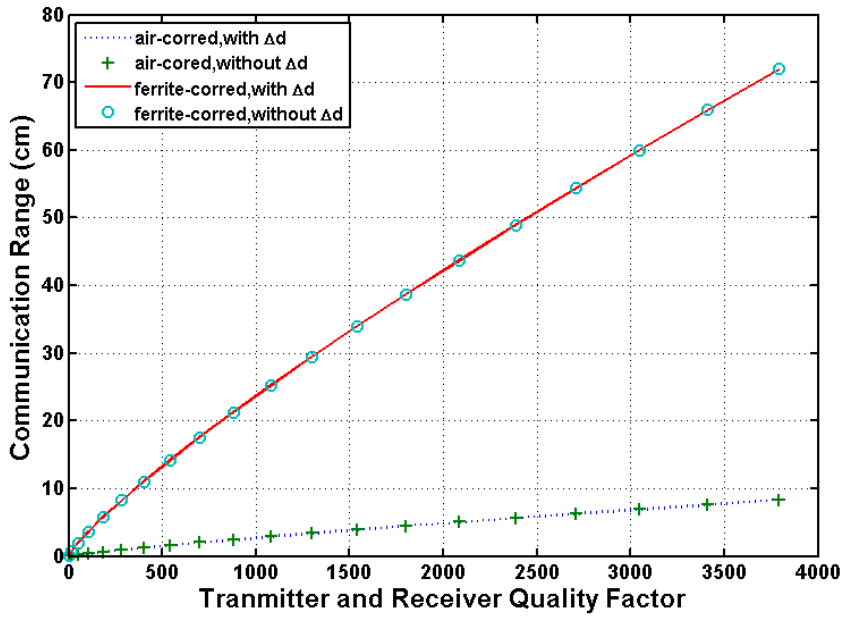

Figure 3.8 Distance versus transmitter and receiver Q-factor

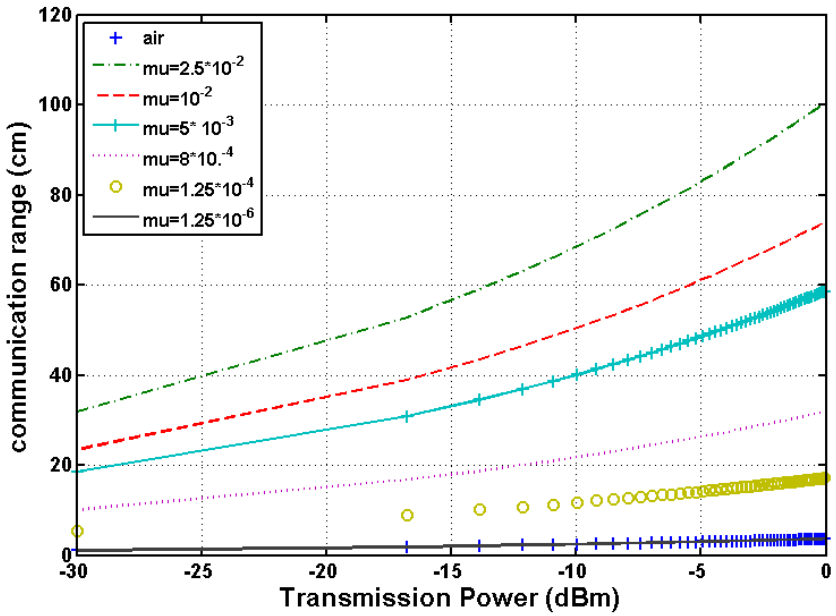

Figure 3.9 Distance versus transmission power

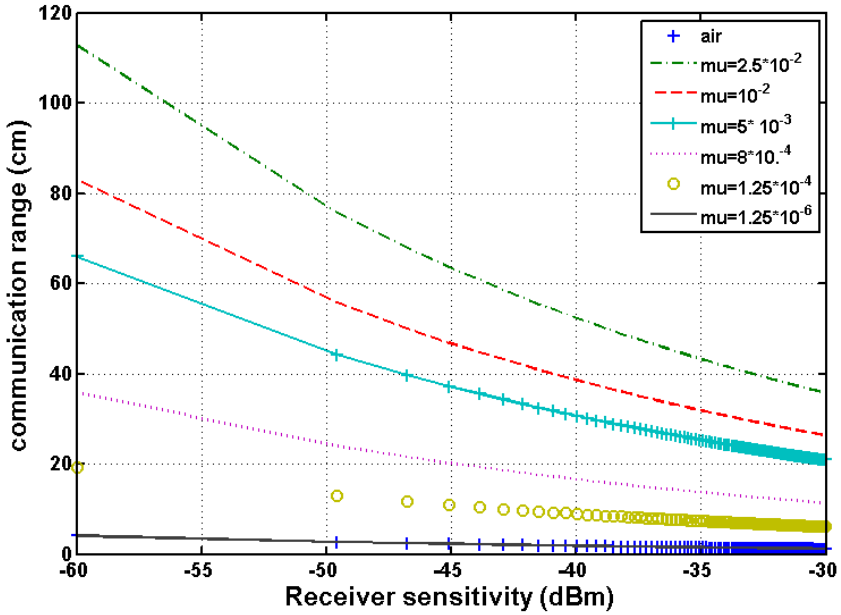

Figure 3.10 Distance versus receiver sensitivity

The transmitted signal needs to be at least equal or grater than the sensitivity of receiver, in order to be successfully received and decoded at the receiver. The higher the transmission power is, the more transmitted signal can travel through the wireless channel. Figure 3.9 shows this tendency, in which by increasing the transmission power communication distance is extended. However, it is not desirable in short range communications such as a BAN, or sensor networks to use high transmission power. To minimize the transmission power while achieving desired communication distance, ferrite-cored coils with high magnetic permeability can be used. Figure 3.10 illustrates how transmission range is reduced as the receiver sensitivity increases. It is shown that by increasing the magnetic permeability of core material, for the same level of receiver sensitivity, longer communication distance is achieved.

3.4 NFMIC Link Budget: AM1 Model and a Comparison between The Two AM Models

This thesis has proposed NFMIC link budget model (AM channel model) to the best of our knowledge, the first (see Section 3.3). AM link budget models a peer-to-peer NFMI communication in free space where LoS exists. The performance of an MI system has been extensively analyzed in the previous section. However, an MI propagation model was proposed by Sun and Akyldiz in [6, 8]. In fact, in this section Sun and Akyldiz model is formulated in the same manner as AM model to be able to compare these two models in terms of achievable communication range based on the design parameters. Their papers [6, 8] study MI communication system where the communication medium is soil, while in AM model the medium is air. However, since the permeability of air and soil are almost equal [6, 8], thus these two models can be compared under the same condition.

Figure 3.11 illustrates MI transceivers with radii of r_T and r_R for the transmitter

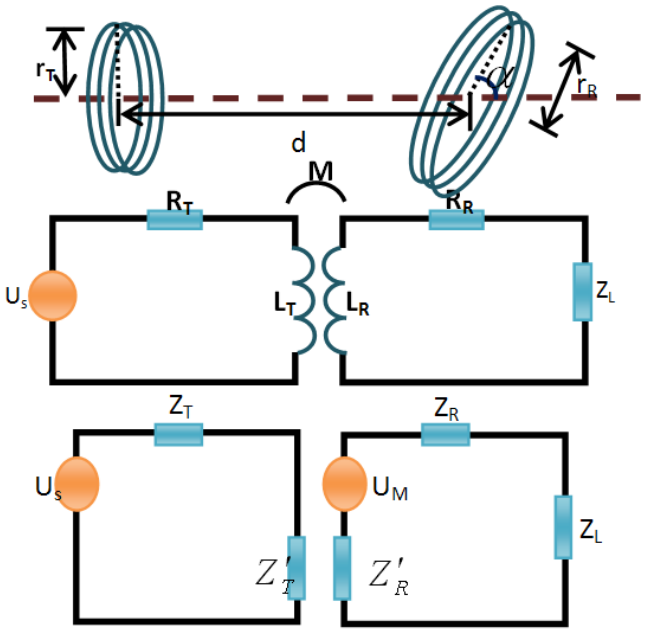

Figure 3.11 MI transceivers and the equivalent circuit model (adapted from [8]

and receiver respectively. Transmitter and receiver are separated from each other by a distance d. α is the angle between the x axis of the transmitter and receiver. However, in this chapter it is assumed that the coils have no angle misalignment in respect to each other (perfect channel); later, in Chapter 5, it is discussed how angle and lateral misalignment may impact the system performance. Figure 3.11 also shows the circuit model of the transmission system. Transmitter circuit consists of a voltage source (U_s), which creates the current in the circuit equal to $I = I_0.e^{-j\omega t}$. It also has an inductor with inductive value of (L_T) and self resistance of (R_T). The inductor in transmitter creates magnetic field around itself which induces a current in the receiver circuit through coupling of magnetic fields with mutual induction M. However, the receiving antenna circuit has a coil with inductive value of (L_R) and self resistance value of (R_R), as well as a load with impedance Z_L. Relationships between the circuit components are shown in the following equations [6, 8]:

$$Z_T = R_T + j\omega L_T; \quad Z'_T = \frac{\omega^2 M^2}{R_R + j\omega L_R + Z_L} \tag{3.28}$$

$$Z_R = R_R + j\omega L_R; \quad Z'_R = \frac{\omega^2 M^2}{R_T + j\omega L_T} \tag{3.29}$$

$$U_M = -j\omega M \frac{U_S}{R_T + j\omega L_T} \tag{3.30}$$

Since the aim of this section is to develop a link budget equation for the MI channel model cited in [6, 8], and compare it with AM link budget, it is firstly required to formulate Sun and Akyildiz model to AM model. Therefore, a common formalism is established for presenting these two models. Common formulism is for the efficiency of transmitter and receiver:

$$\eta_T = \frac{R_S}{R_S + R_T} \cong 1 \tag{3.31}$$

$$\eta_R = \frac{R_L}{R_L + R_R} \cong 1 \tag{3.32}$$

In [6], it is assumed that the resistance of the transmitting antenna and receiving antennas are equal to (R_T) and (R_R) respectively:

$$R_T = 2\pi.r_T N_T R_0 \tag{3.33}$$

$$R_R = 2\pi.r_R N_R R_0 \tag{3.34}$$

Hence the efficiency approaches unity. However the self inductance of coil is a function of the number of turns N, the permeability of core material of the coils μ, coil radius r, the length of coil (l), as well as the area of a single turn A. Therefore the self inductance is estimated using:

$$L = \frac{\mu A.N^2}{l} \tag{3.35}$$

The quality factors of coils are:

$$Q_T = \frac{\omega L_T}{R_T} \tag{3.36}$$

$$Q_R = \frac{\omega L_R}{R_R} \tag{3.37}$$

If identical coils are used at the transmitter and receiver, hence the load and source resistance have equal values. Further, this results in identical Q-factor at transmitter and receiver.

$$Q_T = Q_R = Q \tag{3.38}$$

Hence the power equation derived in [6] (Equation 2.24) becomes:

$$P_R = P_T Q^2 k^2 (d) \tag{3.39}$$

In the power equation, $k(d)$ which is the coupling coefficient, may be viewed as the path loss of NFMIC system at distance d. Coupling coefficient between the transmitting and receiving antennas may refer to the ratio of the coupling volume of a single turn and reactive power density at the receiver and is shown as [16]:

$$k^2 (d) = \frac{V_C}{V_D} \tag{3.40}$$

Where the coupling volume is [16]:

$$V_C = \frac{\mu_0 A^2}{L} \tag{3.41}$$

Reactive power density per unit volume created at the receiver side is [16]:

$$V_D = \frac{\text{Reactive power flowing in transmitting coil}}{Volume\,density\,of\,reactive\,power\,at\,the\,receiver\,created\,by\,transmitter} \tag{3.42}$$

Therefore coupling coefficient can be expressed as:

$$k^2\,(d) = \frac{\mu_0^2 A_R^2 . r_T^4}{4 . L_T L_R (d^2 + r_T^2)^3} \tag{3.43}$$

By substituting the equivalent expressions for $A_R = \pi \times r_R^2$, L_R and L_T, also by making a further assumption that the radius of transmitting coil is far smaller than communication range, therefore path loss becomes:

$$k^2\,(d) = \frac{r_T^3 r_R^3}{N_T N_R d^6} \tag{3.44}$$

The above formulation is used to compare the link budget for two models of AM and AM1.

3.4.1 AM Model:

Based on AM model (Section 3.3) and the assumption discussed earlier, received signal power at receiver for AM model becomes:

$$P_R = \frac{\omega^2 \mu^2 . r_T^3 r_R^3 P_T}{16 N_R N_T R_0^2 d^6} \tag{3.45}$$

According to Equation 3.45, the link budget equation (AM case) can be written as:

$$d_{AM} = 10^{\beta_{(AM)}} \tag{3.46}$$

where,

$$\beta_{(AM)} = \frac{P + 20.\log\mu + 20.\log\omega + 30\log\left(r_T r_R\right) - 10.\log 16 - 20.\log R_0 - 10.\log N}{60} \tag{3.47}$$

and

$$P = \left(P_T - P_R\right); (\mathrm{dBm}) \tag{3.48}$$

$$N = N_T.N_R \tag{3.49}$$

3.4.2 AM1 Model

AM1 channel model is derived from [6,8]. Power equation cited in [6] is shown here:

$$P_R = \frac{P_T \omega \mu N_R r_T^3 r_R^3 \sin^2\alpha}{16.R_0 d^6} \tag{3.50}$$

Using the same formalism as previously discussed (Section 3.4.1), Equation 3.50 cast as a link budget equation and becomes:

$$\begin{aligned} d_{AM1} &= 10^{\beta_{(AM1)}} \\ \beta_{(AM1)} &= \frac{P + 10.\log\mu + 10.\log\omega + 30\log(r_T r_R) - 10.\log 16 - 10.\log R_0 + 10.\log N_R}{60} \end{aligned} \tag{3.51}$$

By comparing these two models (Equations 3.45 and 3.50), it is observed that received signal power for AM model can be higher than received power in AM1 model by a factor equal to Equation 3.52, if $\omega\mu >> N_R^2 N_T R_0$:

$$\frac{P_{R(AM)}}{P_{R(AM1)}} = \frac{\omega\mu}{N_R^2 N_T R_0} \tag{3.52}$$

This implies that by using higher permeable material and also higher frequencies AM model achieves better performance in terms of received signal power and the communication range. This also can be seen in the simulation results in the following section.

3.4.3 Simulation Results

To compare these two models, AM and AM1 link budget models are simulated using Matlab. The design parameters are as discussed in Section 3.3.2. The operating frequency is set to three different frequencies of 13.56 MHz, 300 MHz and 900 MHz, as used for simulations in [6]. The results show the performance of both models for different transceiver coil radii as well as transmission power. However, since transmitter and receiver coil radii have almost the same impact on the communication range, only the results for a range of transmitter coil radius are provided here.

3.4.3.1 Communication range vs. transmitter coil radius and transmission power

Figures 3.12 to 3.14 depict the relationship between communication range and the radius of transmitter coil at 13.56 MHz, 300 MHz and 900 MHz respectively. In each figure, this relationship may be seen for two channel models of AM and AM1. By comparing the graphs showing these two models, it is observed that AM link budget is more efficient in terms of achievable communication range. This means that AM model provides longer communication distance than AM1. For example, at 13.56 MHz (Figure 3.12), in AM model using a transmitter coil with radius of 0.5 cm, achievable range is 6 cm while 4.8 cm can be obtained by considering AM1 model. In this scenario, AM provides 1.25 times longer communication distance. However increasing the operating frequency, this difference is more considerable. While at frequency 300 MHz (Figure 3.13), the achievable range for AM model with the same transmitter coil (radius=0.5 cm) is 17 cm, AM1 results in 7 cm communication range. Using AM link budget equation, the obtained distance at 900 MHz (Figure 3.14) is 2.4 times larger than an AM1 situation, in which by using the same coil more than 24 cm is achieved.

The tendency of signal attenuation with distance at the mentioned frequency bands for AM and AM1 channel models are shown in Figures 3.15 to 3.17. These graphs suggest that AM model achieves longer communication range than AM1 using the

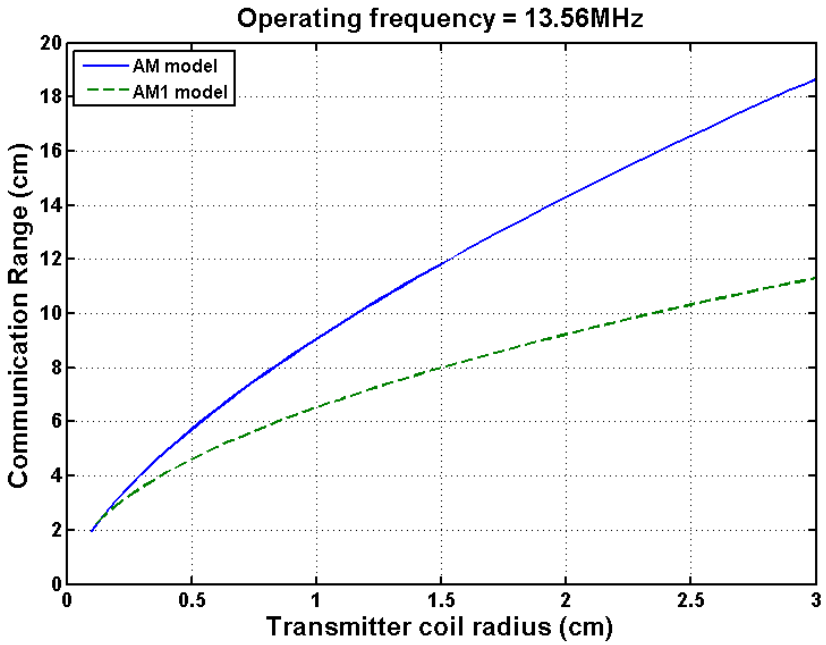

Figure 3.12 Communication range vs. transmitter coil radius at 13.56MHz

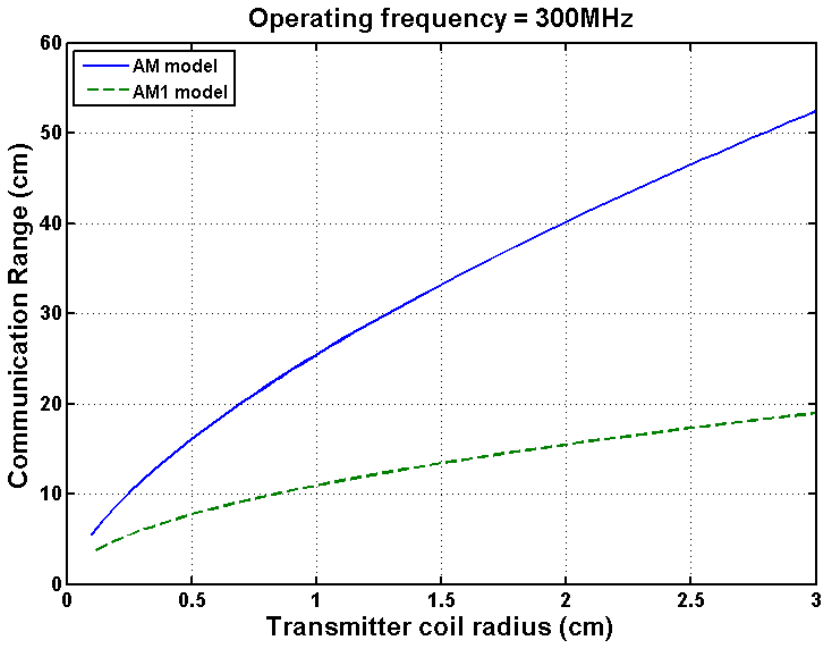

Figure 3.13 Communication range vs. transmitter coil radius at 300MHz

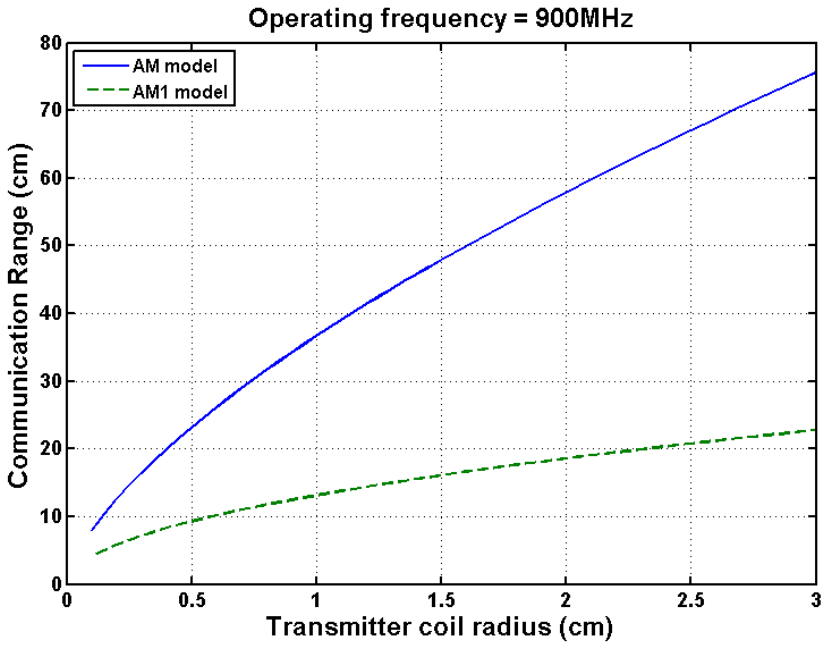

Figure 3.14 Communication range vs. transmitter coil radius at 900MHz

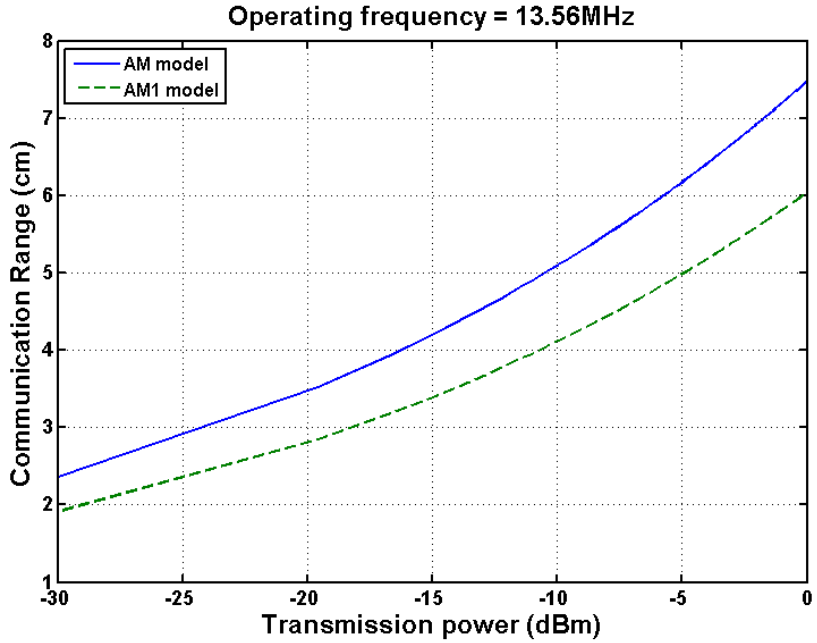

Figure 3.15 Communication range vs. received power at 13.56MHz

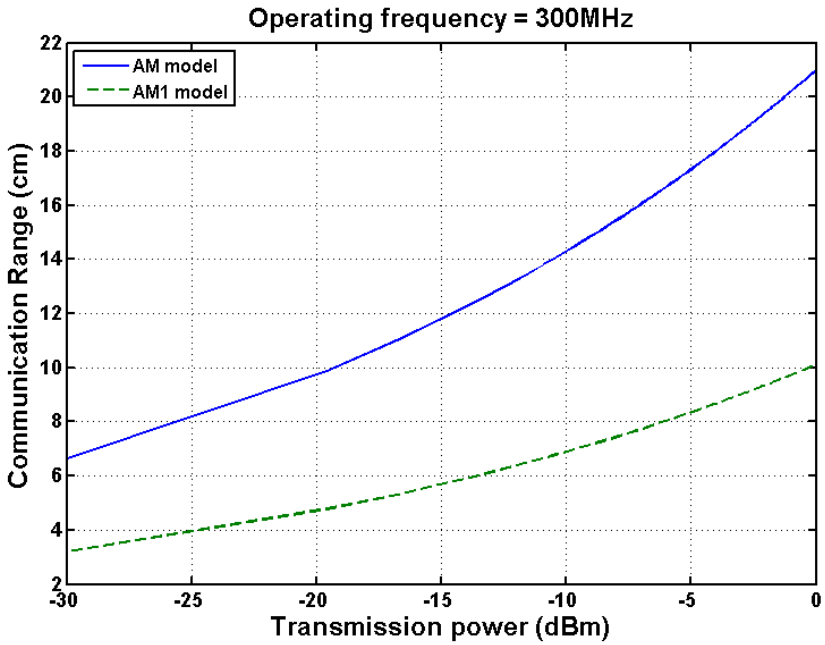

Figure 3.16 Communication range vs. received power at 300MHz

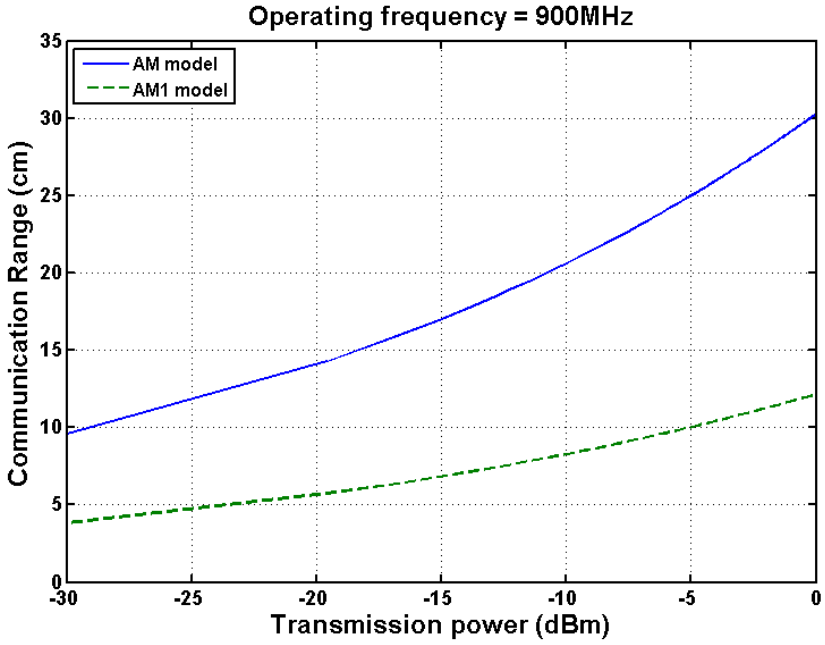

Figure 3.17 Communication range vs. received power at 900MHz

same transmission power. However, as the transmission power increases, AM performs more efficiently.

3.4.3.2 Communication range vs. Operating Frequency

The interesting result observed from simulation is that NFMI systems perform effectively in higher frequencies. Compared to MI, in EM based communication systems the signal attenuates much faster at higher frequencies. The communication range achieved using magnetic waves is much larger at higher frequencies compared to the EM waves. This is observed from simulation result presented in the previous section. As it can be seen from the figures in Section 3.4.2, the achieved communication range at 900 MHz band is much higher than the range at operating frequency 13.56 MHz and 300 MHz. Figure 3.18 presents the relationship between communication range and frequency spectrum for both magnetic and EM-based communication systems. However, this shows the normalized frequencies to illustrate the general trend of these two approaches. As can be seen here, EM waves perform efficient at lower

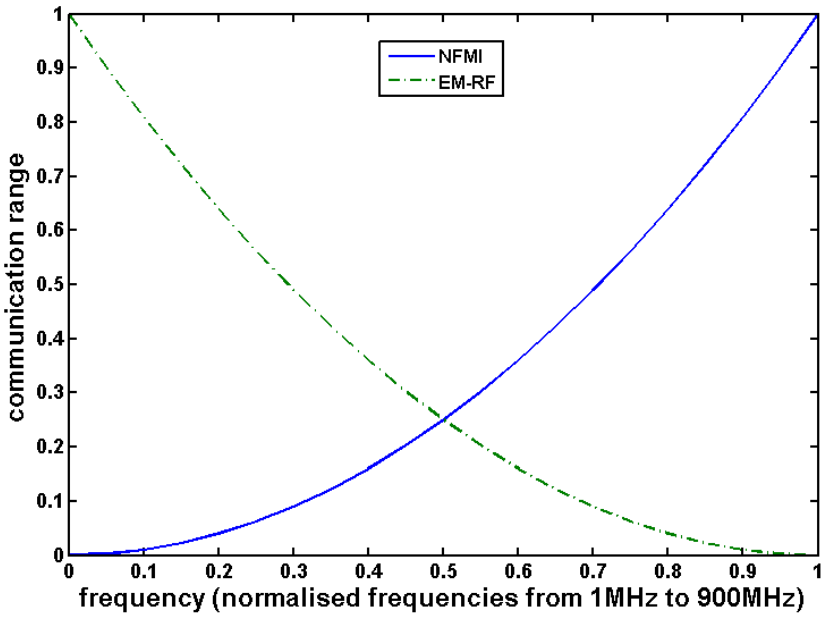

Figure 3.18 Communication range vs. operating frequency

frequencies, while the magnetic waves achieve longer range at higher frequencies. However, it has to be noted that at higher frequencies the near field region tends to have smaller radius as the wavelength decreases. It implies that to maintain the communication within near field region at higher frequencies, the maximum allowable range decreases.

3.5 Summary

This chapter proposed a NFMIC link budget model (AM model) and studied the model theoretically and by simulations. This model determines the achieved communication distance in NFMIC by taking into account the antenna gains as well as the propagation loss. It is concluded that the communication range can be greatly increases if the coils are wound around a high magnetically permeable core. AM1 link budget model is also proposed upon the work of [6, 8], and the two AM models are compared. It is concluded that in AM model, longer communication range can be achieved compared to AM1. However, measurements can be done in order to verify the theory and simulations.

Chapter 4

Magneto Inductive Waveguide Link Budget (Multi-node NFMI Communications)

4.1 Chapter Overview

In this chapter, magneto inductive model is discussed as a method of NFMIC range extension. This method is studied for different section path loss approximations, and link budget models is developed for each case. It is shown that the conventional waveguide model works properly under specific conditions. A distance threshold is proposed, after which the waveguide system works inversely. This means that by increasing the number of relaying nodes in the waveguide chain, the communication distance decreases. It is discussed that this is due to the power reflection between the nodes, the transmission line has to be terminated properly, in order to take advantage of waveguide method for the communication range extension.

Three methods of voltage excitation for a waveguide transmission system are proposed (Array Edge Excitation, Array Centre Excitation and Collinear Array Excitation) and their performances are compared. It is shown that applying a proper voltage excitation method results in higher waveguide performance [62].

4.2 Magneto-Inductive Waveguide Link Budget Model

Magneto Inductive waveguide model is introduced in chapter 2. While Syms, Solymar and Shamonina have studied the waveguide model for proper termination methods of a transmission line [63], Sun and Akyildiz have explored this model for an underground communication system [6, 8]. Syms, Solymar and Shamonina have discussed the termination of a waveguide chain to decrease the power loss due to the power reflection [63]. However, in this section build upon the work of [6, 8, 63], this thesis has developed a link budget for a magneto inductive waveguide communication system. The system uses an array of n antennas in communication channel located between the transmitter and receiver linearly. The pioneering work of Syms, Shamonina and Solymar [63], have established some of the theories for the magneto inductive waveguide discussed in this section. In its simplest form, a one section peer to peer flux coupling system is used for communication with no option of range extension (Figure 2.13). This model has been well analyzed and discussed in Chapter 3 and also by Agbinya et al in [15]. However, multiple section (multi-node) communication is studied in this chapter to evaluate the performance of conventional magneto inductive waveguide and its ability for communication range extension (Figure 2.13).

For a peer to peer communication the power equation is given by the Equation 3.50 and as mentioned earlier, if $(R_0 << \omega\mu N_T)$, the power equation casts as a link budget equation (Equation 3.51). This model supports only a peer-to-peer communication. For range extension, a method using magneto inductive waveguide was studied by the authors of [6, 8, 63]. A typical magneto inductive waveguide consists of n intermediate coils between transmitter and receiver ($n + 1$ sections); a section is referred to as a communication link between any two adjacent nodes. Such a system is depicted in Figure 2.13, where the transmitter couples energy to its nearest neighbor node and the receiving coil couples energy to its next neighboring node and this process is repeated until transmitted data (by the original source node) reaches the final receiver.

Sun and Akyildiz proposed a complex path loss model for a magneto inductive waveguide system. In this section, this model is greatly simplified. In their work, each intermediate node is loaded with a capacitor C to neutralize self-induction and C is [6]:

$$C = \frac{2}{\omega^2 N^2 \mu.\pi.r} \tag{4.1}$$

The path loss expression for an *(n+1)-section* waveguide is given in [6] as:

$$\frac{P_R}{P_T} = \frac{\omega^2 N^2 \mu^2 r_T^3 r_R^3}{4x^6 2R_0 \left(4R_0 + \frac{\omega^2 N^2 \mu^2 r_T^3 r_R^3}{4x^6 2R_0}\right)} \left[\frac{j}{\frac{4R_0}{\omega\mu N}\left(\frac{x}{r_R}\right)^3 + \frac{\omega\mu N}{4R_0}\left(\frac{r_R}{x}\right)^3}\right]^{2n} \tag{4.2}$$

In this expression the variable x is the separation distance between any two adjacent nodes of the MI waveguide (i.e. a single section). Thus, the communication range d is divided into $n+1$ sections of length x, or $d/x = (n+1)$. The path loss expression is simplified for analysis and modeling into the so-called $AM2$ link budget equations (Section 4.2.2) and thus provides insight into the achievable range based on the desirable system variables. The path loss equation may be represented as [74]:

$$\frac{P_R}{P_T} = P_1 P_{2n} \tag{4.3}$$

where [74]:

$$P_1 = \frac{\omega^2 N^2 \mu^2 r_T^3 r_R^3}{4x^6 2R_0 \left(4R_0 + \frac{\omega^2 N^2 \mu^2 r_T^3 r_R^3}{4x^6 2R_0}\right)} \tag{4.4}$$

$$P_{2n} = \left[\frac{j}{\frac{4R_0}{\omega\mu N}\left(\frac{x}{a}\right)^3 + \frac{\omega\mu N}{4R_0}\left(\frac{a}{x}\right)^3}\right]^{2n} \tag{4.5}$$

In [6], the authors discuss that the inductance of transmitting and receiving antennas may be expressed as:

$$L_T = \frac{1}{2}\mu_T \pi N_T^2 r_T \tag{4.6}$$

$$L_R = \frac{1}{2}\mu_R \pi N_R^2 r_R \tag{4.7}$$

Based on the assumption discussed in [6], the load and source resistances are estimated using:

$$R_L = 2\pi N_R r_R R_0 \tag{4.8}$$

$$R_S = 2\pi N_T r_T R_0 \tag{4.9}$$

R_0 is the resistance of wire per unit of length. Therefore, the quality factor of the transmitter and receiver in this case may be shown as:

$$Q_T = \frac{\omega L_T}{R_S} = \frac{\omega \mu_T N_T r_T}{4R_0} \tag{4.10}$$

$$Q_R = \frac{\omega L_R}{R_R} = \frac{\omega \mu_R N_R r_R}{4R_0} \tag{4.11}$$

By substituting Q_T and Q_R in Equation 4.4 and defining $k^2(x) \approx \frac{r_T^3 r_R^3}{x^6}$ (similar to neglecting Δd in the AM model discussed in Section 3.3), P_1 becomes:

$$P_1 = \frac{Q_T.Q_R.k^2(x)}{(2 + Q_T.Q_R.k^2(x))} \tag{4.12}$$

Similarly, relating P_{2n} to the transmitting and receiving quality factor and coupling coefficient, it casts as [62],

$$P_{2n} = \left(Q_T.Q_R k^2(x)\right)^n \left[\frac{j}{(1 + Q_T.Q_R k^2(x))}\right]^{2n} \tag{4.13}$$

Hence, the power equation becomes [74]:

$$\frac{P_R}{P_T} = \frac{Q_T.Q_R k^2(x)}{(2 + Q_T.Q_R.k^2(x))} \left(Q_T.Q_R k^2(x)\right)^n \left[\frac{j}{(1 + Q_T.Q_R k^2(x))}\right]^{2n} \tag{4.14}$$

β is defined as the section path loss, where [74]:

$$\beta = Q_T Q_R k^2(x) \tag{4.15}$$

Therefore, the waveguide path loss is given by the expression [62]:

$$\frac{P_R}{P_T} = \frac{\beta.\beta^n}{(2+\beta)} \left[\frac{j}{(1+\beta)}\right]^{2n} = \left(\frac{\beta^{n+1}}{(2+\beta)}\right) \left[\frac{j}{(1+\beta)}\right]^{2n} \tag{4.16}$$

When $n = 0$, it casts a simple peer-to-peer MI system path loss equation. If the design is such that $r_T = r_R = x$, then $k(x) = 1$. The coupling coefficient cannot be more than unity or $r_T.r_R$ cannot be greater than the section length in practice. Therefore, $r_T.r_R \leq x^2$. $r_T.r_R > x^2$ is an unrealistic situation since it is impractical that the receiver collects more flux than all the flux created by transmitter. For $n = 0$ and β is unity, the received power is a third of the transmitted power and Equation 4.2 by Sun and Akyildiz [6, 8] is simplified to [74]:

$$\frac{P_R}{P_T} = \frac{1}{3}\left(\frac{1}{2}\right)^{2n} \tag{4.17}$$

This means that since $\beta = Q_T Q_R k^2(x)$, the design equation required for determining optimum power transfer between the sections is a function of the coupling coefficients and the quality factors of the coils. This power equation may literally be used to design the antennas for the required receiver sensitivity and communication distance.

4.2.1 One Section Peer to Peer: Line of Sight

The case when $n = 0$ is particularly interesting to study, because it is the one transmitter and one receiver case with the path loss equation [74],

$$\frac{P_R}{P_T} = \frac{Q_T.Q_R k^2(x)}{(2 + Q_T.Q_R k^2(x))} \tag{4.18}$$

- In this equation, when $\beta >> 2$ the power equation approaches the value $\frac{P_R}{P_T} \approx 1$. This is an unrealistic case. The received powers in most communication systems (inductive and radiative) are not usually equal due to losses in the channel and transceiver circuitry.

- When $\beta = 2$ [74],

$$\frac{P_R}{P_T} = \frac{1}{2} \tag{4.19}$$

  Although this approximation promises that half the transmitted power can be received, engineering the scenario could prove very difficult. Hence, a better approximation may be required.

- When $\beta << 2$, which implies $k^2(x)$ is very small, then a more practical situation is [74]:

$$\frac{P_R}{P_T} \approx \frac{Q_T.Q_R k^2\left(x\right)}{2} \tag{4.20}$$

Thus, by using different assumptions, a familiar expression is achieved. The reduced equation and the AM models are equivalent (to within a constant multiplier). This proves the fact that AM model and Sun and Akyildiz model [6] are almost identical and have correctly modeled MI communications.

4.2.2 Multi-Section Waveguide

- Using the approximation $\beta >> 2$, in the expression for a multi-section waveguide, it simplifies to [74]:

$$\frac{P_R}{P_T} \approx \left(Q_T.Q_R k^2\left(x\right)\right)^n \left[\frac{j}{\left(Q_T.Q_R k^2\left(x\right)\right)}\right]^{2n} \tag{4.21}$$

Therefore, the link budget equation becomes [74]:

$$\begin{aligned} &d = 10^{\alpha 1}; \\ &\alpha 1 = \frac{P_T(dBm) - P_R(dBm) - 10 \cdot n[\log Q_T + \log Q_R + 3 \cdot \log(r_R r_T) + 2 \cdot \log(j)]}{60.n} \end{aligned} \tag{4.22}$$

As discussed in previous section, this is an unrealistic situation and hence impractical. Impracticability of this situation is also shown by the simulation results in Section 4.2.3.

- When $\beta = 2$, the difference between the transmitted and received signal power is 3 dBm. In this case, the communication distance approaches a threshold in which the waveguide model performs in a reverse manner. This means that if the transmitted power is larger than the received power for more than 3 dBm, by increasing the number of intermediate nodes the achieved received signal strength decreases. However, the distance threshold is a function of coil characteristics. For example, by increasing the radius of the transmitting and receiving coils, number of turns (i.e. increasing coil Q-factor), the distance

threshold increases. Equation 4.23 shows the relationship between the distance threshold and coil characteristics. When $\beta = 2$, then $P_T - P_R = 3dBm$, therefore, the distance threshold is [74]:

$$d_{threshold} = 10^t\,; \quad t = \frac{10.\log Q_T + 10.\log Q_R + 30.\log(r_T.r_R) - 3}{60} \tag{4.23}$$

Based on this assumption, the received power at distance threshold $d_{threshold}$, for an $n+1$ section MI waveguide system is independent of the number of nodes. However, when $\beta = 2$, the approximation gives [74]:

$$\frac{P_{R(n+1)}}{P_{T(n)}} = \frac{2^n}{4}\left[\frac{j}{3}\right]^{2n} \tag{4.24}$$

Equation 2.24 shows the power transfer function for any adjacent nodes.

- The third assumption and the most practical situation is when $\beta << 2$. Therefore, the power equation simplifies to [74]:

$$\frac{P_R}{P_T} \approx \frac{1}{2}\left(Q_T.Q_R k^2\,(x)\right)^{n+1} j^{2n} \tag{4.25}$$

This expression truly shows an $n+1$ section power terms and if the term in the bracket is less than one, the received power is always less than the transmitted power and depends on the number of sections in the MI waveguide. The link budget equation in this case becomes [74]:

$$\begin{aligned} &d = 10^{\alpha 2};\\ &\alpha 2 = \frac{P_T(dBm) - P_R(dBm) - 3 + 10\cdot(n+1)[\log Q_T + \log Q_R + 3\cdot\log(r_R r_T)] + 20\cdot n\cdot\log(j)}{60\cdot(n+1)} \end{aligned} \tag{4.26}$$

Also using the simulation results provided in the following section, it is discuss that the most realistic situation is the case when $\beta << 2$.

4.2.3 Simulation Results

In this section the simulation results using Matlab are provided. The link budget equations for an $n+1$ section MI waveguide is simulated, based on three different

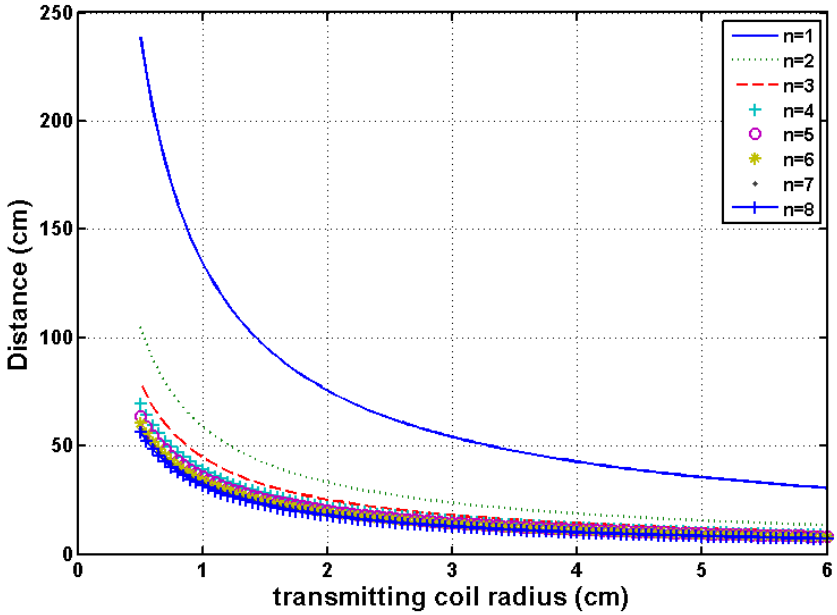

Figure 4.1 Distance vs. transmitting coil radius when $\beta >> 2$

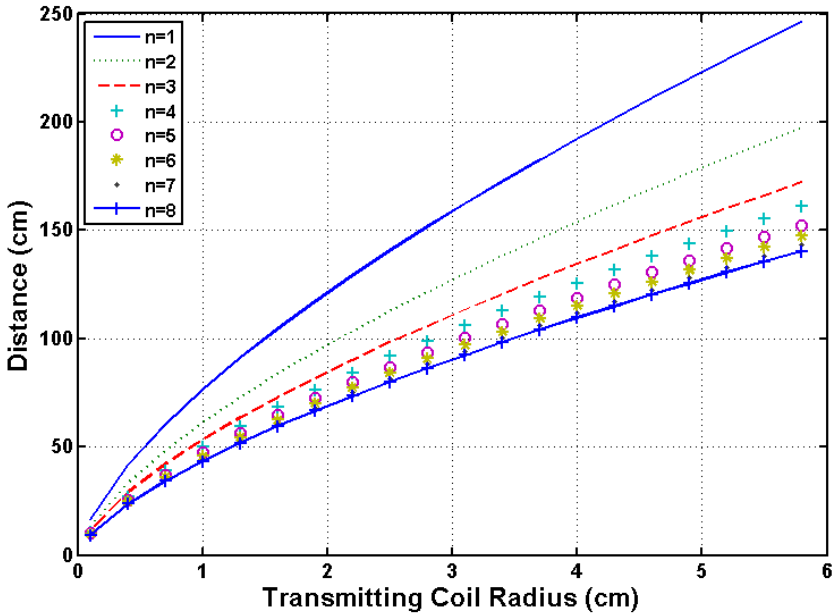

Figure 4.2 Distance vs. transmitting coil radius when $\beta << 2$

assumptions discussed earlier (i.e. when $\beta >> 2$, $\beta << 2$ and $\beta = 2$). In the simulations, most parameters have the same values as discussed in Section 3.3.2. The number of turns are set to 10, 15 and 20 and coils of radius 1 cm are considered since according to [6] the condition $R_0 << \omega\mu N$ should be met. Figure 4.1 shows the achieved communication distance when $\beta >> 2$. This graph implies that by using larger coil, communication range will decrease. This is an unrealistic relationship since it is well know and expected that by increasing the radius of inductors, higher received power and consequently longer communication range should be achieved. Therefore, it is shown that it is impractical to have $\beta >> 2$. The link budget when $\beta << 2$ is shown in Figure 4.2. It is shown how distance increases by increasing the transmitting coil radius for different number of intermediate nodes. It can be seen here that increasing the number of relaying nodes between transmitter and receiver not only does not lead to the range extension but also it decreases the achieved range, since the received power decreases. However, Figure 4.3, which shows the coil radius against the received power, suggests that the waveguide method works properly

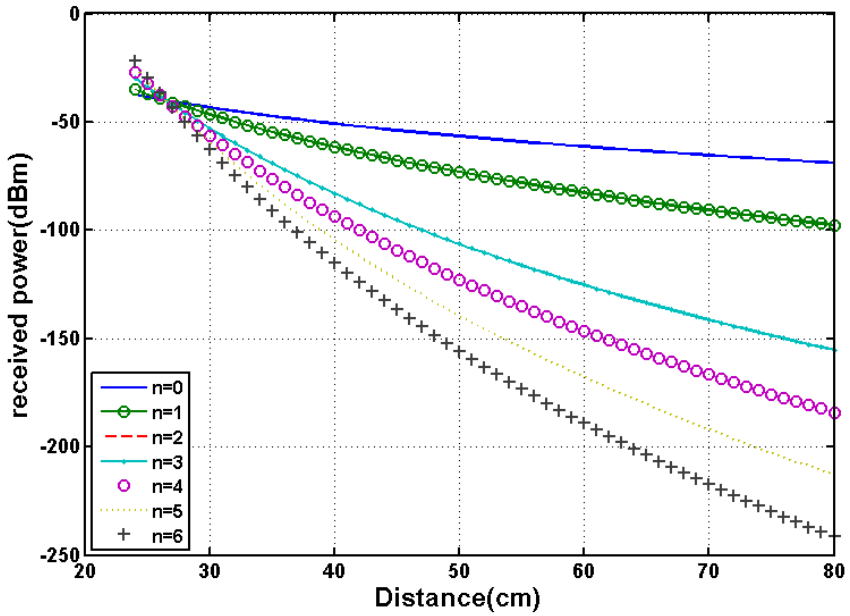

Figure 4.3 Received power vs. transmitting coil radius when $\beta << 2$ and $N = 15$

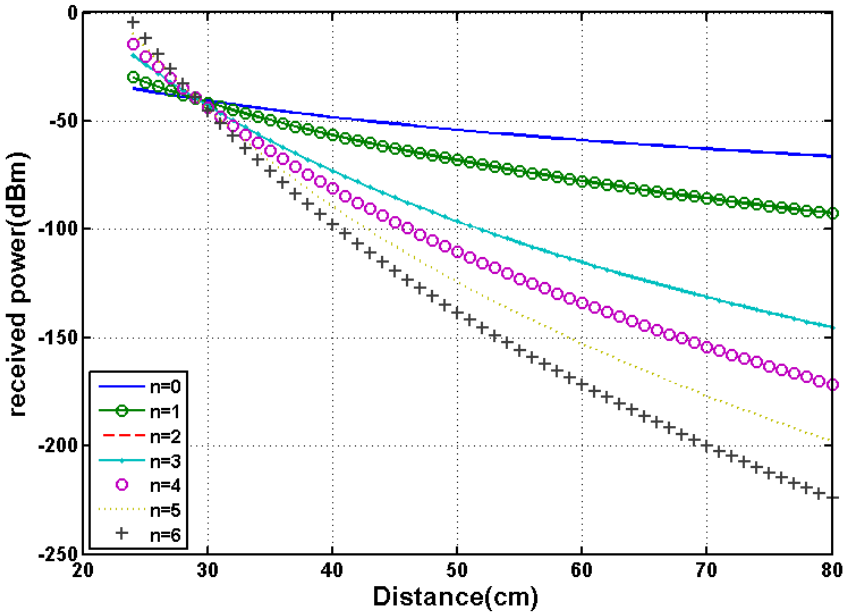

Figure 4.4 Received power vs. communication range when $\beta << 2$ and $N = 20$

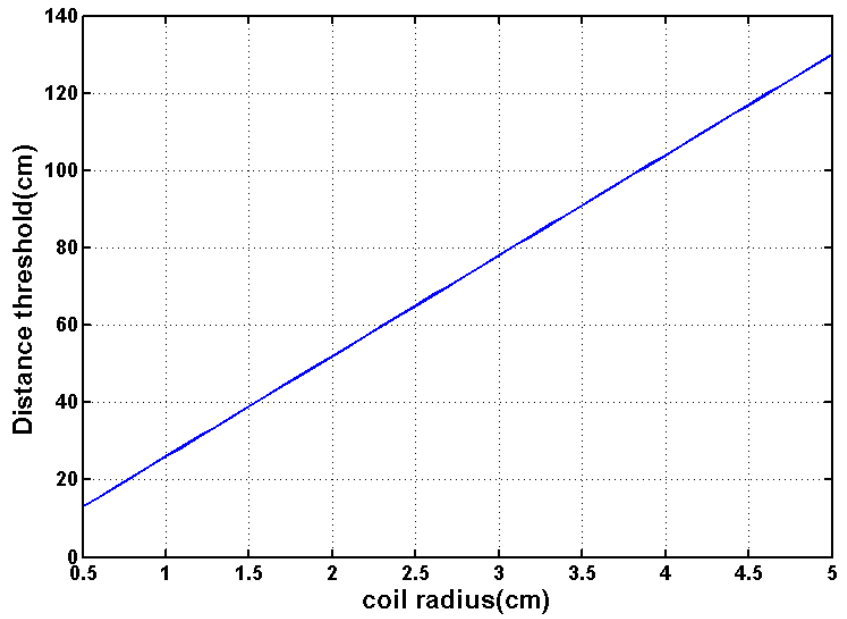

Figure 4.5 Distance Threshold vs. transmitting coil radius when $\beta = 2$

when received power is more than half of the transmission power. As discussed in Section 4.2.2, this point is termed a distance threshold. Once the communication distance exceeds the distance threshold, not only no range extension can be achieved through increasing the number of intermediate nodes, but also it results in shortening the achieved distance. However, distance threshold is a function of system characteristics and configuration. For instance, by increasing the coil size and/or Q-factor, distance threshold can be extended. Figure 4.4 shows the achieved distance as a function of received power when the Q-factor is enhanced by increasing the number of turns from 15 (see Figure 4.3) to 20. As may be seen from these two graphs, the distance threshold can be increased from 26 cm to 30 cm by improving the quality factor achieved through larger number of turns. Figure 4.5 presents the trend in which the distance threshold increases by increasing the coil radii.

Based on the theoretical and simulation analysis, it can be concluded that the waveguide method increases the range if $R_0 << \omega\mu N$ and also $\beta << 2$, where distance threshold is not exceeded. It is achieved through the use of very high frequencies and large number of turns and high relative permeability of the core material of coils; otherwise the waveguide model works inversely within the system. In fact, this is due to the reflected current from the receiving coupled coil toward the source node. This means that reflected current is created between the transmitting and receiving antenna, which results in canceling the desirable induced current at the receiving coil and consequently reduction in the received power at the final receiving coil. In this case by increasing the number of intermediate nodes, the reflected current toward the transmitter is much larger, therefore, the signal transmitted by the original transmitter attenuates much higher. However, the reflected current can be suppressed if the system is terminated properly. Syms, Solymar and Shamonina have discussed the termination of transmission lines in depth in [7, 63]. In general to suppress the reflected current toward the transmitter, it is practical to load the coils with a resistive element. However, how to choose the resistive element and how to implement it in the communication link is critical to provide efficiency (see [7, 63] for more detail).

4.3 Magneto Inductive Waveguide Voltage Excitation Methods

Different methods of voltage excitation of a waveguide system is tested in the laboratory. The waveguide configuration tested in the laboratory is demonstrated in Figure 4.6. Figure 4.7 shows the mean value of measured voltage at each node for the case when waveguide relaying nodes are used and also without the cooperative relaying coils (peer-to-peer) at the frequency 2.65 MHz and at different distances. The input voltage is 30 mV. The result has shown that the waveguide model increases the

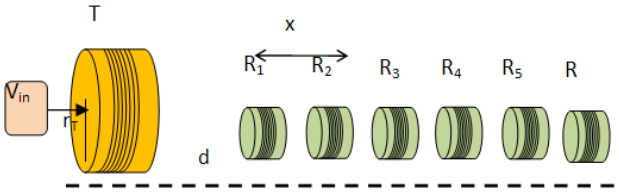

Figure 4.6 Waveguide experiment configuration

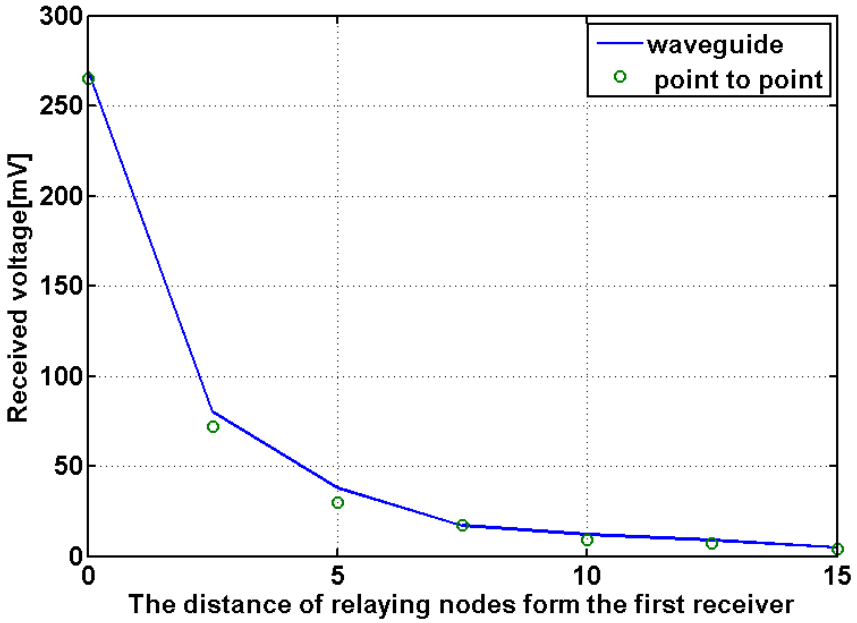

Figure 4.7 Waveguide experiment result

received power at each node and consequently the communication range but not considerably. However, it mitigates interference and noise significantly, since by using relaying nodes clearer signal was observed. The circles in Figure 4.7 show the mean value of voltage received at the receiver without the presence of relaying nodes, at different distances. However, the line corresponds to the case when the six relaying nodes are placed between the transmitter and the final receiver (Figure 4.6). It may be seen that the received voltage, which is proportional to the received power (Equation 4.27) is slightly higher when the relaying nodes are present [62].

$$P = \frac{V}{R}; \text{ for constant R} : P\alpha V \quad (4.27)$$

The relaying nodes are not required to have individual power sources in a magneto inductive waveguide communication system, since the voltage in the transmitting circuit induces currents in the neighboring nodes through mutual inductive coupling. However, the locations and orientations of relaying nodes affect the coupling coefficient k significantly. Therefore, the method of voltage excitation of relaying antenna array has an important role to play to achieve higher received signal power at the receiver. Different placement and orientations of the transceivers in respect to each other result in different received signal power. In this context, three voltage excitation methods for magneto inductive waveguide are proposed and discussed in this section; array edge excitation (AEE), array centre excitation (ACE) and collinear array excitation (CAE) [62]. The performance of each method is measured in laboratory and compared to each other.

In the theoretical analysis here, it is assumed that each node receives its power through the coupling with the transmitter directly and two instant neighboring nodes, which themselves receive the power directly from the transmitter. In other words, when considering the coupling between the adjacent nodes ($n, n+1, n-1$), the inductive coupling between nodes two sections away and their adjacent nodes ($n+2, n+3$ and $n-2, n-3$) are neglected in this work. This is because the value of coupling coefficient is usually very small and is often in the range of 10^{-6}.

4.3.1 Array Edge Excitation

In the array edge excitation method the relaying nodes were excited from the edge of array, by lining up the transmitter directly opposite the relay node 1 as shown in Figure 4.8. The transmitting coil has a radius of 6 mm and the receiving coils have a radius of 3.5 mm with each one wound on a ferrite core (the radius of the coils used in the experiment).

The power received by a receiver is influenced by the mutual coupling between the node and transmitter directly, as well as the coupling with its neighboring nodes, which themselves are powered by their adjacent nodes and the transmitter. Therefore the received power at $Receiver7$ is given by [62]:

$$\begin{aligned} \frac{P_{R7}}{P_T} &\approx \frac{Q^2k^2(d_7)\cos^6\theta_7}{2} + \frac{Q^2k^2(d_6)\cos^6\theta_6}{2} \times \frac{Q^2k^2(x_6)}{2} \\ \frac{P_{R7}}{P_T} &= \frac{Q^2}{2}\left(k^2\left(x_6\right)\frac{Q^2k^2(d_6)\cos^6\theta_6}{2} + k^2\left(d_7\right)\cos^6\theta_7\right) \end{aligned} \tag{4.28}$$

In this equation d_n is the distance between the transmitting coil and the nth node, x_n indicates the distance between the nth and $(n+1)th$ nodes. If define $\alpha = \frac{Q^2}{2}$ and $\beta = \frac{Q^2k^2(x)}{2}$, where the distance between the neighboring relay nodes are identical,

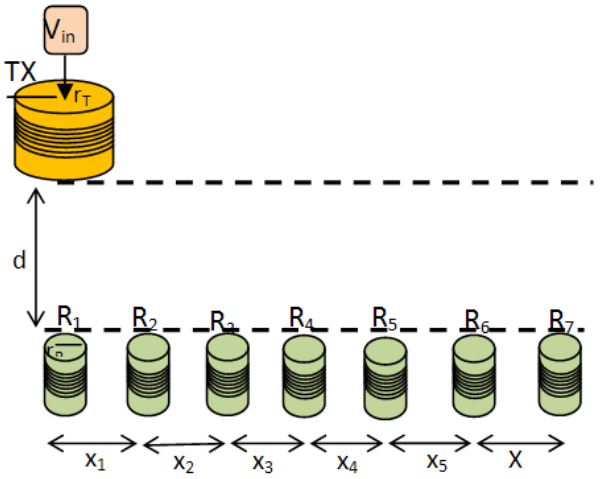

Figure 4.8 Array Edge Excited

then the received power at $Receiver6$ is [62]:

$$\begin{aligned} \frac{P_{R6}}{P_T} &\approx \frac{Q^2k^2(d_5)\cos^6\theta_5}{2} \times \frac{Q^2k^2(x)}{2} + \frac{Q^2k^2(x)}{2} \times \frac{Q^2k^2(d_7)\cos^6\theta_7}{2} + \frac{Q^2k^2(d_6)\cos^6\theta_6}{2} \\ \frac{P_{R6}}{P_T} &= \alpha\left[\beta.k^2\left(d_7\right)\cos^6\theta_7 + \beta.k^2\left(d_5\right)\cos^6\theta_5 + k^2\left(d_6\right)\cos^6\theta_6\right] \end{aligned} \tag{4.29}$$

In general for the jth section in the relaying array the received power is [62]:

$$\frac{P_{Rj}}{P_T} = \alpha[\beta k^2(d_{j+1})\cos^6\theta_{j+1} + \beta k^2(d_{j-1})\cos^6\theta_{j-1} + k^2(d)\cos^6\theta_j] \tag{4.30}$$

However, the first and last receiver only have one neighboring node. This is equivalent to assume that their second adjacent node is located in infinity and consequently it does not receive power from it due to very long distance. In other words, if the distance of neighboring node tends to infinity, θ tend to 90° and hence the last part in Equation 4.30 tends to zero. Therefore, the nodes at either edges receives power from the transmitter directly and only one neighboring node. Therefore, equation (4.30) may be applied to all nodes.

Experiments were conducted using the hardware set up shown in Figure 4.8 consisting of 7 receiving coils. Using AEE method, the received power profile is an

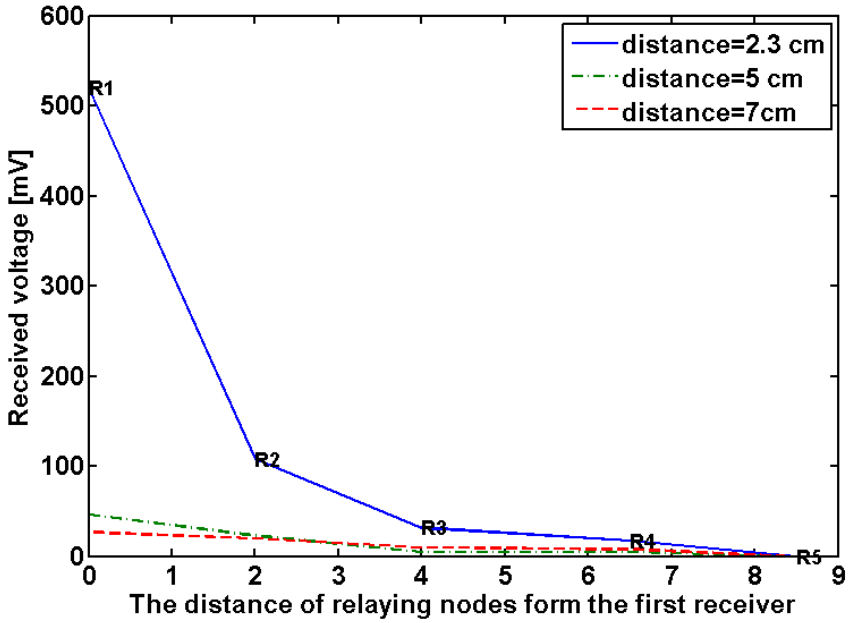

Figure 4.9 Array Edge Excited (measured voltage)

exponential decay and has a maximum value at the node located at the array edge, directly opposite the transmitter. With the transmitter input voltage of 30 mV and the receiving array located at 2.3 cm from it, the highest received voltage is 520 mV, a voltage gain of 17.3 at the bore site of transmitter (see Figure 4.8) The x-axis in Figure 4.8 shows the location of each relaying nodes from the node at the bore sight of the transmitter in cm. y-axis, shows the voltage induced in each coil at three different distances from the transmitting coil (the distance between transmitter and the first node in the waveguide array: 2.3 cm, 5 cm, 7 cm).

The receiving array was moved to 5 cm from the transmitter, and the received voltage at bore sight measured 46 mV, a gain of 1.53 when compared with the input voltage (Figure 4.8). The receiving array again was moved to 7 cm from the transmitter, and the received voltage at the bore sight of transmitter was measured 27 mV, a gain of 0.9 when compared with the input voltage (Figure 4.8).

4.3.2 Array Centre Excitation

In the ACE method, the relaying nodes are excited from the centre of array by lining up the transmitter at a distance d directly opposite the relay node at the middle of

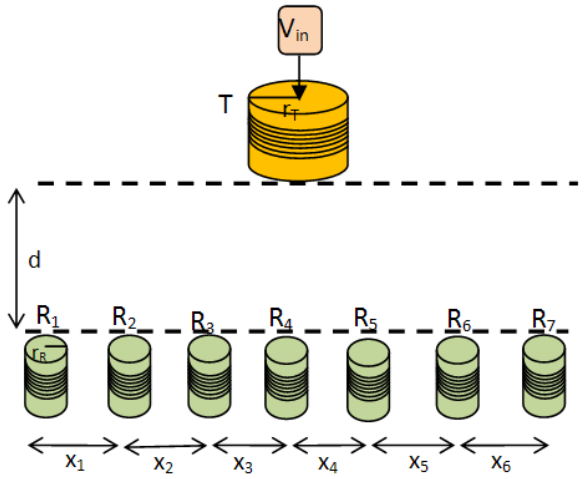

Figure 4.10 Array Centre Excited

array as shown in Figure 4.10. The objective of this design might be to achieve single input multiple output communication.

The power received by the receiving nodes are given by the following expressions (from the left) [62].

Receiver 1:

$$\frac{P_{R1}}{P_T} \approx \frac{Q^2k^2\left(d_1\right)\cos^6\theta_1}{2} + \frac{Q^2k^2\left(x\right)}{2} \times \frac{Q^2k^2\left(d2\right)\cos^6\theta_2}{2} \tag{4.31}$$

Receiver 2:

$$\frac{P_{R2}}{P_T} \approx \frac{Q^2k^2\left(d_2\right)\cos^6\theta_2}{2} + \frac{Q^2k^2\left(d_1\right)\cos^6\theta_1}{2} \times \frac{Q^2k^2\left(x\right)}{2} + \frac{Q^2k^2\left(d_3\right)\cos^6\theta_3}{2} \times \frac{Q^2k^2\left(x\right)}{2} \tag{4.32}$$

Receiver 3:

$$\frac{P_{R3}}{P_T} \approx \frac{Q^2k^2\left(d_3\right)\cos^6\theta_3}{2} + \frac{Q^2k^2\left(d_2\right)\cos^6\theta_2}{2} \times \frac{Q^2k^2\left(x\right)}{2} + \frac{Q^2k^2\left(d_4\right)\cos^6\theta_4}{2} \times \frac{Q^2k^2\left(x\right)}{2} \tag{4.33}$$

Since $\alpha = \frac{Q^2}{2}$ and $\beta = \frac{Q^2k^2(x)}{2}$, then above equation may be simplified to:

$$\frac{P_{R3}}{P_T} = \alpha\left[\beta k^2\left(d_2\right)\cos^6\theta_2 + \beta.k^2\left(d_4\right)\cos^6\theta_4 + k^2\left(d_3\right)\cos^6\theta_3\right] \tag{4.34}$$

In general, for the ith section in the array, the received power is [62]:

$$\frac{P_{Ri}}{P_T} \approx \alpha\left[\beta k^2\left(d_{i+1}\right)\cos^6\theta_{i+1} + \beta.k^2\left(d_{i-1}\right)\cos^6\theta_{i-1} + k^2\left(d_i\right)\cos^6\theta_i\right] \tag{4.35}$$

If the receiving array is symmetrical around the transmitter axis, the total received power at the middle array element (at the bore-sight of transmitter) is [62]:

$$\frac{P_{R(bs)}}{P_T} \approx \alpha\left[\beta k^2\left(d_{bs+1}\right)\cos^6\theta_{bs+1} + \beta.k^2\left(d_{bs-1}\right)\cos^6\theta_{bs-1} + k^2\left(d_{bs}\right)\right] \tag{4.36}$$

Using an ACE, the received power profile is parabolic and has a peak, centered at the middle coil. With a transmitter input voltage of 30 mV and the receiver array located at 2.3 cm from it, the highest received voltage is 1000 mV (1 volt), a voltage gain of 33.3 at bore-sight (see Figure 4.11). The receiving array was moved to 5

cm from the transmitter, and the received voltage at the bore sight of transmitter was 120 mV, a gain of 4 when compared with the input voltage (Figure 4.11). The receiving array was moved further to 7 cm from the transmitter, and the received voltage at the bore sight of transmitter was measured 40 mV, a gain of 1.33 when compared with the input voltage (Figure 4.11). In general, although the transmitted signal degrades with the $6th$ power of distance for MI transmissions, the received power can be enhanced by using an array of receivers and a proper voltage excitation method. Table 4.1 shows the mean value of voltage received at each node in both scenarios and at different distances; this was repeated several times.

According to the observed data, it can be concluded that higher voltage at each receiver is achieved through the ACE. In this case the distance between transmitter and half of the receivers reduce, therefore the angle is also decreases, which results in higher received power at each node (*power* $\propto$ *voltage*).

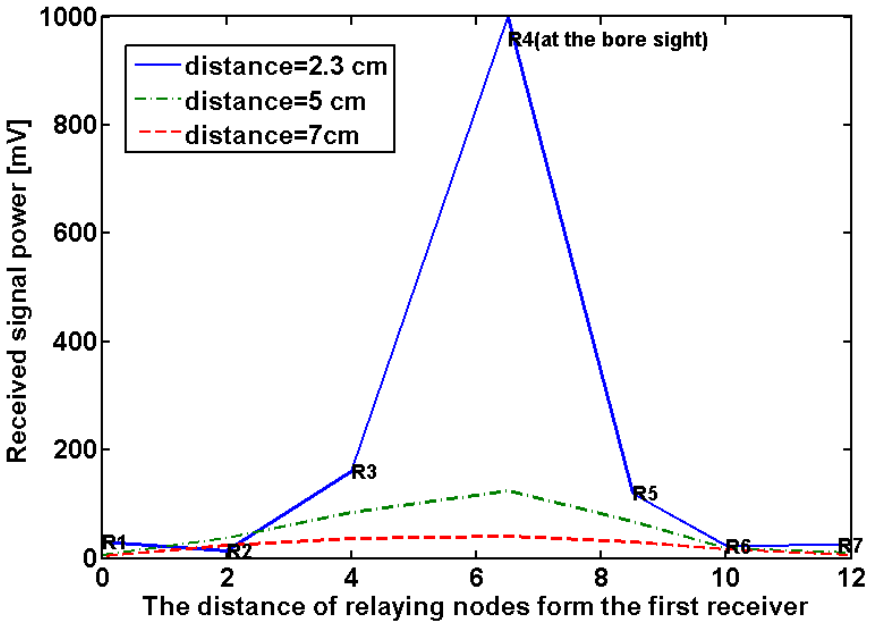

Figure 4.11 Array Centre Excited (measured voltage)

Table 4.1 AEE and ACE received voltages (Note: N indicates Noise)

Nodes	**Voltage measured at the nodes (mV), at distance=23 mm**		**Voltage measured at the nodes (mV), at distance=7 mm**		**Voltage measured at the nodes(mV), at distance=5 mm**	
	AEE	ACE	AEE	ACE	AEE	ACE
R1(at the bore sight of transmitter in AEE)	520	30	46	6	27	4
R2	108	13	23	37	20	24
R3	32	160	5	84	10	36
R4(at the bore sight of transmitter in ACE)	17	1000	5	124	8	40
R5	N	120	N	68	N	30
R6	N	23	N	18	N	16
R7	N	25	N	10	N	6

4.3.3 Collinear Array Excitation

In the CAE (as is in conventional waveguide system), the transmitter x-axis is collinear with the waveguide array x-axis and the coils form a linear chain network of MI

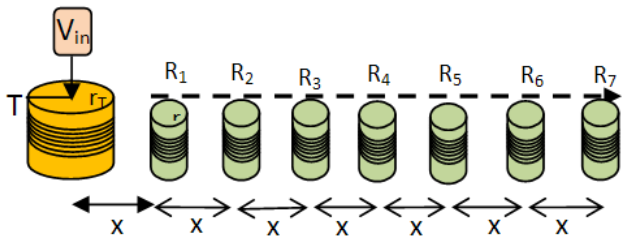

Figure 4.12 Collinear Array Excited

nodes. All the array elements including the transmitter (first node) are separated from each other by a constant designed distance x.

The power received at the first receiver is [62]:

$$P_{R1} \approx \frac{Q^2 k^2 (x)}{2} P_T \tag{4.37}$$

and the second node receives its power from the *receiver 1* [62]:

$$P_{R2} \approx \frac{Q^2 k^2 (x)}{2} P_{R1} = \left(\frac{\pi^2 k^2 (x)}{2} \right)^2 P_T \tag{4.38}$$

Therefore, the received power at the nth relaying node is [62]:

$$P_{Rn} \approx \frac{Q^2 k^2 (x)}{2} P_{R(n-1)} = \left(\frac{Q^2 k^2 (x)}{2} \right)^n P_T \tag{4.39}$$

If there are $n+1$ sections (i.e. n relaying nodes), then the received power at the final node (nth) is [62],

$$P_{Rn} \approx \left(\frac{1}{2} \right)^n \left(Q^2 k^2 (x) \right)^n P_T \tag{4.40}$$

This arrangement has a power expression similar to the magneto inductive waveguide and it may be viewed as a magnetic waveguide [6, 7, 7, 44], which is previously discussed in details.

4.4 Summary

This chapter has proposed link budget models for a waveguide transmission system under different section path loss (β) approximations. It is discussed that it is unrealistic to have $\beta >> 2$ or $\beta = 2$. Therefore, based on a realistic approximation, a link budget model is developed and the performance is studied. It is shown that the waveguide method may work inversely if the so called *distance threshold* is exceeded (due to the power reflection). However, it is shown that the distance threshold is a function of coil characteristics and can be extended. This chapter also discusses that if the waveguide transmission line is terminated properly, the power reflection may be minimised, hence, the waveguide method works properly.

Also in this chapter, three voltage excitation methods -AEE, ACE and CAE- are proposed and their performances have been measured and compared. It is shown that if the array of antennas (waveguide system) is excited from the centre, highest voltage is received at each receiving node among the three methods, while in CAE (conventional placement of waveguide) the voltage received at the receiving nodes are minimum compared to the other two methods.

Chapter 5

Multihop Relay Techniques for Communication Range Extension in NFMIC

5.1 Chapter Overview

Conventional waveguide model is not directly applicable to a BAN for communication range extension. Although it may be useful for fixed sensor networks, such as in pipelines for leakage detection or underground communications in mining application, it may not be directly applied to a BAN, where the nodes may change their location in a 3D environment. Furthermore, they may have angular and lateral displacement in respect to each other. Angle and lateral misalignments may result in performance reduction, and achieving a perfect antenna alignment may not be guaranteed for a BAN. Since conventional magneto inductive waveguide model is not directly applicable to a BAN, in this chapter, cooperative communication methods for a BAN are proposed. Here, NFMIC cooperative communications is approached from two perspectives. Firstly, when a direct LoS exists between the original transmitter and target receiver, and secondly, when the target receiver is out of the direct communication range of transmitting node (NLoS). Three different methods of cooperative communications are proposed for each approach: Magnetic Induction Relay, Master/Assistant Magnetic Induction Relay 1 and 2.

In order to model the cooperative network, different antenna displacements need to be taken into account. Hence, this chapter discusses a point-to-point NFMIC propagation model, where lateral and angular displacement exist. Then, this is used to model the signal propagation for the three relaying methods. The effect of each antenna displacement on each cooperative communication technique is discussed. Firstly, the relay selection is performed based on either separation distance, lateral or angle displacement and performance of each technique is studied and then a new relay selection metric -*relay link indicator*- is proposed that takes into consideration the three factors of separation distance as well as the lateral and angle displacement.

5.2 NFMIC Cooperative Communications

5.2.1 Description of the System

The network consists of a number of nodes, however, for simplicity it is assumed that only 4 nodes contribute to the cooperative communication: a transmitter (source), a receiver (final destination) and two intermediate nodes, which function as cooperative relay nodes. The source and destination are separated from each other by a distance d. However, it is assumed that there are two idle devices between source and sink, which can be exploited to assist the communication by providing an indirect path from the transmitter to the receiver over which information may be relayed. The transmitter is separated from the relay 1 and 2 by a distance $x_{Tx,R1}$ (x-component of the distance) and $x_{Tx,R2}$ respectively, and the receiver is located at a distance $x_{R1,Rx}$ and $x_{R2,Rx}$ from relay 1 and 2 respectively. Relay 1 ($R1$) is assumed to be located closer to the transmitter and R2 is placed closer to the receiver such that any distance-dependent differences in performance may easily be evaluated. Both the source and sink have a direct link with relay 1 and 2. To avoid frequency spectrum contention, it is assumed that the network uses Time Division Multiple Access (TDMA) for channel allocation for each transmission. However, the transmission system requires precise synchronization, which is beyond the scope of this work.

As is usual in single-channel wireless systems a half duplex transmission system is used, meaning that a node can either transmit or receive data during a specific time slot, but cannot do both simultaneously. A relay node receives the signal from the transmitter, amplifies it and then forwards it to the next hop, which can be the final receiver or another relay node (as discussed in chapter 2 this is known as the AF cooperative relaying technique) [75].

Three different relaying methods will be evaluated in this network model to show how the idle intermediate nodes may be used to extend the coverage range and channel data rate. The three techniques are denoted Magnetic Induction Relay (MI Relay), Master/Assistant Magnetic Induction Relay 1 (MAMI Relay1) and Master/Assistant Magnetic Induction Relay 2 (MAMI Relay2). The three proposed cooperative communication strategies are studied for two different scenarios, when a direct LoS exist between the source and sink, as well as the case when the final receiver is out of the direct LoS of source node (NLoS). In the former case, cooperative communication may be used to enhance the capacity. By contrast, in the later case, the aim may be to increase the communication range through cooperative relaying.

5.2.1.1 Peer-to-Peer Communication Model with Lateral and Angular displacement in a 3D environment

To be able to apply NFMIC cooperative communications to a BAN, it is required to model the NFMIC in a 3D environment. Therefore, in this section, first a peer to peer communication model is described, then, this is used to model a multihop NFMIC system. Figure 5.1 illustrates an ideal near field magnetic induction communication system, in which there is no angle and lateral misalignment between the transmitting and receiving antenna coils. The system consists of a transmitter and a receiver separated from each other by distance d. The circuit model of such systems is also shown in Figure 5.1.

According to [9], the power transfer function for this scenario is:

$$\frac{P_{Rx}}{P_{Tx}} = \frac{\mu_0^2 N_T^2 N_R^2 A_R^2 \omega^2}{16\pi^2 R_{Tx} R_{Rx}} H_{INT}^2 \tag{5.1}$$

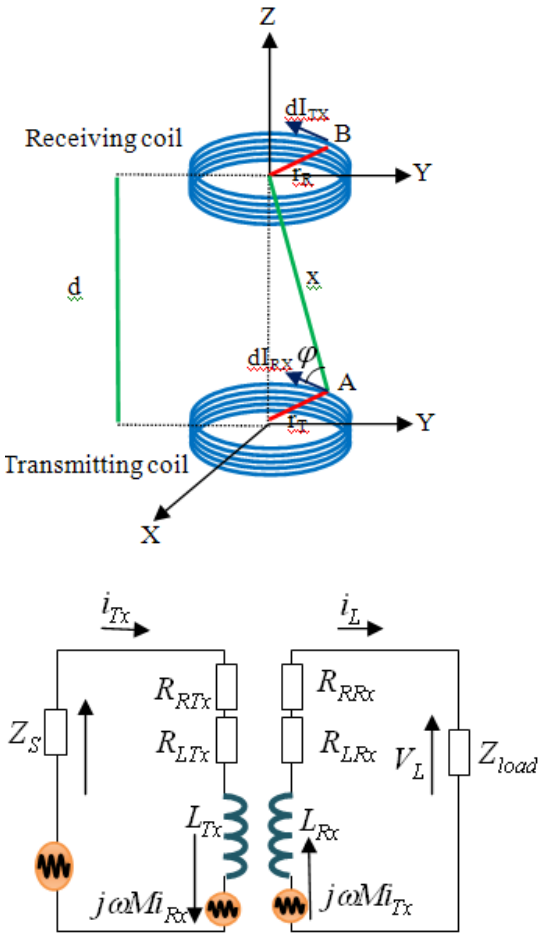

Figure 5.1 ideal transmitting and receiving coil configuration and the circuit model (adapted from [9])

where the magnetic field strength is [9]:

$$H_{INT} = \int_0^{\pi} \frac{\mathrm{dI_{Tx}} \times \mathrm{x}}{\mathbf{x}^3} = \sqrt{\frac{r_T^4 \pi^2}{\left(r_T^2 + d^2\right)^3}} \tag{5.2}$$

The cross sectional area of the receiving coil is:

$$A_R = 2 \cdot \pi \cdot r_R^2 \tag{5.3}$$

The total resistance at the receiving and transmitting circuits are:

$$R_{Rx} = (2 \cdot \pi \cdot r_R \cdot N_R \cdot R_0) + R_L \tag{5.4}$$

$$R_{Tx} = (2 \cdot \pi \cdot r_T \cdot N_T \cdot R_0) + R_S \tag{5.5}$$

R_L and R_s are the resistance of load and source respectively and r_R, r_T, N_T, N_R, are the radius and number of turns of the receiving and transmitting circuit respectively. R_0 is the resistance of wires per unit of length. Therefore, the power transfer function for an ideal communication link becomes [9]:

$$\frac{P_{Rx}}{R_{Tx}} = \frac{\mu_0^2 \cdot N_T^2 \cdot N_R^2 \cdot r_R^4 \cdot \omega^2 \cdot r_T^4}{16.R_{Tx} \cdot R_{Rx} \cdot (r_T^2 + d^2)^3} \tag{5.6}$$

As discussed in chapter 2 and 3, the power transfer function can also be expressed as [16, 17]:

$$\frac{P_{Rx}}{R_{Tx}} = Q_T Q_R k^2 \tag{5.7}$$

where k is the coupling coefficient and Q_T and Q_R denote the quality factor of the transmitting and receiving antennas [17]:

$$Q_T = \frac{\omega L_T}{R_{Tx}} = \frac{\omega \left(\mu_0 \pi N_T^2 r_T^2\right)}{l_T R_{Tx}} \tag{5.8}$$

$$Q_R = \frac{\omega L_R}{R_{Rx}} = \frac{\omega \left(\mu_0 \pi N_R^2 r_R^2\right)}{l_R R_{Rx}} \tag{5.9}$$

L_T and L_R are the inductance of the transmitting and receiving coils respectively and l_T and l_R are the length of the two coils. Thus, by substituting Q-factor in the power equation, the power transfer function reduces to:

$$\frac{P_{Rx}}{R_{Tx}} = Q_T Q_R \frac{r_T^2 r_R^2 l_T l_R}{16(r_T^2 + d^2)^3} \tag{5.10}$$

Hence, the coupling coefficient may be expressed as:

$$k = \sqrt{\frac{r_T^2 r_R^2 l_T l_R}{16(r_T^2 + d^2)^3}} \tag{5.11}$$

In reality achieving a perfect antenna alignment is difficult and this results in some degrees of performance reduction in terms of achievable communication range or data rates. There are two main sources of performance degradation known as *angle* and *lateral* misalignment. This chapter is made of two sections: when only lateral

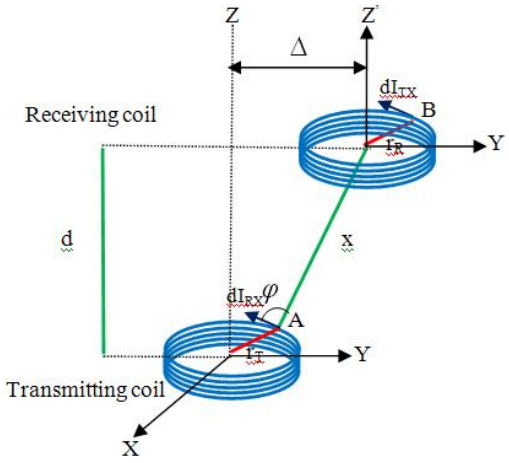

Figure 5.2 Lateral Misalignment (adapted from [9])

displacement exist (perfect angle alignment) and when there are both lateral and angle misalignment.

When there is lateral misalignment (Figure 5.2), the x and y component of the receiver plane are parallel to the transmitting antenna coil plane. Therefore, they have no contribution in flux cutting through the receiving coil. In fact, the dominating component will be the z-component [9]. According to [9], the power transfer function in this case is,

$$\frac{P_{Rx}}{R_{Tx}} = \frac{\mu_0^2 \cdot N_T^2 \cdot N_R^2 \cdot r_R^4 \cdot \omega^2 \cdot m^2}{64 . R_{Tx} \cdot R_{Rx} \cdot r_T \cdot \Delta^3} \cdot \left[\Delta \cdot K + \frac{(r_T \cdot m) - (2-m)\Delta}{2-2m} \cdot E\right]^2 \tag{5.12}$$

where K and E are the complete elliptic integrals of the first and second kind respectively, and m is the elliptic modulus and is always a positive value between 0 and 1 [9]. The equivalent equations for this three parameters are shown in the following equations:

$$K(m) = \int_0^{\pi/2} \frac{d\gamma}{\sqrt{1 - m^2 \sin^2\gamma}}; \; 0 \leq m \leq 1 \tag{5.13}$$

$$E(m) = \int_0^{\pi/2} \sqrt{1 - m^2 \sin^2\gamma} \cdot d\gamma \,; 0 \leq m \leq 1 \tag{5.14}$$

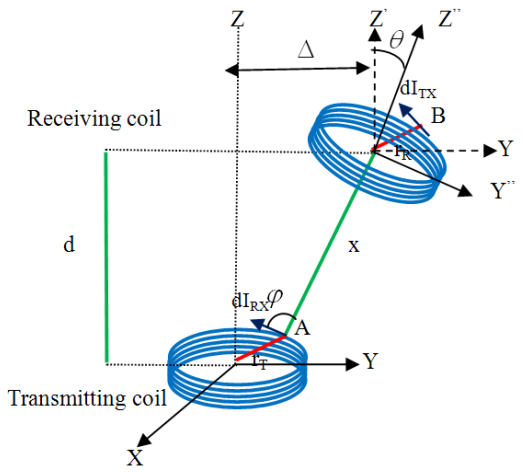

Figure 5.3 Angle Misalignment (adapted from [9])

$$m = \left[\frac{4 \cdot r_T \cdot \Delta}{(r_T + \Delta)^2 + d^2}\right]; 0 \leq m \leq 1 \tag{5.15}$$

To simplify the power transfer function, the Q-factor is substituted in the power equation and therefore it becomes $P_{Rx} = R_{Tx} Q_T Q_R k^2$. In this case, the coupling coefficient is,

$$k^2 = \frac{r_R^2 \cdot \Delta^2 \cdot l_T \cdot l_R}{16.\pi^2 \cdot \left((r_T+\Delta)^2+d^2\right)^2 \cdot r_T \cdot \Delta^3} \cdot \left[\Delta \cdot K + \frac{(r_T \cdot m)-(2-m)\Delta}{2-2m} \cdot E\right]^2 \tag{5.16}$$

When there is an angular displacement (Figure 5.3) at the receiver (in respect to the transmitter), the x and y components of magnetic field vector cancel out each other, as a result of the circular symmetry at the centre of the receiving antenna coil [9]. Hence, according to [9], the z-component of magnetic field with angle misalignment of α, is expressed as [9]:

$$H_{INT-AMz} = \sqrt{\frac{r_T^4 \pi^2}{\left(r_T^2 + d^2\right)^3}} \cdot \cos\alpha \tag{5.17}$$

Therefore, in this case, the power transfer function becomes [9]:

$$\frac{P_{Rx}}{R_{Tx}} = \frac{\mu_0^2 \cdot N_T^2 \cdot N_R^2 \cdot r_R^4 \cdot \omega^2 \cdot r_T^4}{16.R_{Tx} \cdot R_{Rx} \cdot \left(r_T^2 + d^2\right)^3} \cdot \cos^2\alpha \tag{5.18}$$

By substituting the Q-factor in the above equation, it is expressed as:

$$\frac{P_{Rx}}{R_{Tx}} = Q_T Q_R \frac{r_T^2 r_R^2 l_T l_R}{16(r_T^2 + d^2)^3} \cdot \cos^2\alpha \tag{5.19}$$

This results in the coupling coefficient to be,

$$k = \sqrt{\frac{r_T^2 r_R^2 l_T l_R}{16(r_T^2 + d^2)^3} \cdot \cos^2\alpha} \tag{5.20}$$

In [9], the power transfer function for the case, when there is both angle and lateral misalignment has not been discussed. In [76], the authors analyse the case when both angle and lateral misalignment exist. However, in [76], it is assumed that $\Delta < r_T$ in their analysis, while Δ can be larger than the radius of transmitter in real applications, such as a BAN. This model cannot be applied when $\Delta \geq r_T$. Therefore, the same method as in [76] is used in this work in order to model both angle and lateral misalignment for any values of Δ, regardless of its relationship with radius of the transmitting coil.

When there is an angle misalignment, then the power transfer function is proportional to the cosine square of the angle:

$$\frac{P_{Rx}}{R_{Tx}} \propto k^2 \propto \cos^2\alpha \tag{5.21}$$

Therefore, a proper approximation is to scale the power transfer function by $\cos^2\alpha$, when there is a lateral misalignment. Hence, if there are both angle and lateral misalignment the power transfer function is estimated as,

$$\frac{P_{Rx}}{R_{Tx}} = Q_T Q_R \frac{r_R^2 \Delta^2 l_T l_R}{16\pi^2\left((r_T + \Delta)^2 + d^2\right)^2 r_T \Delta^3} \left[\Delta K + \frac{(r_T m) - (2-m)\,\Delta}{2 - 2m} E\right]^2 \cos^2\alpha \tag{5.22}$$

This implies that the coupling coefficient is scaled by $\cos\alpha$, and it casts as:

$$k = \sqrt{\frac{r_R^2 \Delta^2 l_T l_R}{16\pi^2\left((r_T + \Delta)^2 + d^2\right)^2 r_T \Delta^3} \left[\Delta K + \frac{(r_T m) - (2-m)\,\Delta}{2 - 2m} E\right]^2 \cos^2\alpha} \tag{5.23}$$

The model, as discussed above, is used to develop three multihop communication methods for NFMIC in order to extend the communication range and enhance data rates. In Section 5.2.2 , the methods are studied for NLoS case to enhance the communication range and in Section 5.2.3 the same strategies are applied when all the receiving nodes are in the direct LoS of the original source. In this case, higher data rates may be the primary objective of cooperative communications within the network.

5.2.2 NLoS NFMIC Multihop Relay Strategies

5.2.2.1 NLoS MI-Multihop Relay

Figure 5.4 illustrates the transmission system described previously in Section 5.2.1. In this scenario, transmission to an out of range receiver is required. Here the transmission to the target receiver is achieved through two time phases:

Phase 1: the transmitter broadcasts the signal to all nodes and the nodes within its transmission range receive the signal (R1 and R2 in this case).

Phase 2: the selected receiving relay (R1 or R2), which has a direct line of sight with the target receiver, amplifies and forwards the data to the final destination. According to the following theoretical analysis and simulation results in section Section 5.3.1, it will be determined later, which relay node can achieve higher received signal strength

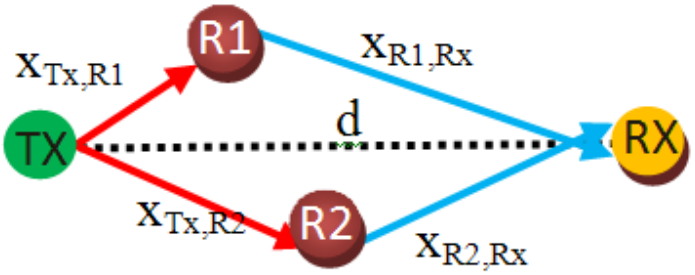

Figure 5.4 NLoS-MI Relay

(RSS) and hence longer communication range. The relay selection may be done based on different metrics such as the separation distance, relative lateral and angular displacement of the relaying nodes in respect to the transmitter, and/or receiver.

Phase 1: During the first phase, the transmitting antenna coil (which has a quality factor Q_{Tx} and efficiency η_{Tx}) sends the data to relays R1 and R2 through magnetic field coupling with transmission power P_{Tx}. Let the transmitting antenna gain to be:

$$G_{Tx} = Q_{Tx}\eta_{Tx} \tag{5.24}$$

Similarly the gain of the relaying antennas i is defined as:

$$G_{Ri} = Q_{Ri}\eta_{Ri} \tag{5.25}$$

According to model described in Section 5.2.2.1, the received signal power at R1 from the transmitter (Tx) is:

$$P_{R1}^{Tx} = P_{Tx}G_{Tx}G_{R1}k_{Tx,R1}^2(x_{Tx,R1}) \tag{5.26}$$

where $k_{i,j}^2(x_{i,j})$ is the coupling coefficient for any given node i (transmitter) and j (receiver), at distance $x_{i,j}$ and is defined as [9, 76]:

$$k_{i,j}^2(x_{i,j}) = S_{i,j} \cdot W_{i,j} \cdot \cos^2\alpha_{i,j} \tag{5.27}$$

where,

$$S_{i,j} = \frac{r_j^2 \cdot \Delta_{i,j}^2 \cdot l_i \cdot l_j}{16.\pi^2 \cdot \left(\left(r_i + \Delta_{i,j}\right)^2 + x_{i,j}^2\right)^2 \cdot r_i \cdot \Delta_{i,j}^3} \tag{5.28}$$

$$W_{i,j} = \left[\Delta_{i,j} \cdot K + \frac{(r_i \cdot m_{i,j}) - (2 - m_{i,j})\,\Delta_{i,j}}{2 - 2m_{i,j}} \cdot E\right]^2 \tag{5.29}$$

In this case $m_{i,j}$ is (for the given transmitting node i and receiving node j):

$$m_{i,j} = \left[\frac{4 \cdot r_i \cdot \Delta_{i,j}}{\left(r_i + \Delta_{ij}\right)^2 + x_{i,j}^2}\right] \tag{5.30}$$

where $0 \leq m_{i,j} \leq 1$, and $\Delta_{i,j}$ is the lateral misalignment between node i and j (Figure 5.2) and $x_{i,j}$ is the separation distance between node i and j on the x-axis.

Similarly the received power at R2 will be:

$$P_{R2}^{Tx} = P_{Tx} G_{Tx} G_{R2} k_{Tx,R2}^2(x_{Tx,R2}) \tag{5.31}$$

Phase 2: based on the relay selection criterion, which in this study could be the separation distance between the relay and transmitter/receiver, angular or lateral misalignment, one of the intermediate nodes is selected to forward the data to the final receiver.

If R1 is selected as the cooperative relay, the final received signal power at the receiver is estimated as:

$$\begin{aligned} P_{Rx}^{R1} &= P_{R1}^{Tx} G_{Rx} G_{R1} k_{Rx,R1}^2 \\ P_{Rx}^{R1} &= \left(P_{Tx} G_{Tx} G_{R1} k_{Tx,R1}^2\right) G_{Rx} G_{R1} k_{Rx,R1}^2 \end{aligned} \tag{5.32}$$

which may be further simplified to:

$$P_{Rx}^{R1} = G^t G_{R1}^2 k_{Tx,R1}^2 k_{Rx,R1}^2 \tag{5.33}$$

where,

$$G^t = P_{Tx} G_{Tx} G_{Rx} \tag{5.34}$$

However, if R2 is selected, the received signal power is:

$$P_{Rx}^{R2} = G^t G_{R2}^2 k_{Tx,R2}^2 k_{Rx,R2}^2 \tag{5.35}$$

Therefore, in general the received power at the destination through relay i will be:

$$P_{Rx}^{Ri} = G^t G_{Ri}^2 k_{Tx,Ri}^2 k_{Rx,Ri}^2 \tag{5.36}$$

5.2.2.2 NLoS-MAMI (Master-Assistant Magnetic Induction) Relay1

Another cooperative relaying technique can be applied to utilize two idle nodes in the network to enhance the system performance, compared to relaying through only one node. The system is shown in Figure 5.5. Transmission of information is now achieved in three phases:

Phase1: The transmitter broadcasts the signal to all nodes in its communication range. Both idle devices which are in the listening state can receive the data from the transmitter.

Phase2: R1 and R2 receive the data; one of the relay nodes (Relay Assistant) amplifies and forwards the data to the other relay (Relay Master) as well as to the final destination. The selection of each node, to act as a relay master or relay assistant impacts the achieved communication distance, and this needs to be done based on an optimum metric. This concept is studied in Section 5.4.

Phase3: The relay master receives the data, amplifies it and forwards it to the final receiver. The receiver (Rx) receives the signal and combines it with the previously arrived copy of the same signal and decodes it.

Therefore, in this scenario, the receiver receives the signal from two different paths via the two relay nodes.

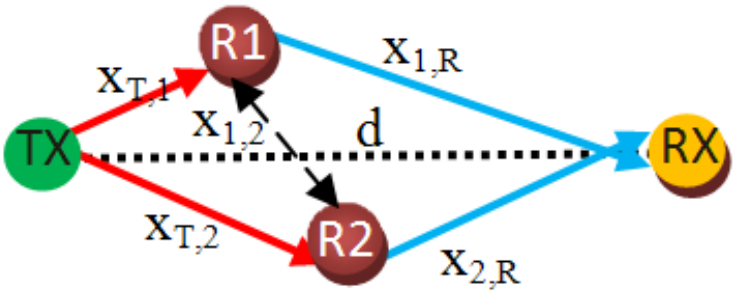

Figure 5.5 NLoS- MAMI Relay1

In phase 1, the strength of the signal received by each relay node is the same as Equation 5.26 and 5.31. However, in stage 2, where the signal is transmitted from the relay assistant to the relay master and the destination, the received signal power at the relay master via the relay assistant is:

$$\begin{aligned} P_{Rm}^{Ra} &= P_{Ra}^{Tx} G_{Ra} G_{Rm} k_{Ra,Rm}^2 \\ P_{Rm}^{Ra} &= P_{Tx} G_{Tx} G_{Ra}^2 G_{Rm} k_{Tx,Ra}^2 k_{Ra,Rm}^2 \end{aligned} \tag{5.37}$$

Similarly, the received power at the final destination through the relay assistant at this stage (S2) is:

$$\begin{aligned} P_{Rx}^{Ra} &= P_{Ra}^{Tx} G_{Rx} G_{Ra} k_{Rx,Ra}^2 \\ P_{Rx}^{Ra} &= P_{Tx} G_{Tx} G_{Ra}^2 k_{Tx,Ra}^2 G_{Rx} k_{Rx,Ra}^2 \end{aligned} \tag{5.38}$$

The relay master now combines the signal received directly from the transmitter with the signal from the relay assistant and forwards the combined signal to the final receiver. Therefore, the signal power at the relay master during this phase is:

$$\begin{aligned} P_{Rm-total}^{S2} &= P_{Rm}^{Ra} + P_{Rm}^{Tx}; \\ P_{Rm-total}^{S2} &= P_{Tx} G_{Tx} G_{Rm} \left(G_{Ra}^2 k_{Tx,Ra}^2 k_{Ra,Rm}^2 + k_{Tx,Rm}^2 \right) \end{aligned} \tag{5.39}$$

In the last phase (stage 3), the relay master sends the signal received in stage 1 and 2 on to the final destination. Receiver receives and decodes it. The received signal power at this stage at the final receiver is estimated by:

$$\begin{aligned} P_{Rx}^{total} &= \left(P_{Rx}^{Ra} + P_{Rx}^{Rm} \right); \\ P_{Rx}^{Rm} &= P_{Rm-total}^{S2} G_{Rx} G_{Rm} k_{Rx,Rm}^2 \end{aligned} \tag{5.40}$$

By substituting the equivalent equations for P_{Rx}^{Ra} and P_{Rx}^{Rm} into Equation 5.40, the received power at the receiver becomes:

$$P_{Rx}^{total} = G^t \left(k_{Tx,Ra}^2 k_{Rx,Ra}^2 G_{Ra}^2 + k_{Rx,Rm}^2 \beta \right) \tag{5.41}$$

where $\beta = G_{Rm}^2 \left(G_{Ra}^2 k_{Tx,Ra}^2 k_{Ra,Rm}^2 + k_{Tx,Rm}^2 \right)$.

5.2.2.3 NLoS-MAMI (Master-Assistant Magnetic Induction) Relay2

The final cooperative communication technique that can be applied in such systems is denoted MAMI Relay2. This method is suitable where there is no direct link between one of the intermediate nodes and the target receiver (although it still works in the case where there is a direct line of sight between the receiver and both relay nodes). However, even if there is a direct LoS between the relay assistant and the receiver, Ra does not transmit to the receiver; transmission to the final receiver is performed only through the relay master. Transmission is achieved in three phases:

Phase 1: The transmitter broadcasts the signal to the idle intermediate nodes. Both R1 and R2 receive the signal. The received power at Ra is given by:

$$P_{Ra}^{Tx} = P_{Tx} G_{Tx} G_{Ra} k_{Tx,Ra}^2 \tag{5.42}$$

While at the relay master (Rm), it is

$$P_{Rm}^{Tx} = P_{Tx} G_{Tx} G_{Rm} k_{Tx,Rm}^2 \tag{5.43}$$

Phase 2: The relay assistant, which is the relay with no direct link with the receiver, forwards the received data to Rm. The difference between MAMI Relay1 and MAMI Relay2 methods is that in stage 2 in MAMI Relay2, the relay assistant does *not* transmit to the final destination (unicast transmission to the Rm), while in MAMI

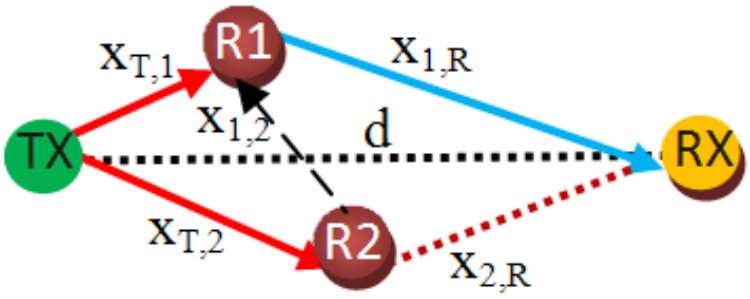

Figure 5.6 NLoS- MAMI Relay2

Relay1, both receiver and relay master receive data from the relay assistant in phase 2 (broadcast or multicast). The received signal power at the relay master via relay assistant during this stage is:

$$P_{Rm}^{Ra} = P_{Ra}^{Tx} G_{Ra} G_{Rm} k_{Ra,Rm}^2 \tag{5.44}$$

Since the transmission power at this stage is equal to the signal power received by the relay assistant at the previous stage, Equation 5.44 can be rewritten as:

$$P_{Rm}^{a} = P_{Tx} G_{Tx} G_{Rm} G_{Ra}^2 k_{Tx,Ra}^2 k_{Ra,Rm}^2 \tag{5.45}$$

Phase 3: The relay master combines the signals, received through Tx and Ra in stage 1 and 2, and forwards it to the final destination. The total signal power received by the relay master at this stage is:

$$\begin{aligned} P_{Rm}^{S2} &= P_{Rm}^{Tx} + P_{Rm}^{Ra}; \\ P_{Rm}^{S2} &= P_{Tx} G_{Tx} G_{Rm} \left(k_{Tx,Rm}^2 + G_{Ra}^2 k_{Tx,Ra}^2 k_{Ra,Rm}^2 \right) \end{aligned} \tag{5.46}$$

The target receiver receives the signal relayed by the relay master and decodes it. The received signal power at the target destination at this stage is:

$$\begin{aligned} P_{Rx}^{total} &= P_{Rm}^{S2} G_{Rx} G_{Rm} k_{Rm,Rx}^2 \\ P_{Rx}^{total} &= \left(G^t G_{Rm}^2 k_{Rm,Rx}^2 \left(k_{Tx,Rm}^2 + G_{Ra}^2 k_{Tx,Ra}^2 k_{Ra,Rm}^2 \right) \right) \end{aligned} \tag{5.47}$$

Using Matlab, the propagation model has been simulated for each of the three methods, in order to compare the performance of the proposed relaying strategies. The results are shown and discussed in Section 5.3.1. However, in the following section these three methods are studied for the case, when direct LoS exist between the original transmitter and the target receiver.

5.2.3 LoS NFMIC Multihop Relay Strategies

In the LoS scenario, although the receiver may receive information directly from the source, data rates may not be sufficient due to low RSS, which results from long

distance between the transmitter and receiver (Rx may be located at the coverage edge of the Tx). Thus, cooperative communication may be used to enhance RSS and subsequently data rates.

5.2.3.1 LoS-MI Relay

Figure 5.7 illustrates an LoS MI-Relay system. In comparison with NLoS-MI Relay, the receiver receives the transmitted data through two independent paths: directly from the source and also via a relaying node. This is performed through two steps or two time phases:

Phase1: transmitter broadcast the message to all nodes and each node including the final receiver receive the signal.

Phase2: selected relay -either relay1 or relay2- send the message to the final receiver, and the target receiver combines the two copies of received signal.

Phase1: the transmitter broadcasts the message to all nodes. R1, R2 and Rx, which are at the listen state, receive the transmitted signal. However, the received signal strength is different at each node. Since the final receiver is assumed to be around the edge of communication, the received power at the target receiver may be minimum

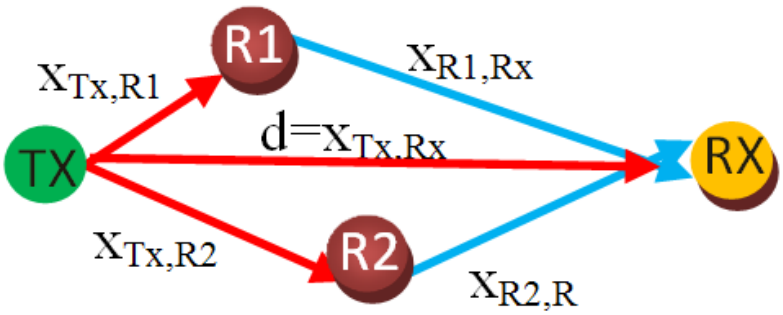

Figure 5.7 LoS-MI Relay

among all receiving nodes at this stage. Let the gain of transmitting and relaying antenna be defined as Equation 5.24 and 5.25. Similarly the gain of receiver is defined as:

$$G_{Rx} = Q_{Rx}\eta_{Rx} \tag{5.48}$$

Where Q_{Rx} and η_{Rx} are the quality factor and efficiency of final receiver.

The received signal power at each relaying node is estimated using Equation 5.26 and 5.31, and the received signal power at the final receiver at this stage is:

$$P_{Rx}^{Tx} = P_{Tx}G_{Tx}G_{Rx}k_{Tx,Rx}^2 \tag{5.49}$$

The coupling coefficient is estimated using Equation 5.27, where i denotes the transmitting node index and j denotes the receiving node.

Phase2: transmitter goes to idle state and Rx is still in the listen mode. However, selected relay (R1 or R2) transmits the received signal -received at phase 1- to the receiver. At this stage, the power received by the destination through relay i is:

$$P_{Rx}^{Ri} = P_{Ri}^{Tx}G_{Rx}G_{Ri}k_{Ri,Rx}^2 \tag{5.50}$$

where $P_{Ri}^{Tx} = P_{Tx}G_{Tx}G_{Ri}k_{Tx,Ri}^2$.

It further simplifies to:

$$P_{Rx}^{Ri} = G^t G_{Ri}^2 k_{Tx,Ri}^2 k_{Ri,Rx}^2 \tag{5.51}$$

Finally, receiver combines the received signals, received from the two paths. Therefore, based on the selected relaying node ($i = 1$ or 2), the final received signal power can be estimated using the following equations:

$$\begin{aligned} &P_{Rx\_total}^{Ri} = P_{Rx}^{Tx} + P_{Rx}^{Ri}; \\ &P_{Tx}G_{Tx}G_{Rx}k_{Tx,Rx}^2 + P_{Tx}G_{Tx}G_{Ri}^2G_{Rx}k_{Tx,Ri}^2k_{Ri,Rx}^2 = \\ &G^t\left[k_{Tx,Rx}^2\left(x_{Tx,Rx}\right) + G_{Ri}^2k_{Tx,Ri}^2k_{Ri,Rx}^2\right] \end{aligned} \tag{5.52}$$

The signal power seen by the receiver can be used to determine the channel capacity. According to the Shannon-Hartley capacity theorem (Equation 5.53), the channel

capacity at the receiver for MI Relay method is (when the relay is performed through relay i):

$$C_{Rx}^{Ri} = B_f f_0 \log_2 \left(1 + \frac{P_{Rx-total}^{Ri}}{N}\right) \; ; \; B_f = \frac{B}{f_0} \tag{5.53}$$

As can be seen from Equation 5.53, higher received signal power for a given noise level results in a higher channel capacity. In this equation B_f is the 3 dB fractional bandwidth, f_0 is the operating frequency and N shows the system noise.

The 3 dB fractional bandwidth can be estimated if the quality factor of the antennas are known [39]:

$$B_f = \frac{B}{f_0} = \frac{\sqrt{-\left(Q_i^2 + Q_j^2\right) + \sqrt{\left(Q_i^2 + Q_j^2\right)^2 + 4Q_i^2 Q_j^2}}}{\sqrt{2} Q_i Q_j} \tag{5.54}$$

In RF communications, interference from other spectrum users is frequently the main source of noise. However, such interference is not as severe in short-range NFMIC. Thus, in the analysis of noise in the NFMIC relay network, it is assumed that the noise affecting the system is principally thermal noise, and its power may be calculated using the well know Johnson noise equation:

$$N_{Power} = kTB; (Watt) \tag{5.55}$$

In this equation, K is Boltzmann's constant (1.38×10^{-23}), T is the temperature in degree of Kelvin, and B is the communication bandwidth. The system is assumed to be operating on a person's body, therefore, the temperature will be around 37∘C (310∘K).

5.2.3.2 LoS-MAMI Relay1

Figure 5.8 shows an LoS-MAMI-Relay system, in which the transmitted signal is received by the receiver through three paths.

Phase1: the transmitter broadcasts the signal. Rx, R1 and R2 receive the transmitted signal. The power received at each node is shown in the Equations 5.26, 5.31 and 5.49.

Phase2: similar to NLoS-MAMI Relay1, at this stage, the relay assistant send the data to the relay master as well as the target receiver.

Power received at relay master at stage2 is:

$$P_{Rm}^{Ra-S2} = P_{Ra}^{Tx} G_{Ra} G_{Rm} k_{Ra,Rm}^2 + P_{Rm}^{Tx} \tag{5.56}$$

where $P_{Ra}^{Tx} = P_{Tx} G_{Ra} G_{Tx} k_{Tx,Ri}^2$. It further simplifies to:

$$P_{Rm}^{Ra-S2} = P_{Tx} G_{Tx} G_{Ra} \left[G_{Ra} G_{Rm} k_{Tx,Ra}^2 k_{Ra,Rm}^2 + k_{Tx,Rm}^2 \right] \tag{5.57}$$

However, the power received at the final receiver at this stage, through the relay assistant is:

$$\begin{aligned} P_{Rx}^{Ra-S2} &= P_{Ra}^{Tx} G_{Rx} G_{Ra} k_{Ra,Rx}^2 \\ P_{Rx}^{Ra-S2} &= G^t G_{Ra}^2 k_{Ra,Rx}^2 k_{Tx,Ra}^2) \end{aligned} \tag{5.58}$$

Phase 3: the relay master, which has received the signal from the original transmitter, as well as the relay assistant, combines the two received signals and sends it to the

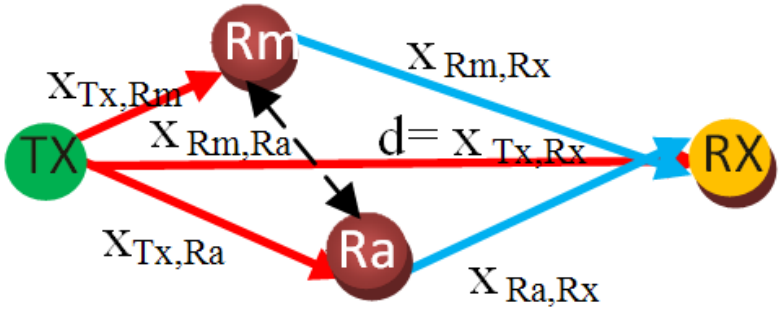

Figure 5.8 LoS- MAMI Relay1

final destination. Therefore, the received signal power at the final receiver at this stage, via Rm is:

$$\begin{aligned} P_{Rx}^{Rm} &= P_{Rm}^{Ra-S2} G_{Rm} G_{Rx} k_{Rm,Rx}^2 \\ P_{Rx}^{Rm} &= G^t G_{Ra} G_{Rm} k_{Rm,Rx}^2 \left[G_{Ra} G_{Rm} k_{Tx,Ra}^2 k_{Ra,Rm}^2 + k_{Tx,Rm}^2 \right] \end{aligned} \tag{5.59}$$

Finally, the target receiver combines the three copies of the received signal. Hence, the final received signal power at the final receiver is:

$$\begin{aligned} P_{Rx-total}^{MAMI1} &= P_{Rx}^{Tx} + P_{Rx}^{Ra-S2} + P_{Rx}^{Rm} \\ P_{Rx-total}^{MAMI1} &= G^t k_{Tx,Rx}^2 + G^t G_{Ra}^2 k_{Ra,Rx}^2 k_{Tx,Ra}^2 + P_{Rm}^{Ra-S2} G_{Rm} G_{Rx} k_{Rm,Rx}^2 \\ P_{Rx-total}^{MAMI1} &= G^t \left(k_{Tx,Rx}^2 + G_{Ra}^2 k_{Ra,Rx}^2 k_{Tx,Ra}^2 + \right. \\ &\left. \left(G_{Ra} G_{Rm} k_{Rm,Rx}^2 \left(G_{Ra} G_{Rm} k_{Tx,Ra}^2 k_{Ra,Rm}^2 + k_{Tx,Rm}^2 \right) \right) \right. \end{aligned} \tag{5.60}$$

Therefore, the channel capacity for LOS-MAMI Relay1 is estimated as:

$$C_{total}^{MAMI1} = B_f f_0 \log_2 \left(1 + \frac{P_{Rx-total}^{MAMI1}}{N} \right) \tag{5.61}$$

5.2.3.3 LoS-MAMI Relay2

As described in Section 5.2.2.3 for the NLoS case, MAMI-Relay 2 is different from MAMI-Relay1 at stage 2, when the relay assistant transmits the signal. In MAMI-Relay 2, the relay assistant transmits the signal only to the relay master instead of sending it to both the receiver and relay master (similar to NLoS MAMI Relay2).

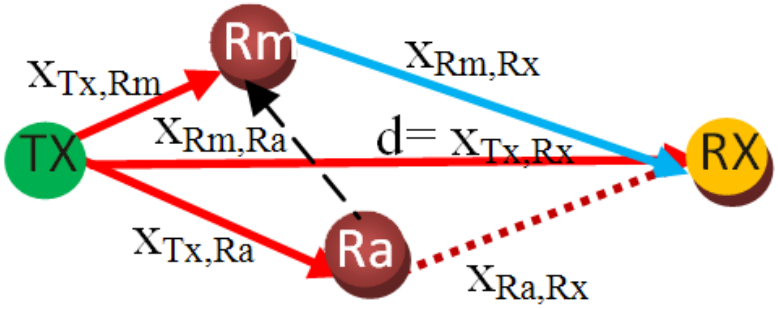

Figure 5.9 LoS- MAMI Relay2

In this scenario (Figure 5.9), transmission to Rx is done through three time phases:

Phase 1: transmitter broadcasts the signal to all nodes (Rm, Ra, Rx). The power received by each node at this stage is the same as Equations 5.42, 5.43, 5.49.

Phase 2: relay assistant sends the data to the relay master but not to the receiver. As mentioned previously, this case may be applied when the relay assistant has no direct line of sight with the final receiver. However, Ra may be used to enhance the transmitted signal to the Rx through the relay master. At this stage, the received signal power by Rm via Ra is:

$$P_{Rm}^{Ra} = P_{Ra}^{Tx} G_{Ra} G_{Rm} k_{Ra,Rm}^2 \tag{5.62}$$

The received power by the relay master from the relay assistant can be expressed as:

$$P_{Rm}^{Ra} = P_{Tx} G_{Ra}^2 G_{Tx} G_{Rm} k_{Ra,Rm}^2 k_{Tx,Ra}^2 \tag{5.63}$$

However, the total received power seen by Rm, at stage 2 will be:

$$\begin{aligned} P_{Rm}^{S2} &= P_{Rm}^{Tx} + P_{Rm}^{Ra}; \\ P_{Rm}^{S2} &= P_{Tx} G_{Tx} G_{Rm} k_{Tx,Rm}^2 + P_{Tx} G_{Ra}^2 G_{Tx} G_{Rm} k_{Ra,Rm}^2 k_{Tx,Ra}^2 \end{aligned} \tag{5.64}$$

It can also be shown as:

$$P_{Rm}^{S2} = P_{Tx} G_{Tx} G_{Rm} \left(k_{Tx,Rm}^2 + G_{Ra}^2 k_{Ra,Rm}^2 k_{Tx,Ra}^2 \right) \tag{5.65}$$

Phase 3: relay master sends the message to the receiver. Therefore, the received power by the receiver at stage 3, through relay master is:

$$P_{Rx}^{Rm} = P_{Rm}^{S2} G_{Rx} G_{Rm} k_{Rm,Rx}^2 \tag{5.66}$$

At this stage, the transmission power of the relay master equals to its received power at the previous stages. Thus, the received power by Rx through the relay master, at this stage is simplified to:

$$P_{Rx}^{Rm} = P_{Tx} G_{Tx} G_{Rm}^2 G_{Rx} k_{Rm,Rx}^2 \left(k_{Tx,Rm}^2 + G_{Ra}^2 k_{Ra,Rm}^2 k_{Tx,Ra}^2 \right) \tag{5.67}$$

Finally, at this phase, the final receiver combines the two copies of the received signal via the transmitter and the relay master. Hence, the total received power at the final receiver is:

$$P_{Rx-total}^{MAMI2} = P_{Rx}^{Tx} + P_{Rx}^{Rm} \tag{5.68}$$

By substituting the equivalent equations for P_{Rx}^{Tx} and P_{Rx}^{Rm} (Equations 5.49 and 5.66) in above equation, it can be expressed as:

$$\begin{aligned} P_{Rx-total}^{MAMI2} &= G^t k_{Tx,Rx}^2 + G^t G_{Rm}^2 k_{Rm,Rx}^2 \left(k_{Tx,Rm}^2 + G_{Ra}^2 k_{Ra,Rm}^2 k_{Tx,Ra}^2\right) \\ P_{Rx-total}^{MAMI2} &= G^t \left(k_{Tx,Rx}^2 + G_{Rm}^2 k_{Rm,Rx}^2 \left(k_{Tx,Rm}^2 + G_{Ra}^2 k_{Ra,Rm}^2 k_{Tx,Ra}^2\right)\right) \end{aligned} \tag{5.69}$$

Therefore, the total capacity of the system according to Shannon-Hartley theorem is:

$$C_{total}^{MAMI2} = B_f f_0 \log_2 \left(1 + \frac{P_{Rx-total}^{MAMI2}}{N}\right) \tag{5.70}$$

5.3 Relay selection based on separation distance

Different relay selection criteria can be considered to choose either of the intermediate nodes as the relaying node, such as RSS, SNIR, angle of arrival (AoA), time difference of arrival (TDoA) and separation distance between the nodes. In NFMIC, communication distance has a critical impact on the received signal strength and on the achievable data rates. As described earlier, signal attenuation is proportional to the sixth power of distance rather than the square as in the case of RF communications. Thus, it is one of the dominant factors in determining achievable system performance. Furthermore, since in an NFMIC personal area network, the communication occurs over very short distances, shadowing and multipath effects are not as critical as in RF communications. Hence, the separation distance between the nodes may be an appropriate criterion for optimum performance achievement. In the following section, the relay selection based on the separation distance is discussed for the proposed relaying strategies.

5.3.1 NLOS

Simulation Methodology

Matlab has been used to simulate the propagation model for each of the three proposed multihop methods. In the simulation, the transmission power is defined as 200 μW, which is sufficient power for short range communications systems such as in sensor networks, and BANs. The receiver sensitivity is 10 μW, which leads to 18 cm communication range for the peer to peer line of sight scenario in this study. The antenna coils have radius of 0.5 cm and the number of turns is 10. The operating frequency is set to 13.56 MHz. The system is assumed to be homogenous and all the nodes use identical antennas which results in identical quality factors. The coils quality factor is 830, where a high magnetic permeable material is used for the core of the coils (such as ferrite or manganese zinc). The permeability of the ferrite is 0.0008 H.m^{-1}. However, the location of each node is chosen in which the transmitter and the target received have no direct link with each other and have no misalignment in respect to each other. Transmitter is located at the reference location Tx (x y z)=(0 0 0). The two relay nodes are located at a distance between transmitter and receiver and have the same lateral misalignment in respect to Rx and Tx. In this analysis, identical lateral misalignment are chosen to measure the performance of the relaying method based on the separation distance only. The effect of lateral and angular misalignment will be discussed in Section 5.4.4. R1 is located close to the transmitter R1(5 2 5) and R2 is located at the edge of the communication range of the transmitter R2(-5 -2 18). The location of receiver is changed on the x axis to determine the maximum achievable distance using each relaying strategy Rx (19:60 0 0). The receiver is located out of the direct communication range of Tx ($d > 18$ (cm)).

Relay selection

Using this scenario, the three multihop techniques are simulated to determine the extent of performance improvement achieved and hence to determine which multihop technique is the most effective. The results are shown in Figure 5.10 to 5.14.

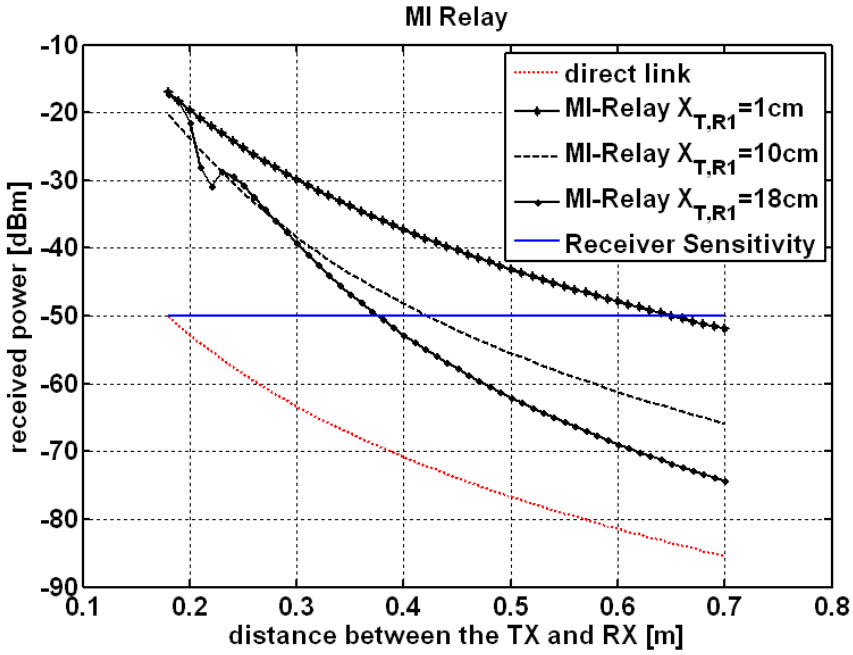

Figure 5.10 NLOS-MI Relay-relay node at different distances

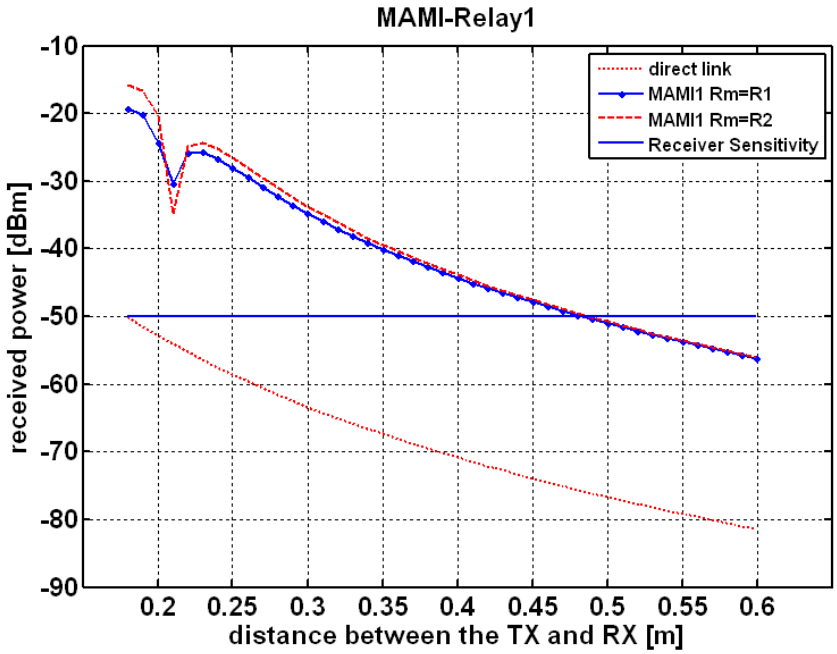

Figure 5.11 NLOS-MAMI Relay1-achieved range

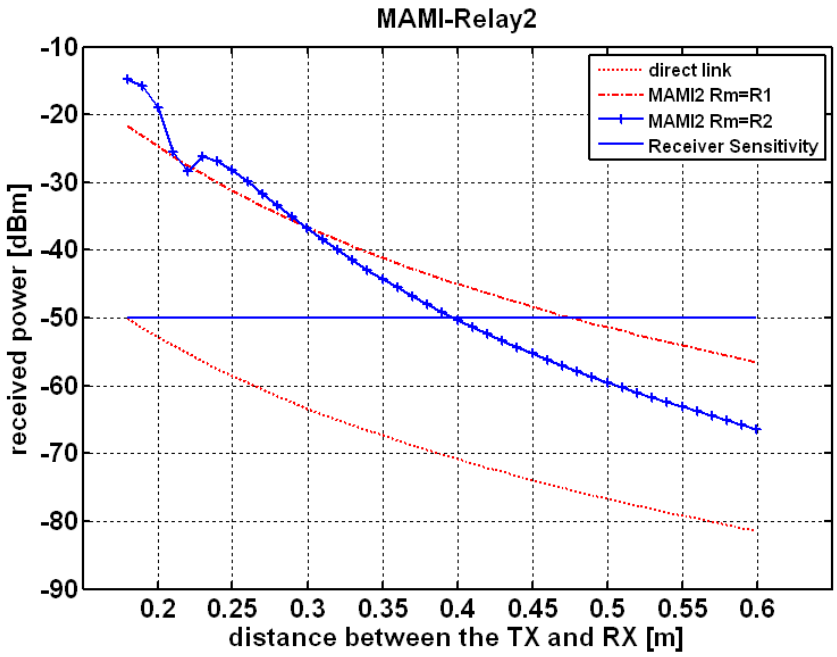

Figure 5.12 NLOS-MAMI Relay2-achieved range

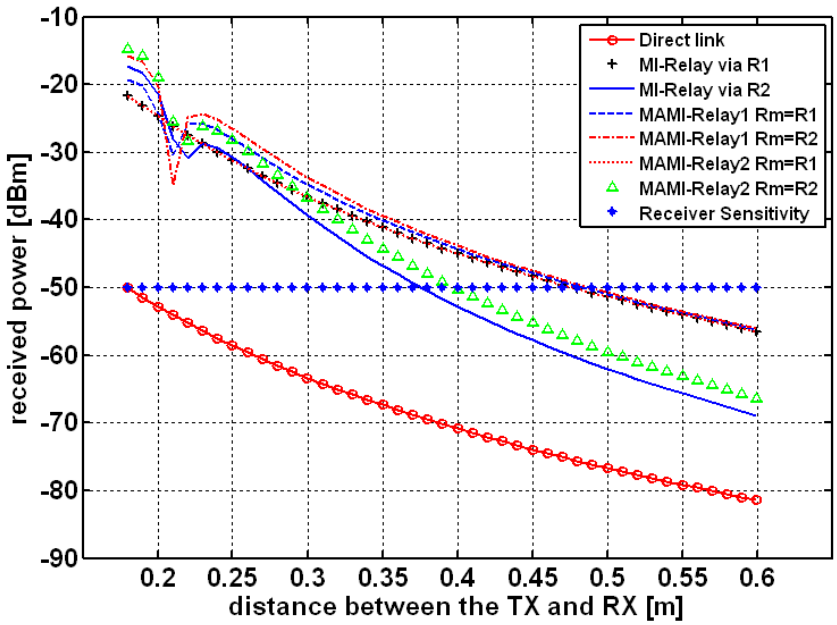

Figure 5.13 RSS and achieved distance-comparison between the three methods

Figure 5.10 shows the achieved received signal strength and the communication distance for the NLoS-MI Relay case where the relaying node is located in different distances (1, 10 and 18 cm) from the original transmitter. The straight line shows the receiver sensitivity which is -50 dBm. In other words, to be able to decode the transmitted signal with minimal bit error rate, the final receiver requires the received signal strength of at least -50 dBm. The dotted line shows the received signal power against the communication range for the final receiver, where there is no cooperative relay. As can be seen from Figure 5.10, at distances above 8 cm, the receiver would not be able to decode the transmitted signal with an acceptable bit error rate, therefore, it is out of the communication range of the original transmitter. The other three plots in the figure show the received signal strength at the out of range receiver, where an idle intermediate node is used to relay the data from the source to destination. It is observed that a relay node can be used to enhance the communication range.

Based on the location of the relaying node, the communication range can be en-

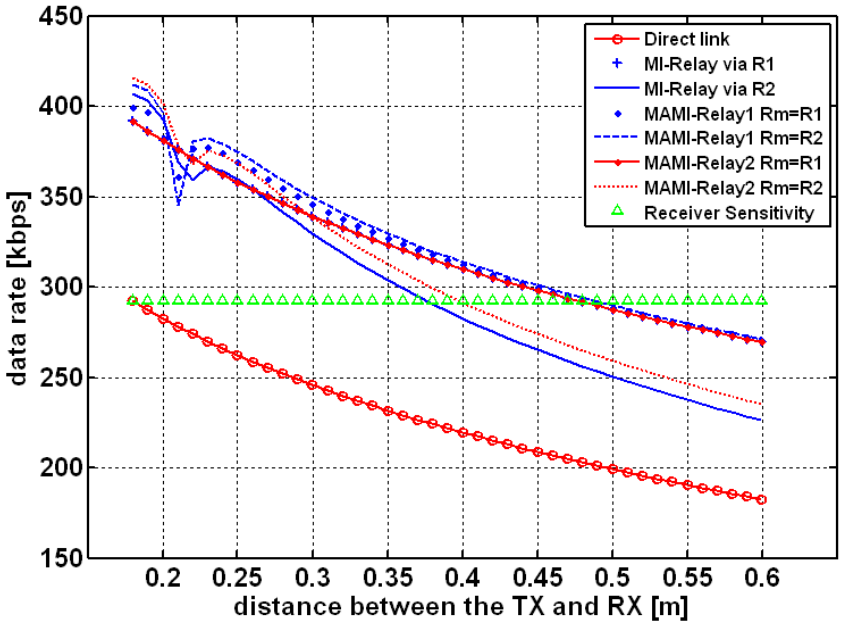

Figure 5.14 achieved data rate-comparison between the three methods

hanced up to 65 cm. However in the worst case scenario (relay is located at the edge of the communication range) the achieved range is 37 cm, which in comparison with 18cm is a significant enhancement. Since the location of the relaying node has a very significant role to play in range extension, the relay node is located at different distances from the transmitter to observe the optimum location of the relay node in respect to the transmitter and receiver. It can be seen from the graph that as the relaying node moves toward the transmitter, longer distances can be achieved. Therefore, if there are more than one node between the transmitter and the out of range receiver, the node closer to the transmitter can achieve the longer distances, as well as higher data rates. For instance, using R1 -relay closer to the transmitter (5 cm)- results in an additional 20 kb/s of channel capacity at distance 30 cm in comparison with relaying through R2 (18 cm) (see Figure 5.10).

Figure 5.11 shows the performance of the NLoS-MAMI Relay1 strategy. As can be seen from Figure 5.11, the graphs showing the two cases of Rm=R1 and Rm=R2 tend to overlap as the receiver is moved away from the transmitter toward the receiver. This implies that in MAMI Relay1, the achievable communication range and data rates are almost identical for both cases (Rm=R1 and Rm=R2). However, when Rm=R2 slightly higher RSS is achieved compared to the case where Rm is closer to the transmitter (Rm=R1). It also may be seen here, that using this strategy, the communication distance can be increased to 48 cm. Therefore, by applying this relaying strategy to the communication system, the range can be dramatically extended. When the final receiver is located close to the edge of the transmission range of the transmitter, using this technique the capacity can be improved from 292 kb/s to more than 400 kb/s (Rm=R2) and up to 412 kb/s (Rm=R1) (see Figure 5.14).

In Figure 5.12, it may be seen that unlike MAMI Relay1, in NLoS-MAMI Relay2, if the relay master is selected to be closer to the transmitter, longer ranges can be achieved. For example in the given scenario, relaying through R1 as the relay master, can improve the range by 8 cm in comparison with the case when the relay master is R2. However, similar to the other two techniques, this cooperative communication

method improves the communication range significantly.

In Figure 5.13 and 5.14, the performance of all proposed relaying techniques are compared to each other. Figure 5.13 and 5.14 show the communication range against the received signal strength and achieved data rate respectively for the three methods: MI relay, MAMI Relay 1 and 2. It is observed that MAMI-Relay1 outperforms the other two multihop methods (MI-Relay and MAMI-Relay2). Although MI-Relay strategy enhances the achieved data rates and the communication range, its performance is highly dependent to the location of the relaying node. For example if the node close to the edge is selected, it results in minimal range and data rate improvement, while if the relay is in close proximity of the transmitter it can achieve almost the same performance improvement as MAMI Relay2 where, Rm=R1.

Similarly, the optimum selection of the relay master and relay assistant in MAMI-Relay2 leads to considerable performance achievement. For instance, when the target receiver is located 40 cm away from the transmitter, the achieved data rate is 18 kb/s higher if the relay master is closer to the transmitter (Figure 5.14).

Based on the simulation results and the theoretical discussion, it is derived that the location of each relaying node and selection of the nodes to act as master or assistant can impact the achieved data rates and the communication range significantly. Table 5.1 describes how the position of each node impacts the performance of MAMI-Relay 1 and 2.

To obtain the optimum location of each node, two approaches have been taken. First, the relay master is located as close as possible to the transmitter and moved the relay assistant from the transmitter toward the receiver for each method. Then the location of the master is chosen to be at the edge of the communication range, while the assistant is placed in different distances from the transmitter. Secondly, the relay assistant is fixed to 2 cm and then 18 cm from the transmitter and the relay master is moved to different locations (2, 10 and 18 cm from the transmitter). The result has shown that in MAMI-Relay1, very similar performance is achieved if either of

the nodes acts as a master or assistant. However, the best result is obtained in both methods, where both the master and relay assistant are located as close as possible to the transmitter. As they move toward the edge the performance degrades. In comparison with MAMI-Relay1, MAMI-Relay2 is highly affected by the selection of the master and assistant node. As described previously, where the two nodes have different distances from the transmitter, if the node closer to the edge is selected as master, the system performance can be improved considerably.

In MAMI-Relay1, as Ra moves toward the edge, the impact of the location of Rm becomes more critical. For example if Ra is located 2 cm away from the transmitter and Rm is located at 2 cm to 18 cm from the original source, the achieved distance varies from 58 cm to 64.6 cm, while if Ra is located at the communication edge (18 cm), the achieved range varies from 40 cm to 60 cm by moving Rm from 2 cm to 18 cm. In the later scenario achieved range varies by 20 cm, while in the former case the difference is below 7 cm. This implies that in MAMI-Relay1, if the node closer to the edge acts as the relay master, not only higher distances is achieved but also more stable system may be obtained.

By contrast, MAMI-Relay2 can achieve longer range and more robustness, as the relay master is moved closer to the transmitter. For instance, when Rm is located at 2 cm away from the transmitter, the achieved distance varies from 56.6 cm to 59 cm if the relay assistant is moved from the source to the communication edge (see Table 5.1). Almost the same variation is observed when the relay master is located at the edge, but the achieved distance is reduced by 20 cm.

Quality Factor

From the power equations discussed in Section 5.2.1.1, it can be seen that to increase the received signal strength and the achieved communication range, antennas with higher quality factor should be used. However, Equation 5.54 suggests that higher quality factor not necessarily results in higher data rates. For a homogenous system, with identical quality factors, this equation simplifies to $B_f = (0.644/Q)$. Therefore,

Table 5.1 MAMI Relay1 and 2 comparison-Master/Assistant Selection

dis. between Tx and Ri (cm)		**Rm=2cm**			**Rm=18cm**			**Ra=2cm**			**Ra=18cm**		
		Ra(cm)=			**Ra(cm)=**			**Rm(cm)=**			**Rm(cm)=**		
		2	10	18	2	10	18	2	10	18	2	10	18
Achieved dis.	MAMI Relay1	65	44	40	65	59	58	64.6	59	58	60	44	40
	MAMI Relay2	59	58.8	56.6	39	38	36.8	56	41	39	37	42	59

to achieve the highest data rate, the optimum Q-factor should be determined. Figure 5.15 to 5.17 show the optimum Q-factor for different communication distance at an operating frequency of 13.56MHz, for the three multihop relay techniques.

As can be seen from Figure 5.15, if the optimum Q-factor (120) is obtained, a data rate up to 870 kb/s is achieved where the receiver is located at 25 cm away from the

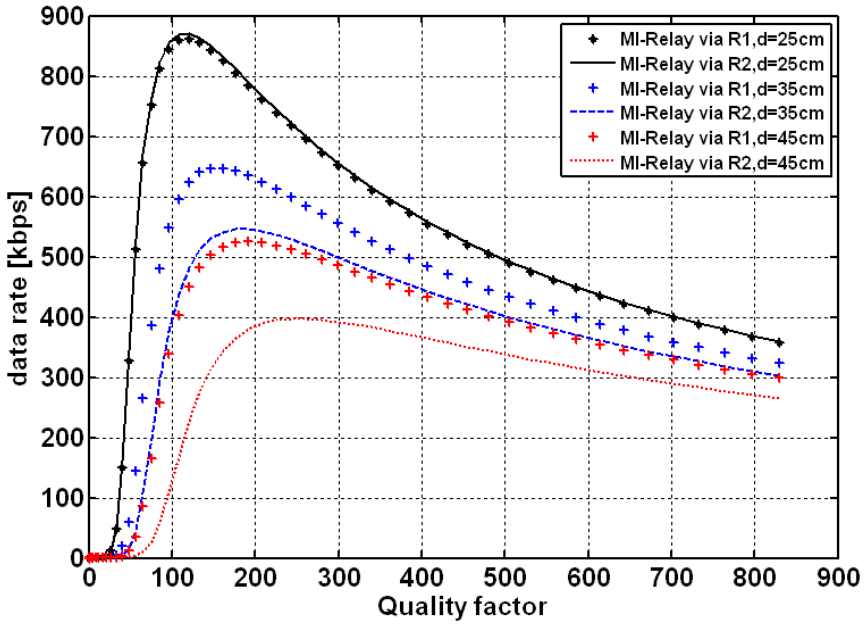

Figure 5.15 NLOS-MI Relay-Optimum Q-factor

source (MI-Relay method). As distance increases, the optimum Q-factor to achieve the maximum data rate also increases. For example, at distance 45 cm, in MI-Relay via R1, Q-factor 191 is required to achieve 525 kb/s data rate, while this amount is 243 to achieve 397 kb/s if relaying is performed via R2. The same tendency can be seen for MAMI-Relay 1 and 2 in Figure 5.16 and 5.17. The graphs also suggest that as the Q-factor increases, the achieved data rates decrease and asymptotically approaches the same data rate for all the cases.

Figure 5.16 suggests that, for MAMI-Relay1, a specific Q-factor at a given communication distance, results in very similar data rates regardless of which node is selected to function as master or assistant. However, in MAMI-Relay2 (5.17) and MI-Relay (Figure 5.15), the selection of each node as master and assistant can impact the optimum Q-factor to achieve the highest data rate. Proper and optimal selection of each node as relay master and relay assistant in each method results in the reduction on the value of Q-factor in order to obtain higher data rates.

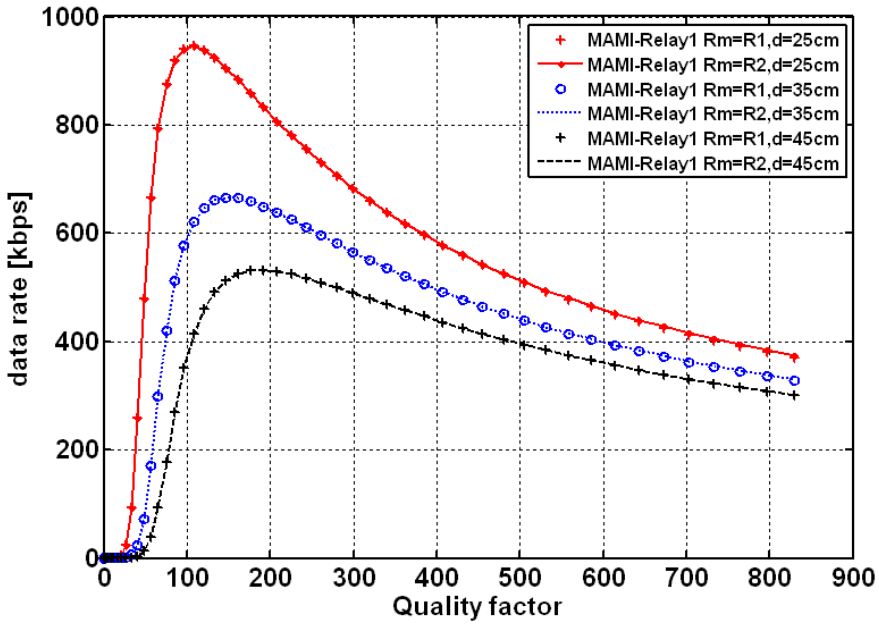

Figure 5.16 NLOS-MAMI Relay1-Optimum Q-factor

The size of antenna coil is one of the important factors to determine the value of the Q-factor. Thus smaller Q-factor often means smaller devices. Hence, by choosing the proper proposed multihop method for a specific scenario, and selecting the optimal node as relay master and assistant, the size of device may be reduced without degrading the data rate. However, the optimum Q-factor to achieve maximum data rate does *not* automatically lead to a longer communication range. Therefore, in every application it is important to determine the most critical requirement, whether it is the high data rates or the communication range extension. Therefore, the optimum Q-factor, data rates and the communication range can be determined.

5.3.2 LoS

To study the relay selection concept in LoS case, the parameters are kept similar to the NLoS case for the simulations. However, the final receiver is moved toward the transmitter, in which it is in direct coverage range of the source node; which in this case is a separation distance less than 18 cm. The performance of each LoS relaying

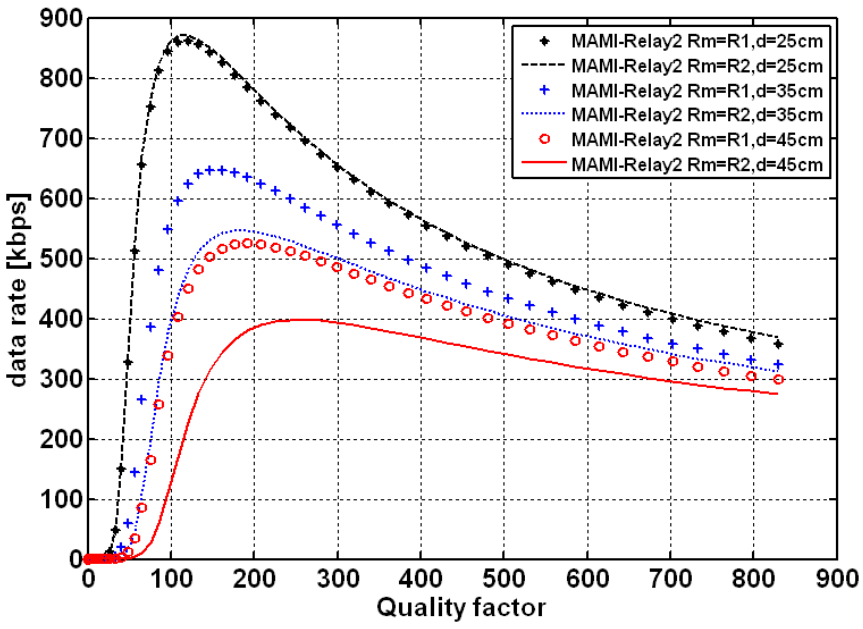

Figure 5.17 NLOS-MAMI Relay2-Optimum Q-factor

techniques is compared with each other, as well as to a conventional point-to-point communication (when there is no cooperative communication).

Figure 5.18 shows the achieved data rates by applying MI relay technique. As can be seen here, if the node closer to the sink is selected to relay the data, slightly higher data rates can be achieved. However, as shown in Figure 5.18, when there is cooperative communication, achieved data rate is significantly higher. For example at the edge of communication (at 18 cm), receiver achieves an additional 125 kb/s data rate if data is receives through two different paths (direct and relay path), compared to a point to point communication.

Figure 5.19 and 5.20 show the achieved data rates against the communication distance for LoS-MAMI Relay1 and 2. The Figures show that, these two methods achieve higher data rates if the relay assistant is chosen to be located closer to the source. It may also be seen here, that applying either of these relaying techniques can improve the achieved data rates considerably. However, in MAMI Relay2, if the

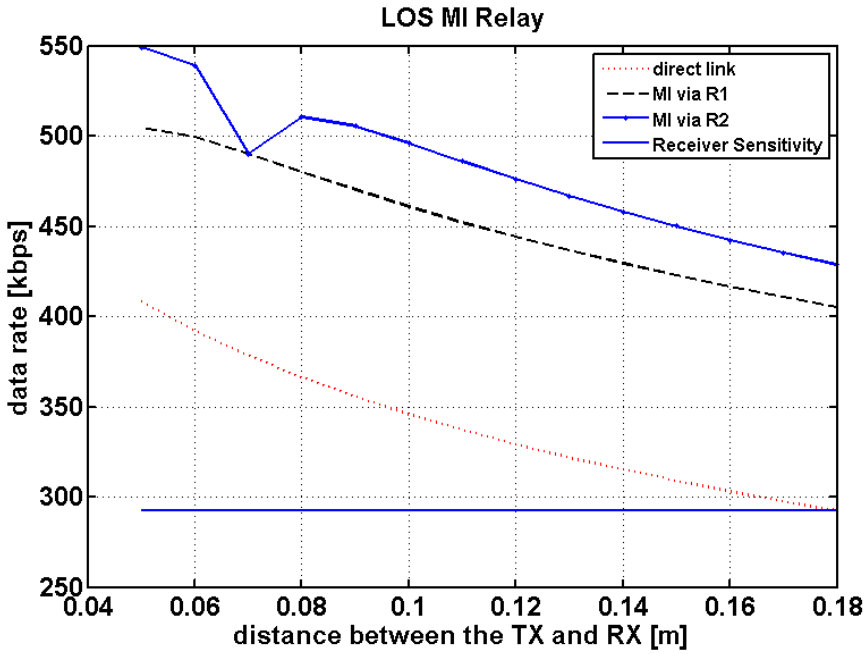

Figure 5.18 LOS-MI Relay-achieved data rates

relay master and assistant are chosen improperly, the achieved data rates degrade notably (about 25 kb/s at the edge in this scenario). This value is about half for MAMI Relay1 (in case of improper master/assistant relay selection).

Figure 5.21 shows a comparison between the three discussed LoS MI cooperative relaying models. As it can be seen from the graphs, the best method is MAMI-Relay1, where the relay master is chosen to be closer to the receiver (Rm=R2). However, if relay is performed through a relay master closer to the transmitter, losses will be higher. As can be seen from the statistics, MAMI-Relay2, where relay master is closer to the transmitter, achieves almost the same performance improvement as the MI-Relay through the closer node to the transmitter. However, MAMI-Relay2 achieves slightly higher channel capacity. Figure 5.21 also illustrates that the worst case scenario is MI-Relay relaying through the node closer to the transmitter (R1). Figure 5.21 also suggest that the MAMI Relay 1 and 2 achieve very similar data rates when Rm=R2, and also the highest among all; while if Rm=R1, MAMI Relay

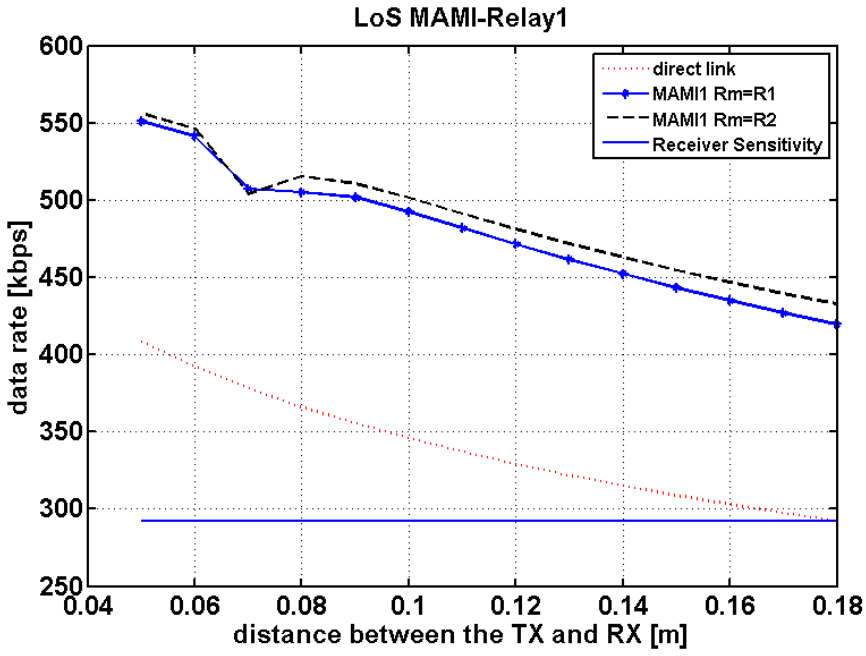

Figure 5.19 LOS-MAMI Relay1-achieved data rates

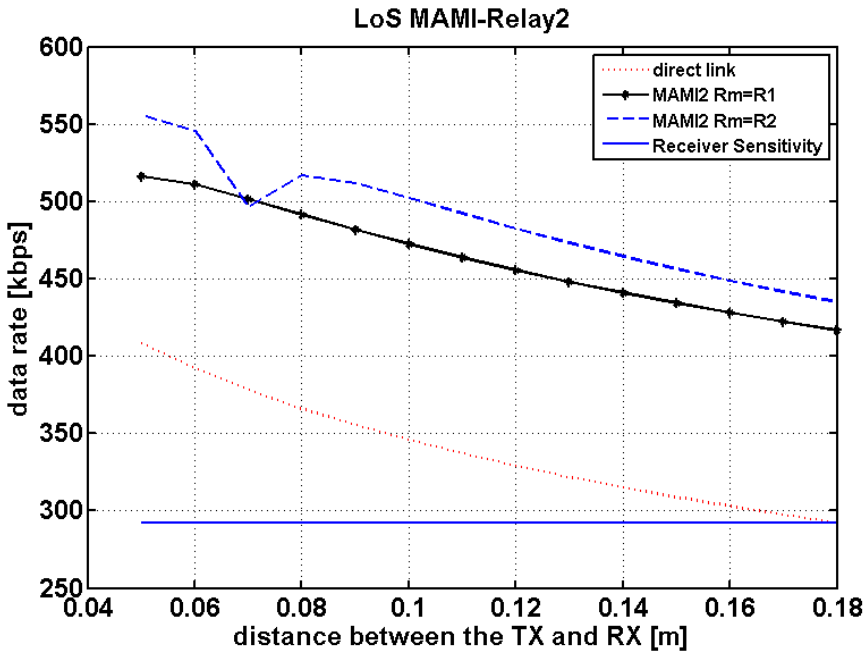

Figure 5.20 LOS-MAMI Relay2-achieved data rates

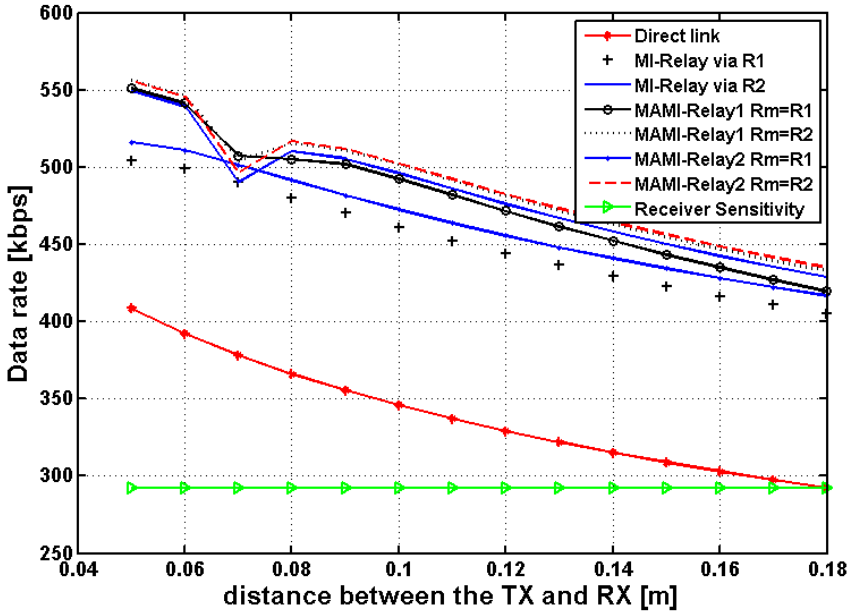

Figure 5.21 LOS-achieved data rates comparison between the three methods

1 outperforms MAMI Relay2.

5.4 Relay selection based on a new metric (*relay link indicator*)

Although the separation distance can be considered as a proper relay selection metric in a system with minimal lateral and angular displacement, this may not be a suitable choice when there are performance losses due to large lateral and angular misalignment. This often could be the case in real applications, where the nodes may change their location and angular orientation in respect to each other. In such scenario, separation distance, as a relay selection metric, may not achieve the optimum performance. For example, in MI relay method, if the relay is selected based on its short separation distance with the receiver, while its orientation angle relative to the receiver or transmitter is close to 90°, the receiver *cannot* receive the signal from it, since the total received power approaches 0 W. The same thing applies when the lateral misalignment is large and hence the received power will be highly degraded by this (the plots showing the tendency, of which the whole cooperative communication system is affected by lateral and angular displacement is shown in Appendix B). Therefore, a new metric is required to take into account not only the separation distance, but also lateral and angular misalignments; which are the three critical sources of the system performance degradation. This section proposes a new metric for relay selection in an imperfect NFMI cooperative communication system using either of the proposed relaying strategies.

To develop a new relay selection metric, the coupling coefficient equation for a point to point link, may be defined as a multiplication of two terms $S_{i,j}$ and δ_{ij}, in which δ_{ij} includes all the location and orientation dependent parameters and $S_{i,j}$ is an indicator of the size of transmitting and receiving coils.

$$k_{i,j}^2(x_i) = S_{i,j} \cdot \delta_{i,j} \tag{5.71}$$

where,

$$S_{i,j} = \frac{r_j^2 \cdot l_i \cdot l_j}{4.\pi^2 \cdot r_i} \tag{5.72}$$

$$\delta_{i,j} = \frac{\Delta_{i,j} \cdot \cos^2\alpha_{i,j}}{\left((r_i + \Delta_{i,j})^2 + x_{i,j}^2\right)^2} \left[K + \frac{\left(\frac{r_i \cdot m_{i,j}}{\Delta_{i,j}}\right) - (2 - m_{i,j})}{2 - 2m_{i,j}} \cdot E \right]^2 \tag{5.73}$$

In this case $m_{i,j}$ (for node i and j) is the same as Equation 5.29. Therefore the power transfer function can be expressed as:

$$P_j^i = P_i G_i G_j S_{i,j} \delta_{i,j} \tag{5.74}$$

Equation 5.74 implies that in a homogenous NFMIC system, the quality of the link can be determined if δ_{ij} (*Link Indicator*) is known, and the higher received power can be achieved for larger δ_{ij}. However, for relay selection purposes, the link indicator should be determined for the both links, between the transmitter and relay/receiver and the link between relay nodes and the final receiver; because the determination of the link indicator for only one link, as the relay selection metric, is insufficient in order to achieve optimum performance. Therefore, the *Relay Link Indicator* (δ_{Ri}) is defined, which takes into account, the quality of the link from the source to the destination. Hence, for the relay node i, relay link indicator is:

$$\delta_{Ri} = \delta_{Tx,Ri} \delta_{Ri,Rx} \tag{5.75}$$

Based on the new metric, the power transfer function equations are reconstructed for the NLoS and LoS multihop relay techniques, then the performance of each technique is simulated and discussed in accordance to relay link indicator.

5.4.1 NLoS

MI Relay

In this case the final power equation (received power via Ri) can be expresses as:

$$P_{Rx}^{Ri} = P_{Tx} G_{Tx} G_{Rx} G_{Ri}^2 S_{Tx,Ri} S_{Rx,Ri} \delta_{Tx,Ri} \delta_{Rx,Ri} \tag{5.76}$$

Here, the total link indicator (δ_{Ri}) needs to be determined. Thus, the power equation becomes:

$$P_{Rx}^{Ri} = P_{Tx}G_{Tx}G_{Rx}G_{Ri}^2 S_{Tx,Ri}S_{Rx,Ri}\delta_{Rx,Ri} \tag{5.77}$$

MAMI Relay1

For NLoS-MAMI Relay1 the final received power is:

$$\begin{aligned} P_{Rx}^{total} &= G^t \left(S_{Tx,Ra}S_{Rx,Ra}\delta_{Tx,Ra}\delta_{Rx,Ra}G_{Ra}^2 + S_{Rx,Rm}\delta_{Rx,Rm}\beta\right) \\ \beta &= G_{Rm}^2 \left(G_{Ra}^2 S_{Tx,Ra}S_{Ra,Rm,}\delta_{Tx,Ra}\delta_{Ra,Rm} + S_{Tx,Rm}\delta_{Tx,Rm}\right) \end{aligned} \tag{5.78}$$

which also can be shown as follows, to relate the received power to the relay link indicators (for relay master and relay assistant):

$$\begin{aligned} P_{Rx}^{total} &= G^t \left(S_{Tx,Ra}S_{Rx,Ra}\delta_{Ra}G_{Ra}^2 + S_{Rx,Rm}\left(\frac{\delta_{Rm}}{\delta_{Tx,Rm}}\right)\beta\right) \\ \beta &= G_{Rm}^2 \left(G_{Ra}^2 S_{Tx,Ra}S_{Ra,Rm,}\left(\frac{\delta_{Ra}\delta_{Ra,Rm}}{\delta_{Ra,Rx}}\right) + S_{Tx,Rm}\left(\frac{\delta_{Rm}}{\delta_{Rm,Rx}}\right)\right) \end{aligned} \tag{5.79}$$

MAMI Relay2

Here the total received power is:

$$P_{Rx}^{total} = G^t G_{Rm}^2 S_{Rm,Rx}\left(S_{Tx,Rm}\delta_{Tx,Rm}\delta_{Rm,Rx} + S_{Tx,a}S_{Ra,Rm}\delta_{Tx,a}\delta_{Ra,Rm}\delta_{Rm,Rx}G_{Ra}^2\right) \tag{5.80}$$

It also can be expressed as:

$$P_{Rx}^{total} = G^t G_{Rm}^2 S_{Rm,Rx}\left(S_{Tx,Rm}\delta_{Rm} + S_{Tx,a}S_{Ra,Rm}\left(\frac{\delta_{Ra,Rm}\delta_{Ra}\delta_{Rm}}{\delta_{Ra,Rx}\delta_{Tx,Rm}}\right)G_{Ra}^2\right) \tag{5.81}$$

5.4.2 LoS

LoS MI Relay

The total received power based on the relay link indicator for LoS-MI relay is:

$$P_{Rx\_total}^{Ri} = P_{Tx}G_{Tx}G_{Rx}\left[S_{Tx,Rx}\delta_{Tx,Rx} + G_{Ri}^2 S_{Tx,Ri}S_{Ri,Rx}\delta_{Ri}\right] \tag{5.82}$$

This equation implies that by relaying through the node with higher relay link indicator, the total received power is higher.

LoS MAMI Relay1

The received signal power for LoS-MAMI Relay 1 is also reconstructed here, based on the relay master and relay assistant link indicator and is:

$$\begin{aligned} P_{Rx-total}^{MAMI1} &= G^t \left(S_{Tx,Rx}\delta_{Tx,Rx} + G_{Ra}^2 S_{Tx,Ra} S_{Ra,Rx}\delta_{Tx,Ra}\delta_{Ra,Rx} + \beta^{MAMI1} \right); \\ \beta^{MAMI1} &= G_{Ra}G_{Rm}S_{Rm,Rx}\delta_{Rm,Rx} \left(G_{Ra}G_{Rm}S_{Tx,Ra}S_{Ra,Rm}\delta_{Tx,Ra}\delta_{Ra,Rm} + S_{Tx,Rm}\delta_{Tx,Rm} \right) \end{aligned} \tag{5.83}$$

It may also be shown as:

$$\begin{aligned} P_{Rx-total}^{MAMI1} &= G^t \left[S_{Tx,Rx}\delta_{Tx,Rx} + G_{Ra}^2 S_{Tx,Ra} S_{Ra,Rx}\delta_{Ra} + \beta^{MAMI1} \right]; \\ \beta^{MAMI1} &= G_{Ra}G_{Rm}S_{Rm,Rx} \left(G_{Ra}G_{Rm}S_{Tx,Ra}S_{Ra,Rm} \left(\frac{\delta_{Ra,Rm}\delta_{Ra}\delta_{Rm}}{\delta_{Ra,Rx}\delta_{Tx,Rm}} \right) + S_{Tx,Rm}\delta_{Rm} \right) \end{aligned} \tag{5.84}$$

LoS MAMI Relay2

Similarly for LoS-MAMI Relay2, the final received power is:

$$\begin{aligned} P_{Rx-total}^{MAMI2} &= G^t \left(S_{Tx,Rx}\delta_{Tx,Rx} + G_{Rm}^2 \beta^{MAMI2} \right); \\ \beta^{MAMI2} &= S_{Rm,Rx}\delta_{Rm,Rx} \left(S_{Tx,Rm}\delta_{Tx,Rm} + G_{Ra}^2 S_{Tx,Ra} S_{Ra,Rm}\delta_{Tx,Ra}\delta_{Ra,Rm} \right) \end{aligned} \tag{5.85}$$

It also can be expressed as:

$$\begin{aligned} P_{Rx-total}^{MAMI2} &= G^t \left(S_{Tx,Rx}\delta_{Tx,Rx} + G_{Rm}^2 S_{Rm,Rx} \left(S_{Tx,Rm}\delta_{Rm} + G_{Ra}^2 \beta^{MAMI2} \right) \right); \\ \beta^{MAMI2} &= S_{Tx,Ra} S_{Ra,Rm} \left(\frac{\delta_{Ra}\delta_{Ra,Rm}\delta_{Rm}}{\delta_{Ra,Rx}\delta_{Tx,Rm}} \right) \end{aligned} \tag{5.86}$$

The following section analyses the performance of each relaying strategies based on the new relay selection metric. Using simulation results to verify the theory discussed earlier, it will be shown that, if the relay selection is performed in accordance to the link indicator, more reliable decision can be made. Furthermore, it presents suggestions on how to chose each node as a relay master and relay assistant based on their link indicator value to achieve optimum results.

5.4.3 Simulation Results

Methodology

In this section, using Matlab, the performance of each relaying strategy is studied against the relay link indicator. The coil design parameters and transmission power and receiver sensitivity are the same as discussed in Section 5.3.1. Hence, the system is still homogenous. However to be able to study the system performance against the link indicator, the location and orientation of each node is changed in order to analyse the communication system for the possible range of the link indicator. To achieve the link indicator range for the defined scenario, the distance of each relaying node as well as their lateral misalignments are increased to their maximum value (i.e. until they are out of the range of transmitter), in order to model an increasingly imperfect channel. The angle is also increased from zero to 90°, since in this range, the $cos^2(\alpha)$ can have all the possible values (i.e. 1-0).

The following section shows the simulations results for the three relaying techniques in LoS and NLoS situations. To determine the relay selection based on the relay link indicator R1 is designed in the simulations to have higher link indicator compared to R2. Thus, the impact of the relay link indicator of each node on the total received signal power and the end to end data rate can be studied. It is shown by the theoretical analysis that master and assistant relay link indicator has different levels of impact on the total system performance. Hence, simulation results provide a better insight into the extent of impact of each relay link quality on the multihop relaying strategies.

It is also shown in the simulations how the relay link indicator may be affected by distance, angle and lateral displacements.

Results

Figure 5.22 to 5.27 illustrates that the achieved received power and data rates steadily increase as the link indicator increases. This implies that in MI relay strategy if the relay with higher link indicator is selected, higher received signal power

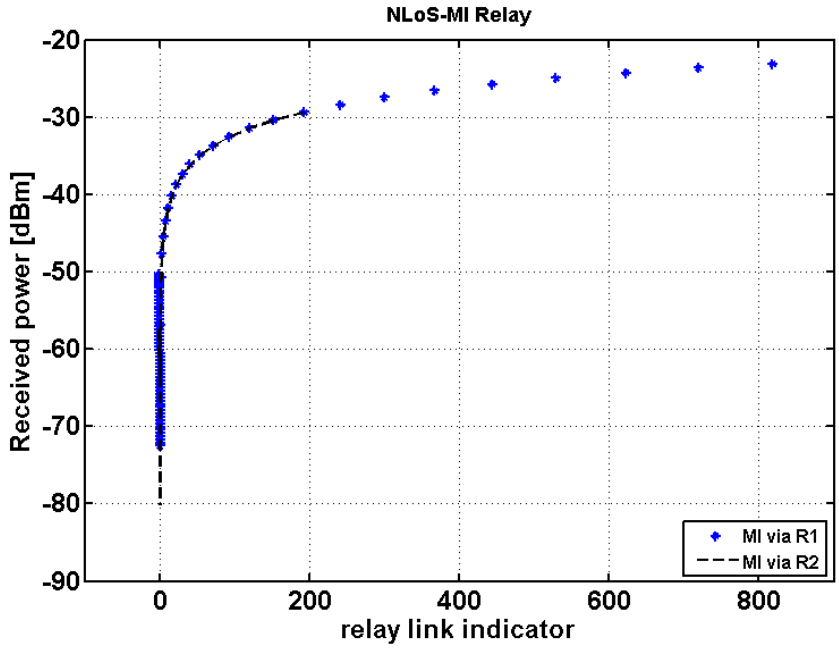

Figure 5.22 NLOS-achieved received power in MI Relay

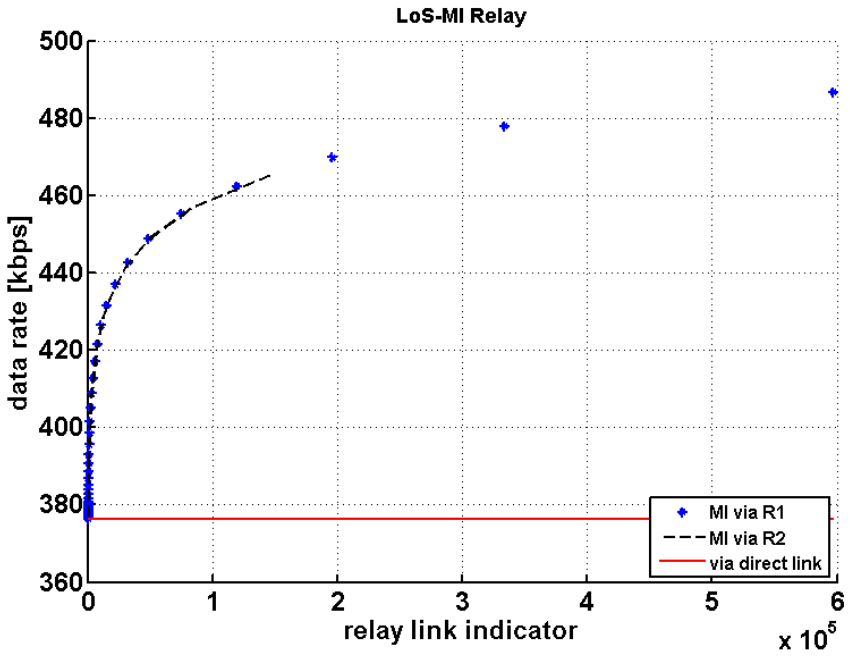

Figure 5.23 LOS-achieved data rates in MI Relay

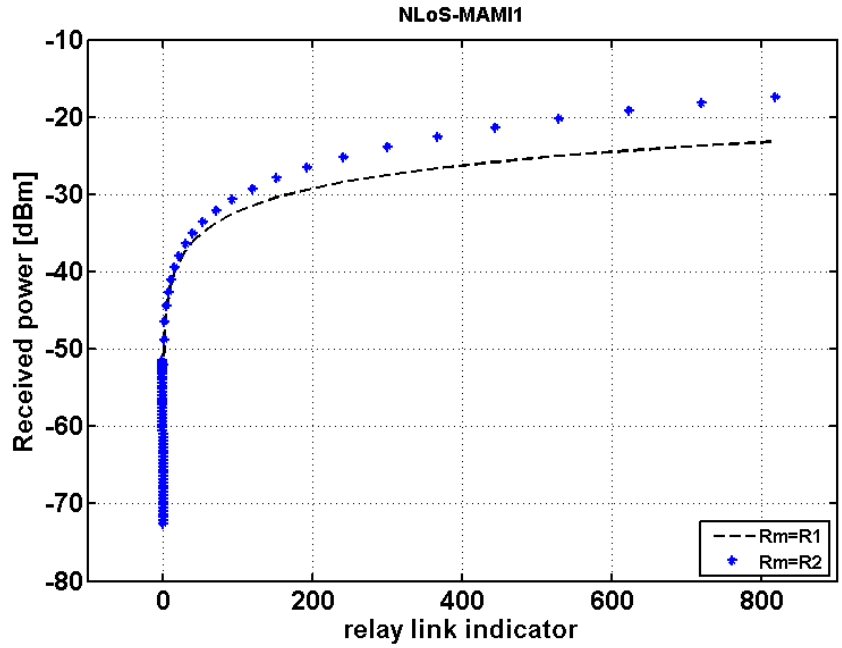

Figure 5.24 NLOS-achieved received power in MAMI Relay1

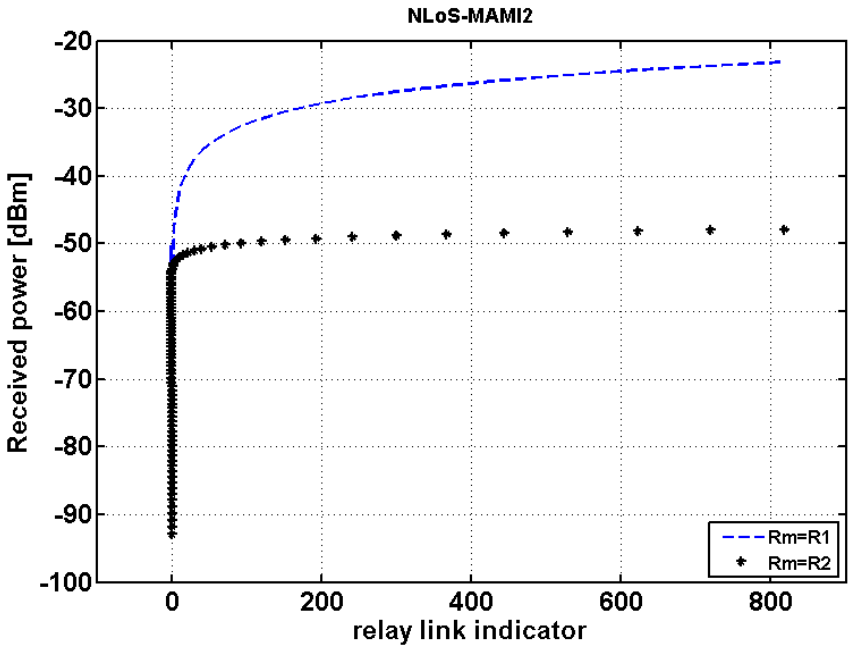

Figure 5.25 NLOS-achieved received power in MAMI Relay2

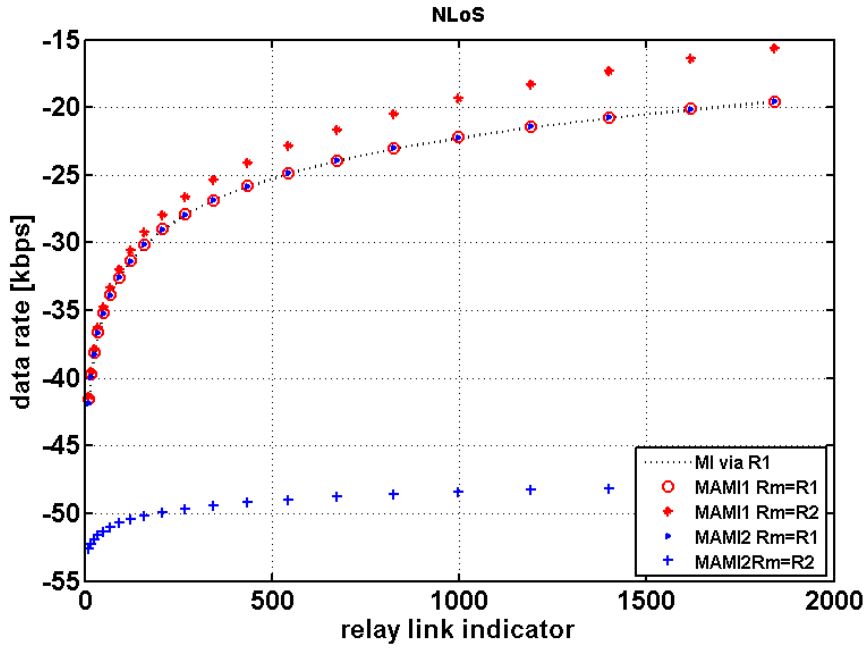

Figure 5.26 NLOS-comparison between the three relaying methods

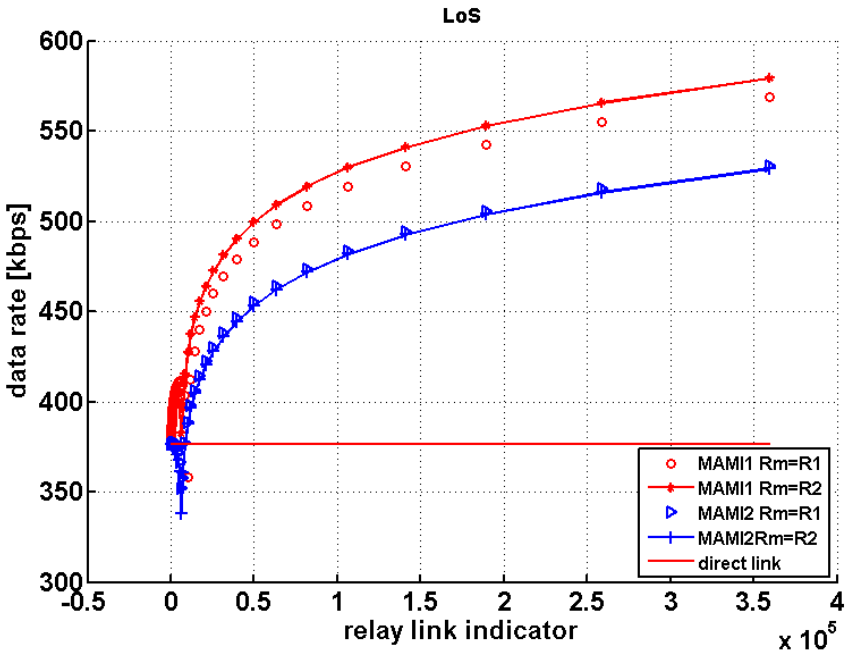

Figure 5.27 LOS-comparison between MAMI Relay1 and MAMI Relay2

and data rates can be achieved. If the relay selection is performed in accordance to the distance alone, it can be seen from Figure 5.10 that although the higher signal strength is achieved by choosing the relay with shorter distance relative to Tx and Rx, this trend is not always stable. The signal experiences a sharp fluctuation at some specific distances, which is dependent on the value of lateral misalignment of the antenna due to the complete elliptic integrals of the first and second kind. It may also be seen from the graphs provided in the Appendix B that relay selection based on the angle, or lateral misalignment alone is also not optimum. However, a reliable decision can be obtained if it is done based on the value of relay link indicator; since higher link indicator achieves higher received power and data rates without experiencing any fluctuations (see Figures 5.22 and 5.23). Figure 5.22 and 5.23 illustrate the achieved received signal power and data rates against the link indicator for both case of NLoS and LoS respectively, when the relaying is through R1 and R2. These results show, since the link indicator of R2 cannot exceed some specific value (this value a function of the location and orientation of the node), it cannot achieve higher data rates and received power at the final destination. Hence, the node with higher link indicator has to be selected for cooperative communication to achieve higher throughput.

Figure 5.24 shows the NLoS-MAMI Relay1, when the relay node with higher link indicator is selected, once as the relay master and also as the relay assistant. As mentioned previously, R1 has a higher link indicator than R2. Furthermore, when the relay node with higher link indicator is selected as the relay assistant, higher received signal can be achieved, consequently, longer communication range will be obtained. For instance, an additional 5 dBm can be achieved for $\delta_{Ra} = 600\ \mathrm{m}^{-3}$ (link indicator has unit of m^{-3}), if the node with better quality (higher δ) is chosen as the relay master.

The same behavior can also be seen for NLoS-MAMI Relay 2 (Figure 5.25); if the relay assistant has higher δ, higher received power is achieved. However, if the the node with greater δ is selected as relay master, the performance degrades

considerably (comparable with NLoS-MI Relay method, relaying via R2). Moreover, the received power is just above the receiver sensitivity if Rm=R1, while this value -received power- is almost twice if Rm=R2.

Figure 5.26 shows a comparison between the performance of the three multihop relaying techniques (for NLoS), when the relaying nodes are selected according to their link indicator. Here, MAMI Relay1 outperforms the other two techniques if the relay assistant has higher δ than the relay master. However, in MAMI Relay1 if Ra=R2, the performance degrades and it becomes very similar to MAMI Relay2 when Ra=R1 and MI Relay via R1. However, in MAMI Relay2 when Ra=R2, no significant improvement is achieved. This implies that in MAMI Relay1, if $\delta_{Rm} > \delta_{Ra}$, it achieves very similar result as MI Relay -via R1- and MAMI Relay1 when $\delta_{Rm} < \delta_{Ra}$, while the number of transmissions are increased.

The above discussion shows that the optimum selection of the relaying nodes is a key factor to achieving optimal system performance. Hence, it is critical to carefully select each node (master/assistant). In this regard, a proper metric for relay selection plays an important role in improving system performance.

Figure 5.27 shows the achieved data rates for LoS MAMI Relay 1 and 2. Similar to the NLoS case, in LoS scenario too, the highest throughput can be achieved through MAMI Relay1 if $\delta_{R_a} > \delta_{R_m}$. However, in MAMI Relay2, if $\delta_{R_a} > \delta_{R_m}$, it results in very similar performance as the case when $\delta_{R_a} < \delta_{R_m}$. Therefore, in LoS-MAMI Relay2 the relay master and assistant selection is not as critical as LoS-MAMI Relay1 (Figure 5.27).

5.4.4 Effect of different antenna displacement on the relay link indicator

The results here show the impact of angle and lateral misalignment, as well as the communication distance on the link quality in terms of the link indicator. Figure 5.28 shows how link indicator changes as the distance ($d_{Tx,Ri}$) increases. It might be

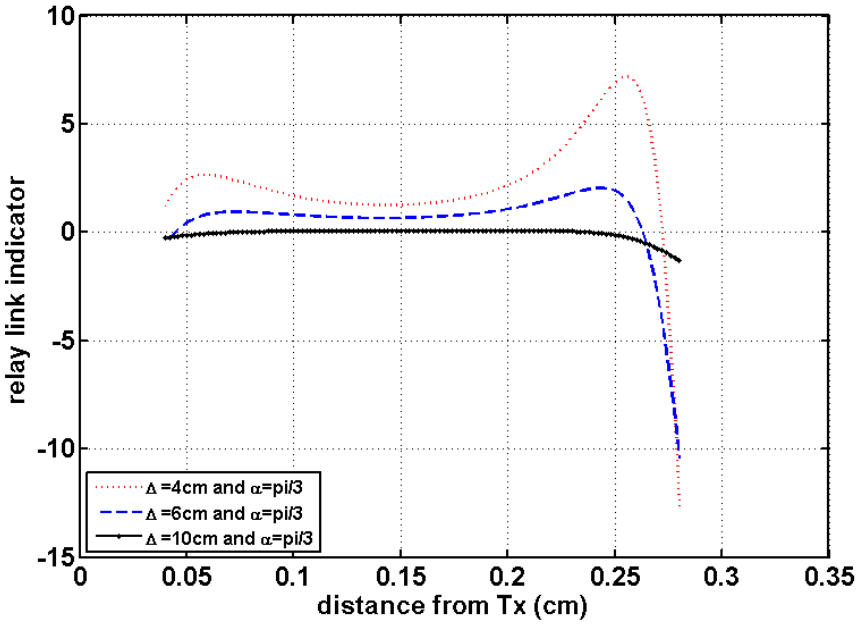

Figure 5.28 Relay link indicator vs. distance

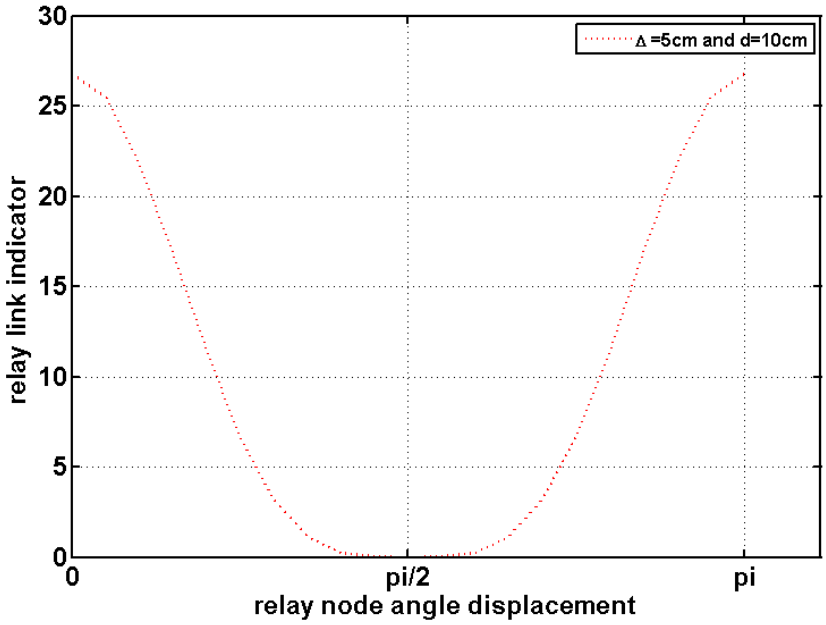

Figure 5.29 Relay link indicator vs. angle misalignment

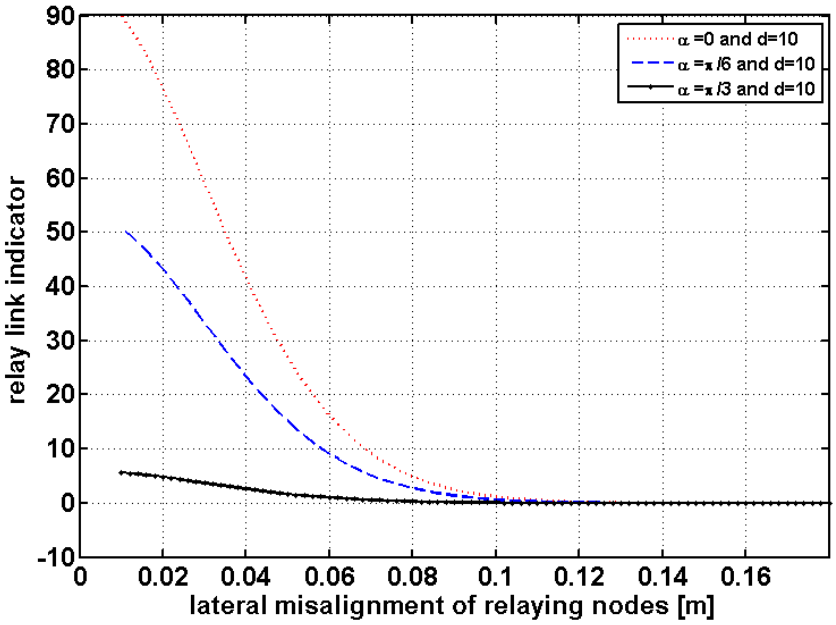

Figure 5.30 Relay link indicator vs. lateral misalignment

expected that as the distance increases, the link quality (δ) should be reduced, while as can be seen here the link indicator decreases with distance until the mid point between the transmitter and receiver and then it increases as it becomes closer to the receiver. However, sharp inflation occurs at specific distances depending on the value of lateral misalignment, since the complete elliptic of the first and second kind is dependent on the distance and lateral displacement. Hence, the distance between the nodes can not determine the optimum relay selection.

Figure 5.29 shows that the link indicator is maximized when the coils are placed with no angle misalignment in respect to each other. When the two nodes are located perpendicular to each other, the link indicator approaches its minimum value ($\delta = 0$). Although, large angle misalignment is undesirable in the system described here, it may be useful for noise reduction in multiple antenna systems. For example to reduce the power transfer between two adjacent antennas in MIMO -it is considered as undesirable noise- if the two antennas are placed with 90° relative to each other, the noise is highly reduced. However achieving exactly 90° may be difficult in practice.

Finally, Figure 5.30 shows how the link quality drops as the lateral misalignment increases. Here, the link indicator is studied for different values of lateral misalignment at distance 10 cm, for different angular orientations in respect to the source ($\alpha = 0$, $\alpha = 30^o$, $\alpha = 60^o$). The figure shows that, link indicator rapidly degrades as the lateral misalignment is increased. This effect can also be used for noise reduction, when the magnetic coupling between two closely located antennas is undesirable and contributes to the noise generation. However, studying the noise effect is out of the scope of this thesis and may be considered for future research.

5.5 Summary

This chapter proposed three cooperative relaying strategies: MI Relay, MAMI Relay 1 and 2. The methods are studied for both cases where a direct LoS exist between the transmitter and the target receiver as well as the case where the target receiver is out of direct range of the transmitter. These models are studied in a 3D environment to model a BAN realistically. The relaying strategies are analysed and compared theoretically and by the simulations. However, to select the relaying nodes to function as master or assistant different metric are studied. The result has shown that, although relay selection based on only separation distance, lateral or angle misalignment may be considered for a fixed network with minimal displacements, they are not optimum where large antenna displacements exist. In this context, a new relay selection metric (relay link indicator) is proposed that considers angular orientation and location of the relaying nodes relative to both transmitter and the target receiver. It is shown by analytical and simulation results that the relay link indicator is an optimum relay selection metric as compared to only the separation distance, lateral and angle misalignment.

Chapter 6

Conclusion

This chapter summarises the contribution of this thesis in Section 6.1. Despite the contribution of this study, there still remain a few research issues for further studies. This issues are discussed in Section 6.2.

6.1 Contributions

In this thesis, four related themes in respect to NFMIC have been studied, and are as follows:

In Chapter 2, a comprehensive literature review, on the topics directly related to the subject of this thesis is presented. This chapter discusses the signal propagation characteristics and path loss in the near field and far field regions. It is concluded that, compared to the far field region, signal attenuation is higher in the near field region. Therefore, this characteristic of the near field makes it suitable for short range communications. Following this, BANs are proposed as an application of the communication in the near field. Different types of BANs -wearable and implant BANs-, their technical requirements and their applications are discussed. It is discussed that a BAN may be used for the purpose of public safety, fitness monitoring, entertainment, assisting elderly people or people with disabilities, as well as for medical and health applications to improve the quality of life.

Then, an overview of the available technologies for the short range BANs are discussed and compared, which includes Bluetooth, UWB, specific low level radio, ZigBee and NFMIC. It is concluded that NFMIC may be the best possible solution for BAN, due to its inherent difficulty of long range detection, low power consumption and its penetration through objects, soil and body tissues. In this context, an overview of NFMIC fundamental concepts is given, and the relevant circuit models and equations are provided. It is shown that the communication range in NFMIC is very limited due to the high path loss (compared to RF communications). To address this limitation, it is proposed that cooperative communications may be applied to NFMIC, in order to increases the achieved communication range and data rates. This consequently may results in higher reliability and robustness in the network as compared to a conventional point-to-point communication.

In order to apply cooperative communications to the NFMIC, a literature review has been conducted, firstly on the concept of cooperative relaying in RF cellular communication networks, and secondly this concept has been studied for NFMIC systems. In the former section, different types of a cooperative network are given, which includes multihop- infrastructure, ad-hoc and hybrid networks, distributed and centralised networks, as well as transparent and non-transparent relaying modes [20]. Usage scenarios are also given for a cooperative relaying networks in RF cooperative communications. However, in the later section (Cooperative Communications in NFMIC), the conventional magnetic inductive waveguide is discussed as a method of range extension in NFMIC systems. Finally, some applications of the waveguide model are presented. However, it is discussed that although this model may be useful for underground sensor networks, it may not be directly applied to a BAN.

In Chapter 3, a link budget model (AM) is proposed for NFMIC. The model estimates the communication range of a point-to-point NFMIC, based on the antenna coil characteristics, the transmission power and the receiver sensitivity. The model is discussed theoretically and by simulations. It is shown that to increase the range of a point-to-point NFMIC, magnetically permeable material can be used in the core of

the transmitting and receiving coils (compared to air-cored coils). Upon the primary work of some researchers on NFMIC [6, 8, 15, 63], AM1 model is also proposed and compared with AM model. It is concluded that AM model results in longer range compared to AM1.

Chapter 4, studies the magneto inductive waveguide as a conventional and primary method of range extension in NFMIC. Firstly, the waveguide model is formulated, in which it relates the power transfer function to the quality factor of the coils, efficiency of the transmitting and receiving antennas and the coupling coefficient (similar to AM model). Then, according to the power transfer function, for an n-section waveguide system, section path loss β is introduced, and the model is analysed for different path loss approximations ($\beta >> 2$, $\beta = 2$ and $\beta << 2$). It is discussed that $\beta >> 2$ is an unrealistic situations, since the receiver collects more power than the transmitted power, and this invades the law of conservation of energy. $\beta << 2$ is a realistic situation, since the received signal is less than the transmitted signal. However, waveguide may not work properly under this situation. This means that by increasing the number of nodes within a given communication distance, the received power decreases, thus, results is shortening the achieved range. This is due to the power reflection back to the transmitting nodes within the transmission line, and can be minimised by a proper method of termination of the waveguide transmission system. However, when $\beta = 2$, the waveguide approaches a distance threshold, at which the waveguide behavior is reversed: by increasing the number of nodes, the achieved distance increases. It is shown that the distance threshold is a function of the coil characteristics and can be extended.

It is also discussed in this chapter that to improve the performance of a waveguide system, the method of voltage excitation of the transmission array is very important. In this context, three voltage excitation methods are proposed and studied: AEE, ACE and CAE. Their performance has been compared, and the result has shown that ACE provides the highest received voltage at each receiving node among the three method, whereas CAE has the lowest received voltage at the receiving nodes.

Finally, it is discussed in this chapter, that the conventional collinear waveguide system cannot directly be applied to a BAN scenario. Therefore, there is a need for a cooperative communication method that takes into account the 3D nature of a BAN.

In Chapter 5, three methods of cooperative communications are proposed for the NFMIC applicable to a BAN: MI Relay, MAMI Relay 1 and 2. Since the nodes in a BAN may change their location and angle orientation in respect to each other, a cooperative communication method should take into consideration the effect of the angle and lateral displacements, as well as the separation distance between the nodes. In this regard, this chapter firstly analyses the effect of different antenna displacements on a point-to-point NFMIC system, then this is used to model the signal propagation for the proposed relaying techniques. The three methods are analysed for both cases, when a direct link exists between the transmitter and the target receiver, as well as the situation when the target receiver is out of the direct range of the transmitter.

These techniques are then simulated in Matlab, in order to analyse their performance. It is discussed that if the relative antenna displacement is minimal within the system, separation distance is a proper metric for the relay selection (M/A selection). However, it is shown that if there are large antenna displacements between the nodes, distance alone cannot be a proper metric. Then, lateral and angle misalignment are studied as the relay selection metric, and it is discussed that none of them alone can be an optimum relay selection criterion. Therefore, relay link indicator is proposed as a new relay selection metric, which considers separation distance, lateral and angle misalignment of the relaying antenna relative to both the transmitter and the receiver.

It is shown that the intermediate nodes with higher link indicator, provides higher received signal at the final receiver. It is also shown that in LoS MAMI Relay 1, if the node with higher link indicator is selected to act as relay assistant, higher data rates can be achieved, and in NLoS case, it achieves longer communication range. Similar result has been observed for NLoS MAMI Relay 2 as well. However, in LoS-MAMI Relay 2, the selection of the relaying node to act as relay master or assistant is not as critical as in LoS-MAMI Relay 1.

Finally, the impact of different antenna displacements and the separation distance on the relay link indicator is analysed. It is shown that as the angle displacement approaches 90°, the link indicator approaches zero, and by increasing the lateral misalignment the link indicator also decreases. However, as the distance between the transmitter and relay node increases to the mid point between the transmitter and receiver, the link indicator decreases; as the relay moves from the mid point toward the receiver, the link indicator increases.

6.2 Future Work

Heterogenous Networks: Although this thesis has studied cooperative communication techniques for homogenous NFMIC networks, the nodes within the network may not always have identical characteristics. Hence, cooperative communication should be analysed for heterogenous NFMIC relaying networks, and an optimum relay selection metric may need to be determined for such a system. For instance, in a NFMIC cooperative communication network consists of nodes with different antenna characteristics -for example different quality factors and efficiencies-, the link indicator as discussed in Chapter 5, may not be an appropriate metric for M/A selection. The metric may need to take into consideration, the specific characteristics of each antenna, such as the type of inductor, in order to achieve optimum relay node selection. Therefore, the cooperative relaying techniques proposed in this thesis may be studied further for heterogenous NFMIC systems.

Timing Synchronization: To achieve optimum cooperative communications, precise timing synchronization is required. There are a few synchronization algorithms for RF communications. This includes, Network Time Protocol (NTP) [77], the Tiny-Sync and Mini-Sync protocols [78], the Reference Broadcast Synchronization (RBS) [79] and Pairwise Broadcast Synchronization (PBS) [80]. Either of the mentioned synchronization protocols may be directly applied to NFMIC relaying networks, or some modifications may be required. However, there may be a need for a

novel synchronization algorithm for NFMIC relaying networks to suit specific characersitics of NFMIC. This concept requires further research and studies.

Mobility: A BAN may be a network of static or mobile nodes. Implant BANs often form a static network, since BAN nodes such as artificial organs and condition monitoring sensors are implanted inside the human body. Therefore, they are usually required to be fixed at a specific position. In contrast, the nodes in an on-body BAN tend to be mobile. The person carrying the devices may intentionally change the location of each node, or the node position may be changed as the person moves. Hence the network topology is dynamic and may be changed frequently. There may also be topology changes due to a node failure and new joining nodes. Therefore, there is a need for a routing and medium access control protocol design that takes into consideration, the mobility and frequent network topology changes of a multihop BAN. Issues such as fairness, delay, energy efficiency and bandwidth utilisation have been somewhat relaxed in wireless MAC protocols, while addressing mobility in such networks still requires further work and research [81]. There are MAC protocols such as mobility adaptive-collision free MAC (MMAC) [81], that have introduced a mobility adoptive frame structure that is able to dynamically adapt to the topology changes. In fact, MMAC uses the location information to estimate the future topology of the network (based on the prediction of the nodes mobility behaviour). Mobility-aware MAC protocol for Sensor Networks (MS-MAC) is another protocol that is designed for mobile sensor networks [82]. In MS-MAC nodes use RSS changes, after a specific time period, to learn about the mobility of their neighbouring nodes. This protocol supports for multihop communications in wireless sensor networks. However, a BAN, as a specific type of a sensor network, has its own requirements and challenges. Hence, this concept needs to be studied for BANs. Most of the existing MAC protocols for BANs are designed for stationary networks or single hop intra-BAN communications, such as MAC for in-vivo BAN [83] and MST protocols [84]. Therefore, applicability of such algorithms to a multihop NFMIC BAN with mobility should be studied.

Interference and Noise Analysis: Interference and noise analysis in multihop NFMIC systems also require further research. As previously discussed , NFMIC and RF communication systems may coexist without interfering each other, due to the perpendicularity of the magnetic and electric waves with respect to each other. However, within a BAN using NFMIC device, there may be interference between the simultaneous transmissions by different transmitters. Moreover, if different BANs are located in close proximity of each other, intra-BAN interference may exist and impact the system performance. Interference impacts the total system throughput and packet delay. Hence, the overall system performance degrades. Interference mitigation is still a major challenge in many wireless communication systems. Different interference mitigation algorithms have been proposed for RF communications. However, since the signal behavior is different in NFMIC, further study is required for NFMIC noise and interference analysis.

Bibliography

[1] P. Nikitin, K. Rao, and S. Lazar, "An overview of near field uhf rfid," in *RFID, 2007. IEEE International Conference on*, March 2007, pp. 167 –174.

[2] H. Schantz, "Near field channel model," pp. 1–13, Oct. 2004.

[3] (2010, Jan.) Freelinc near field magnetic induction technology. [Online]. Available: www.freelinc.com

[4] H. Jing and Y. Wang, "Capacity performance of an inductively coupled near field communication system," in *Antennas and Propagation Society International Symposium, 2008. AP-S 2008. IEEE*, July 2008, pp. 1 –4.

[5] S. W. Peters and R. W. Heath, "The future of wimax: Multihop relaying with ieee 802.16j," *Communications Magazine, IEEE*, vol. 47, no. 1, pp. 104–111, 2009.

[6] S. Zhi and I. F. Akyildiz, "Underground wireless communication using magnetic induction," in *Communications, 2009. ICC '09. IEEE International Conference on*, pp. 1–5.

[7] R. R. A. Syms, E. Shamonina, and L. Solymar, "Magneto-inductive waveguide devices," *Microwaves, Antennas and Propagation, IEE Proceedings* -, vol. 153, no. 2, pp. 111–121, 2006.

[8] I. F. Akyildiz, Z. Sun, and M. C. Vuran, "Signal propagation techniques for wireless underground communication networks," *Physical Communication*,

vol. 2, no. 3, pp. 167–183, Sep. 2009. [Online]. Available: http://www.sciencedirect.com/science/article/pii/S1874490709000408

[9] K. Fotopoulou and B. Flynn, "Optimum antenna coil structure for inductive powering of passive rfid tags," in *RFID, 2007. IEEE International Conference on*, March 2007, pp. 71 –77.

[10] FreeLink. (2009) Near field products. [Online]. Available: http://www.freelinc.com/products/

[11] (2010) Human body 3d model. [Online]. Available: http://www.3dmodelfree.com/models//262080.htm

[12] J. Flores, S. Srikant, B. Sareen, and A. Vagga, "Performance of rfid tags in near and far field," in *Personal Wireless Communications, 2005. ICPWC 2005. 2005 IEEE International Conference on*, Jan. 2005, pp. 353 – 357.

[13] J. I. Agbinya, *Principles of Inductive Near Field Communications for Internet of Things*. Denmark: River Pub., 2011.

[14] J. Agbinya, *Planning and optimization of 3G & 4G wireless networks*. Denmark: River Pub., 2009.

[15] J. I. Agbinya, N. Selvaraj, A. Ollett, S. Ibos, Y. Ooi-Sanchez, M. Brennan, and Z. Chaczko, "Size and characteristics of the 'cone of silence' in near-field magnetic induction communications," *Battlefield Technology*, vol. 13, 2010.

[16] (2010, Feb.) Beamforming and array processing. [Online]. Available: http://www.eleceng.adelaide.edu.au/personal/peter/peter/L5EMT&RFID10/HelpOnCouplingVolume.pdf

[17] H. C. Jing and Y. E. Wang, "Capacity performance of an inductively coupled near field communication system," in *Antennas and Propagation Society International Symposium, 2008. AP-S 2008. IEEE*, pp. 1–4.

[18] I. P. Chochliouros, A. Mor, K. N. Voudouris, G. Agapiou, A. Aloush, M. Belesioti, E. Sfakianakis, and P. Tsiakas, "A multi-hop relay station software architecture design, on the basis of the wimax ieee 802.16j standard," in *Vehicular Technology Conference, 2009. VTC Spring 2009. IEEE 69th*, pp. 1–6.

[19] D. Soldani and S. Dixit, "Wireless relays for broadband access [radio communications series]," *Communications Magazine, IEEE*, vol. 46, no. 3, pp. 58–66, 2008.

[20] J. Sydir and R. Taori, "An evolved cellular system architecture incorporating relay stations," *Communications Magazine, IEEE*, vol. 47, no. 6, pp. 115–121, 2009.

[21] C. Capps. (2001) Near field of far field. [Online]. Available: www.edn.com/contents/images/150828.pdf

[22] T. Lecklider. (2005, Oct.) The world of the near field. [Online]. Available: http://archive.evaluationengineering.com/archive/articles/1005/1005the_world.asp

[23] S. Vasisht. Near field magnetic communication for low power wireless devices @ONLINE. [Online]. Available: http://www.auracomm.com

[24] Sony. (2010) Near field communications. [Online]. Available: international.org/activities/Communications/TC32tg19_110603.old.pdf

[25] NFCforum. (2010) Near field communications. [Online]. Available: www.nfc-forum.org

[26] H. Schantz, "Near field propagation law a novel fundamental limit to antenna gain versus size," in *Antennas and Propagation Society International Symposium, 2005 IEEE*, vol. 3A, July 2005, pp. 237 – 240 vol. 3A.

[27] N. Selvaraj and J. Agbinyar, *Planning and optimization of 3G & 4G wireless networks*, ch. 6.

[28] H. B. Li and R. Kohno, *Body Area Network and Its Standardization at IEEE 802.15.BAN*, ser. Lecture Notes in Electrical Engineering. Springer Berlin Heidelberg, 2008, vol. 16, pp. 223–238.

[29] B. Latré, B. Braem, I. Moerman, C. Blondia, and P. Demeester, "A survey on wireless body area networks," *Wirel. Netw.*, vol. 17, pp. 1–18, January 2011. [Online]. Available: http://dx.doi.org/10.1007/s11276-010-0252-4

[30] S. Drude, "Requirements and application scenarios for body area networks," in *Mobile and Wireless Communications Summit, 2007. 16th IST*, July 2007, pp. 1 –5.

[31] R. Hoyt, J. Reifman, T. Coster, and M. Buller, "Combat medical informatics: present and future," in *Proc AMIA Symp*, December 2002, pp. 335–339.

[32] bluetooth. [Online]. Available: www.bluetooth.com

[33] S. Sadeghzadeh, S. Shirazani, and M. Mosleh, "Notice of violation of ieee publication principles a new secure scheme purposed for recognition and authentication protocol in bluetooth environment," in *Advanced Communication Technology (ICACT), 2010 The 12th International Conference on*, vol. 2, Feb. 2010, pp. 1326 –1331.

[34] S. Wang, A. Waadt, S. Rickers, C. Kocks, D. Xu, A. Viessmann, G. Bruck, and P. Jung, "Java implementation of localization and tracking application based on hdr-uwb platform," in *Applied Sciences in Biomedical and Communication Technologies, 2009. ISABEL 2009. 2nd International Symposium on*, Nov. 2009, pp. 1 –5.

[35] R. Xu, Y. Jin, and C. Nguyen, "Power-efficient switching-based cmos uwb transmitters for uwb communications and radar systems," *Microwave Theory and Techniques, IEEE Transactions on*, vol. 54, no. 8, pp. 3271 –3277, Aug. 2006.

[36] S. H. Kim, J. S. Kang, H. S. Park, D. Kim, and Y. joo Kim, "Upnp-zigbee internetworking architecture mirroring a multi-hop zigbee network topology," *Consumer Electronics, IEEE Transactions on*, vol. 55, no. 3, pp. 1286 –1294, August 2009.

[37] I. Ramachandran and S. Roy, "Analysis of throughput and energy efficiency of p-persistent csma with imperfect carrier sensing," in *Global Telecommunications Conference, 2005. GLOBECOM '05. IEEE*, vol. 6, Dec. 2005, pp. 5 pp. –3432.

[38] R. Bansal, "Near-field magnetic communication," *Antennas and Propagation Magazine, IEEE*, vol. 46, no. 2, pp. 114–115, 2004.

[39] N. Jack and K. Shenai, "Magnetic induction ic for wireless communication in rf-impenetrable media," in *Microelectronics and Electron Devices, 2007. WMED 2007. IEEE Workshop on*, pp. 47–48.

[40] V. Palermo, "Near field magnetic comms emerges," Nov 2003.

[41] C. Bunszel, "Magnetic induction: A low-power wireless alternative," 15/11/2010 2001.

[42] J. Agbinya and M. Masihpour, "Power equations and capacity performance of magnetic induction communication systems," *Wireless Personal Communications*, pp. 1–15, 2011.

[43] C. Bunszel, "Magnetic induction:a low-power wirelessalternative," 2001.

[44] Z. Sun and I. Akyildiz, "Magnetic induction communications for wireless underground sensor networks," *Antennas and Propagation, IEEE Transactions on*, vol. 58, no. 7, pp. 2426 –2435, July 2010.

[45] S. Zhi and I. Akyildiz, "Deployment algorithms for wireless underground sensor networks using magnetic induction," in *GLOBECOM 2010, 2010 IEEE Global Telecommunications Conference*, Dec. 2010, pp. 1 –5.

[46] A. Vaios, "Incorporation of the short-range multi-hop communication model in infrastructure-based wireless local area networks," Ph.D. dissertation, 2009.

[47] X. J. Li, B.-C. Seet, and r. H. J. Chong, "Multihop cellular networks: Technology and economics," *Computer Networks*, vol. 52, no. 9, pp. 1825–1837, 2008.

[48] H. Lee and C. C. Lee, "An integrated multihop cellular data network," in *Vehicular Technology Conference, 2003. VTC 2003-Fall. 2003 IEEE 58th*, vol. 4, pp. 2232–2236 Vol.4.

[49] I. Ioannidis and B. Carbunar, "Scalable routing in hybrid cellular and ad-hoc networks," in *Mobile Ad-hoc and Sensor Systems, 2004 IEEE International Conference on*, pp. 522–524.

[50] I. F. Akyildiz, X. Wang, and W. Wang, "Wireless mesh networks: a survey," *Computer Networks*, vol. 47, no. 4, pp. 445–487, 2005.

[51] G. Hongju and D. G. Daut, "Performance evaluation of multihop wpans based on a realistic ofdm uwb physical layer," in *Vehicular Technology Conference, 2007. VTC2007-Spring. IEEE 65th*, pp. 90–94.

[52] M. A. B. Sarijari, R. A. Rashid, M. R. A. Rahim, and N. H. Mahalin, "Wireless home security and automation system utilizing zigbee based multi-hop communication," in *Telecommunication Technologies 2008 and 2008 2nd Malaysia Conference on Photonics. NCTT-MCP 2008. 6th National Conference on*, pp. 242–245.

[53] A. A. Janefalkar, K. Josiam, and D. Rajan, "Cellular ad-hoc relay for emergencies (care)," in *Vehicular Technology Conference, 2004. VTC2004-Fall. 2004 IEEE 60th*, vol. 4, pp. 2873–2877 Vol. 4.

[54] K. Gosse, "New radio interfaces for short range communications," Tech. Rep.

[55] M. Krunz, A. Muqattash, and L. Sung-Ju, "Transmission power control in wireless ad hoc networks: challenges, solutions and open issues," *Network, IEEE*, vol. 18, no. 5, pp. 8–14, 2004.

[56] S. Jang-Ping, L. Chen-Wei, and C. Chih-Min, "Power-aware routing for energy conserving and balance in ad hoc networks," in *Networking, Sensing and Control, 2004 IEEE International Conference on*, vol. 1, pp. 468–473 Vol.1.

[57] A. Torok, L. Vajda, P. Laborezi, Z. Fulop, and A. Vidaes, "Analysis of scatternet formation in high-rate multi-hop wpans," in *Personal, Indoor and Mobile Radio Communications, 2006 IEEE 17th International Symposium on*, pp. 1–6.

[58] N. Ben Salem, L. Buttyan, J. P. Hubaux, and M. Jakobsson, "Node cooperation in hybrid ad hoc networks," *Mobile Computing, IEEE Transactions on*, vol. 5, no. 4, pp. 365–376, 2006.

[59] R. R. A. Syms, I. R. Young, and L. Solymar, "Low-loss magneto-inductive waveguides," *Journal of Physics D: Applied Physics*, vol. 39, no. 18, p. 3945, 2006. [Online]. Available: http://stacks.iop.org/0022-3727/39/i=18/a=004

[60] J. J. Sojdehei, P. N. Wrathall, and D. F. Dinn, "Magneto-inductive (mi) communications," in *OCEANS, 2001. MTS/IEEE Conference and Exhibition*, vol. 1, pp. 513–519 vol.1.

[61] M. Masihpour and J. I. Agbinya, "Cooperative relay in near field magnetic induction: A new technology for embedded medical communication systems," in *Broadband and Biomedical Communications , 2010 International Conference on*, pp. 1–6.

[62] J. I. Agbinya and M. Masihpour, "Excitation methods for magneto inductive waveguide communication systems," in *Broadband and Biomedical Communications , 2010 International Conference on*, pp. 1–6.

[63] R. Syms, L. Solymar, and E. Shamonina, "Absorbing terminations for magneto-inductive waveguides," *Microwaves, Antennas and Propagation, IEE Proceedings* -, vol. 152, no. 2, pp. 77 – 81, Apr 2005.

[64] R. R. A. Syms and L. Solymar, "Magneto-inductive cable arrays: Estimation and reduction of crosstalk," *Journal of Applied Physics*, vol. 109, no. 4, pp. 044 902 –044 902–10, Apr 2011.

[65] O. Zhuromskyy, O. Sydoruk, E. Shamonina, and L. Solymar, "Slow waves on magnetic metamaterials and on chains of plasmonic nanoparticles: Driven solutions in the presence of retardation," vol. 106, no. 10, p. 104908, 2009. [Online]. Available: http://dx.doi.org/10.1063/1.3259397

[66] J. Agbinya, "Framework for wide area networking of inductive internet of things," *Electronics Letters*, vol. 47, no. 21, pp. 1199 –1201, 12 2011.

[67] O. Zhuromskyy, O. Sydoruk, E. Shamonina, and L. Solymar, "Slow waves on magnetic metamaterials and on chains of plasmonic nanoparticles: Driven solutions in the presence of retardation," *Journal of Applied Physics*, vol. 106, no. 10, pp. 104 908 –104 908–7, Nov 2009.

[68] J. Agbinya and M. Masihpour, *Planning and optimization of 3G and 4G wireless networks*. Denmark: River Pub., 2009, ch. Part III Wimax and LTE Link Budge.

[69] R. Ezzine, A. Al-Fuqaha, R. Braham, and A. Belghith, "A new generic model for signal propagation in wi-fi and wimax environments," in *Wireless Days, 2008. WD '08. 1st IFIP*, Nov. 2008, pp. 1 –5.

[70] J. Milanovic, S. Rimac-Drlje, and K. Bejuk, "Comparison of propagation models accuracy for wimax on 3.5 ghz," in *Electronics, Circuits and Systems, 2007. ICECS 2007. 14th IEEE International Conference on*, Dec. 2007, pp. 111 –114.

[71] J. I. Agbinya, *IP Communications and Services for NGN*. Denmark: Taylor Francis., 2010.

[72] A. H. I. O. Tamaz Javornik, Gorazd Kandus, *Software in Telecommu- nication and Computer Networks*, 2006.

[73] J. I. Agbinya and M. Masihpour, "Near field magnetic induction communication link budget: Agbinya-masuhpour model," in *Broadband and Biomedical Communications , 2010 International Conference on*, pp. 1–6.

[74] J. Agbinya and M. Masihpour, *Principles of Inductive Near Field Communications for Internet of Things*. Denmark: River Pub., 2011, ch. Magneto Inductive Link Budget.

[75] J. N. Laneman, D. N. C. Tse, and G. W. Wornell, "Cooperative diversity in wireless networks: Efficient protocols and outage behavior," *Information Theory, IEEE Transactions on*, vol. 50, no. 12, pp. 3062–3080, 2004.

[76] M. Soma, D. C. Galbraith, and R. L. White, "Radio-frequency coils in implantable devices: Misalignment analysis and design procedure," *Biomedical Engineering, IEEE Transactions on*, vol. BME-34, no. 4, pp. 276–282, 1987.

[77] D. Mills, "Internet time synchronization: the network time protocol," *Communications, IEEE Transactions on*, vol. 39, no. 10, pp. 1482 –1493, Oct 1991.

[78] S. Yoon, C. Veerarittiphan, and M. L. Sichitiu, "Tiny-sync: Tight time synchronization for wireless sensor networks," *ACM Trans. Sen. Netw.*, vol. 3, June 2007. [Online]. Available: http://doi.acm.org/10.1145/1240226.1240228

[79] J. Elson, L. Girod, and D. Estrin, "Fine-Grained Network Time Synchronization using Reference Broadcasts," 2002. [Online]. Available: http://citeseerx.ist.psu.edu/viewdoc/summary?doi=10.1.1.17.4097

[80] K. lae Noh, E. Serpedin, and K. Qaraqe, "A new approach for time synchronization in wireless sensor networks: Pairwise broadcast synchronization," *Wireless Communications, IEEE Transactions on*, vol. 7, no. 9, pp. 3318 –3322, September 2008.

[81] M. Ali, T. Suleman, and Z. Uzmi, "Mmac: a mobility-adaptive, collision-free mac protocol for wireless sensor networks," in *Performance, Computing, and Communications Conference, 2005. IPCCC 2005. 24th IEEE International*, April 2005, pp. 401 – 407.

[82] H. Pham and S. Jha, "Addressing mobility in wireless sensor media access protocol," in *Intelligent Sensors, Sensor Networks and Information Processing Conference, 2004. Proceedings of the 2004*, Dec. 2004, pp. 113 – 118.

[83] L. Lin, K.-J. Wong, A. Kumar, S. L. Tan, and S. J. Phee, "An energy efficient mac protocol for mobile in-vivo body sensor networks," in *Ubiquitous and Future Networks (ICUFN), 2011 Third International Conference on*, June 2011, pp. 95 –100.

[84] H. Kwon and S. Lee, "Energy-efficient multi-hop transmission in body area networks," in *Personal, Indoor and Mobile Radio Communications, 2009 IEEE 20th International Symposium on*, Sept. 2009, pp. 2142 –2146.

[85] A. C. Boucouvalas and P. Huang, "Obex over irda: Performance analysis and optimization by considering multiple applications," *Networking, IEEE/ACM Transactions on*, vol. 14, no. 6, pp. 1292 –1301, Dec. 2006.

Appendix A

NFMIC-GUI

A.1 Overview

Using Matlab, a graphical user interface (*NFMIC-GUI*) is developed, which can be used to model AM link budget, discussed in Chapter 3 for NFMIC. Researchers in the field can benefit from NFMIC-GUI by evaluating the signal power at the receiver and communication range against different antenna coil parameters, such as transmitter and receiver coil efficiency, Q-factor, permeability, radius as well as the transmission power. Here, a description of NFMIC-GUI is provided. The theoretical background is discussed in Chapter 3.

These codes are published in *Principles of Inductive Near Field Communications for Internet of Things* authored by Johnson Agbinya in 2011.

A.2 NFMIC-GUI

Firstly by running the program, the *'home page'* window as shown in Figure A.1 appears. The home page is divided into two sections: the left column shows four push buttons, each operates a specific function. The right column, which can be seen in yellow, shows the brief description of the function of each push button. Therefore, the user can easily find the part of the program that suits his/her intention. By clicking

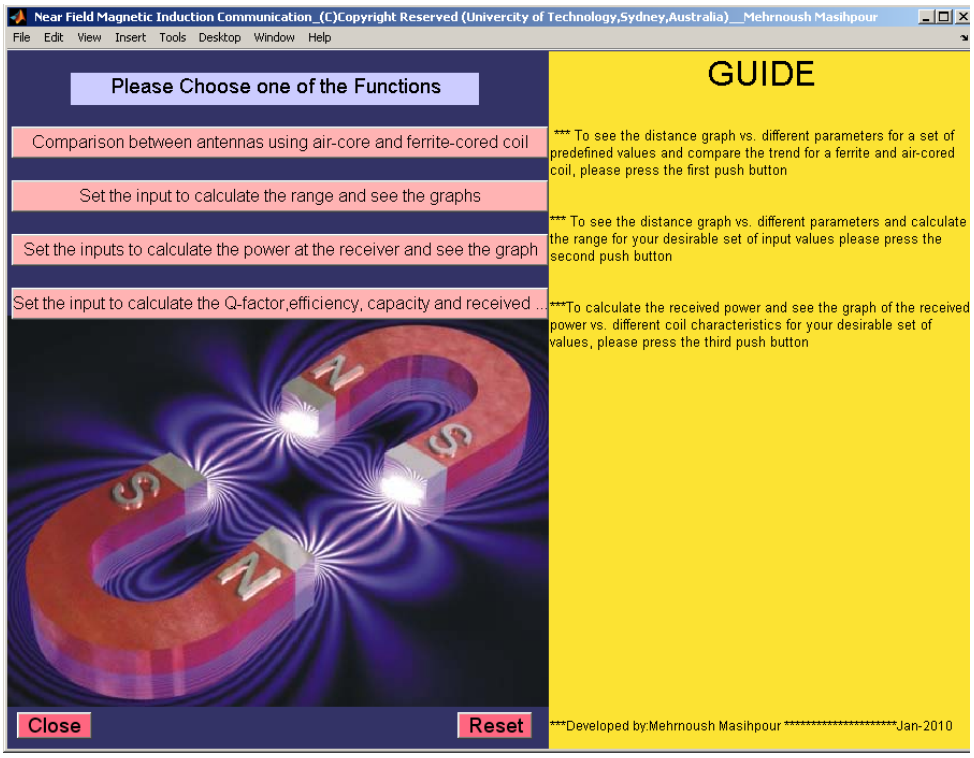

Figure A.1 Home Page

on either push buttons, a new window will appear, which the tasks are as follows:

First Push Button: ***"Comparison between antennas using air-cored and ferrite-cored coils"***

By clicking on the first push button, a window as shown in Figure A.2 opens, which has two positions to show different axis, in order to demonstrate the achieved distance against a range of antenna coil parameters that can impact the communication range, for two cases of using air and ferrite-cored antenna coils (see Chapter 3 for detail). By choosing one of the desirable graphs from the pop-up menu for each case, two graphs can be seen and compared; this shows how ferrite material at the core can improve the communication range. The assigned values for different parameters are shown in the left column of the window. In each positions, there are two plots, which show the communication range, when considering or neglecting Δd at the AM link budget equation. Therefore, the difference between these two cases can be seen on

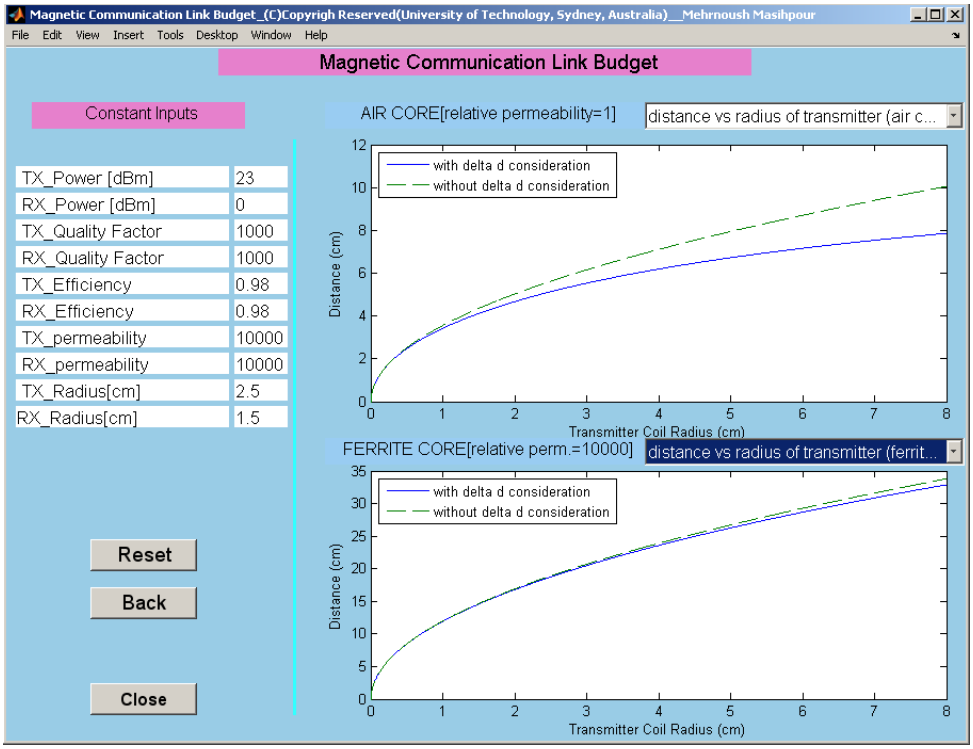

Figure A.2 Air and Ferrite-cored coil comparison

the axis. There is a *'Reset'* button in this window which clears the axis.

Second Push Button: ***"Set the values to calculate the range and see the graphs"***

The second interface, as shown in Figure A.3 is more dynamic and useful for design purposes. Using this interface, the value of each parameter is determined by the user at the edit boxes in the upper left column, and simply by pushing one of the radio buttons the communication range against the desirable coil parameter can be observed on the axis, for both ferrite-cored and air-cored antenna coil. To return the values to their default and clear the axis, the *'Reset'* button needs to be clicked on. Moreover, by clicking on the *"Calculate the Distance (cm)"* button, the value of communication distance for the assigned values to each parameter will appear in front of the buttons, for either case.

Third Push Button: ***"Set the values to calculate the power at the receiver and see***

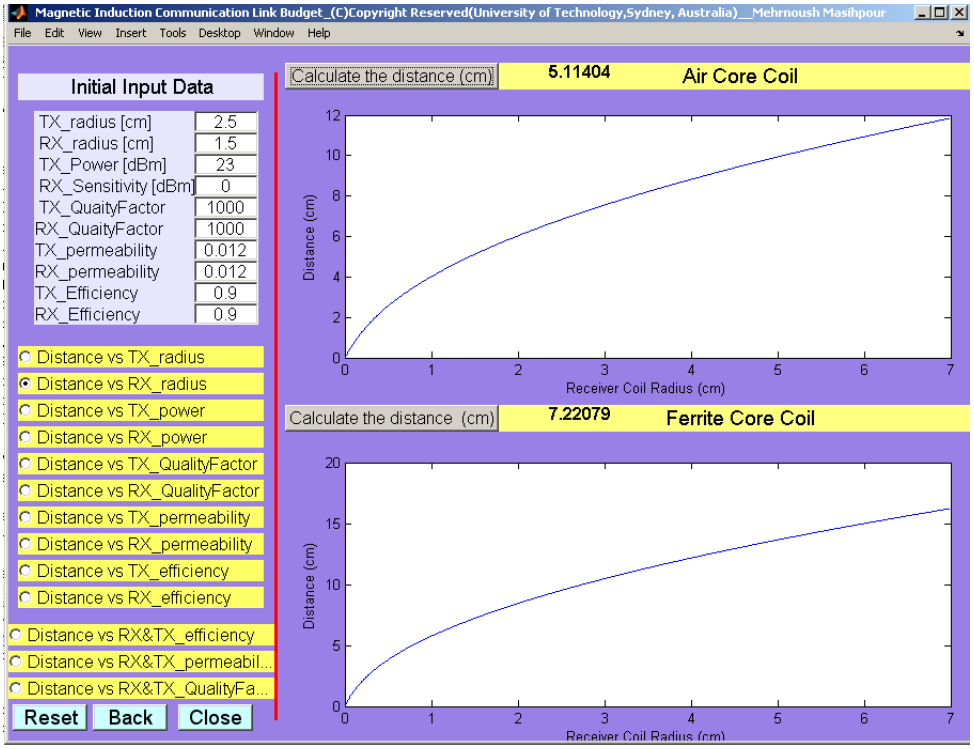

Figure A.3 Air and Ferrite-cored coil comparison and link budget calculations for various inputs

the graphs"

This part of the GUI is useful for the estimation of received signal power for different scenarios. As can be seen from Figure A.4, there is a column at the upper left side of the window, indicating the input data, in which the default value can be replaced with the desirable values. Then, by choosing one of the radio buttons underneath, the received power plot against the required parameters appears on the axis. Calculation of the received power for the assigned set of values can also be shown on the window, by clicking on the push button below the axis.

The estimated received power can be seen in both units of dBm and mW. The *'Reset'* button returns the default values back to the edit boxes, and the program can be run for another set of design parameter values. The *'Back'* button in each window, returns the user to the home page, and the *'close'* button in each window will close

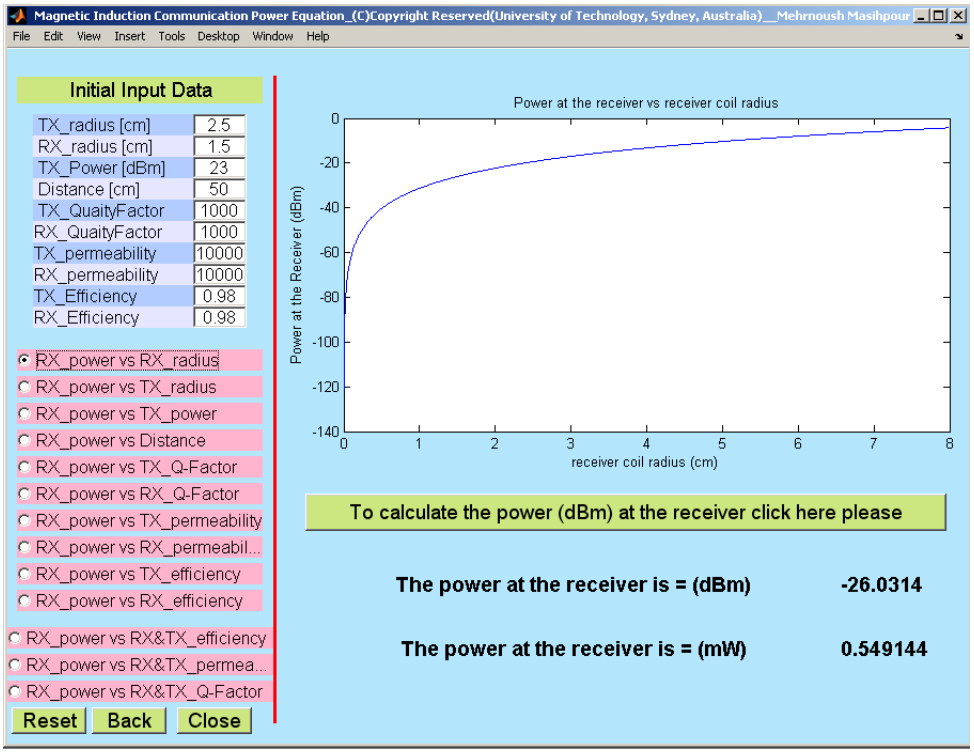

Figure A.4 Received power calculations and graphs vs. antenna coil components

the *NFMIC-GUI*.

Fourth push button: ***"set the input to calculate the Q-factor, efficiency, received power and capacity"***

In this section of the NFMIC-GUI (Figure A.5), the operating frequency can be set to any value. However, the radio buttons next to the *"centre frequency"* edit box, allows the user to choose the frequency in the range of MHz and GHz. The self inductance of the coils, source or load resistance, coil resistance, transmitting and receiving coil radii, desirable communication range and transmission power can also be set to the required values. Therefore, by clicking on the first push button, this tool, which may be referred to as an NFMIC calculator, calculates the quality factor of the coils. Second button calculates the coil efficiency and the following button estimates the capacity at the edge of the communication bubble in unit of bps. Finally, by clicking on the last button, received power at a desirable distance can be seen in unit

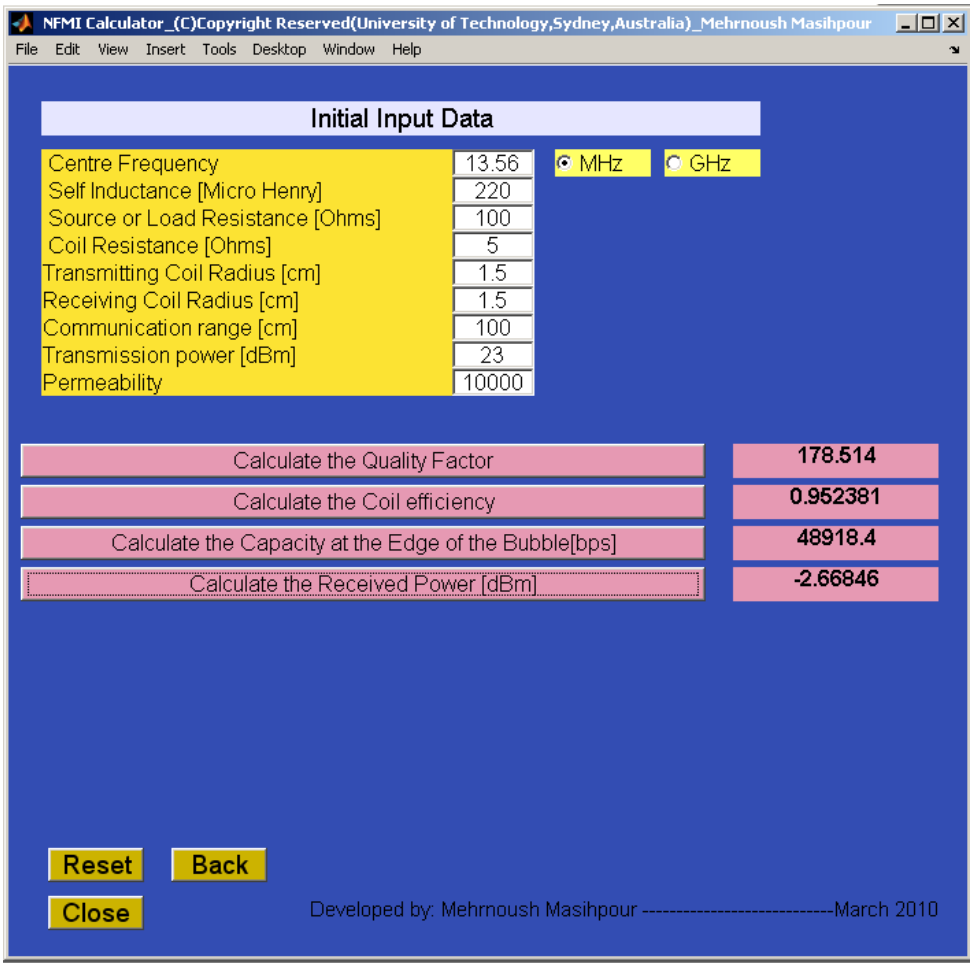

Figure A.5 Q-factor, efficiency, received power and capacity calculation for a set of parameters

of dBm. To run the program for a new set of design parameter values, the *'Reset'* button should be clicked on. *'Back'* Button returns the user to the home page and *'close'* button exits the program.

Appendix B

Master/Assistant Relay Selection Based on Angle and Lateral Displacements

B.1 Overview

This chapter provides the Matlab simulation results, for the case when Master/Assistant (M/A) relay selection is performed based on the angle and lateral displacement of the relaying nodes. In Chapter 5, it is discussed that although the separation distance may be considered as a proper relay selection metric in a perfect condition (i.e. no angle and lateral displacement), or minimal displacement, it is not optimum when large lateral and angular misalignments exist. It is also discussed theoretically that M/A selection based on the lateral and angle displacement alone is not optimum. In this chapter, the simulation results are provided for these two cases, in order to show that a reliable decision cannot be obtained based on only one of the parameters. The following section shows the plots for the achieved RSS and data rates for NLoS and LoS MAMI Relay 1 and 2 against the relaying nodes Δ and α (relative to the Tx). The design parameters are the same as discussed in Chapter 5.

B.2 Figures

Figure B.1 shows the achieved received signal for NLoS MAMI Relay 1, when M/A are selected based on their angle misalignments (in respect to the reference node, which is Tx). In this scenario, $\alpha_{R1} = \pi/4$ and $\alpha_{R2} = \pi/3$ to be able to analyse the impact of the relaying node lateral displacement, when the M/A selection is performed based on their angle misalignment. As can be seen from Figure B.1 if the relay selection is performed based on the angle misalignment of the relaying nodes, the received signal at the final receiver experiences a rapid decline as the lateral misalignment increases. However, a sharp fluctuation can be seen here; as discussed previously in Chapter 5, this is due to the impact of the complete elliptic integrals of the first and second kind. The Δ at which this fluctuation occurs, depends on the relative distance and angular orientation of the relaying nodes and Tx/Rx, as well as the applied relaying strategy. Very similar behavior can be seen for NLoS-MAMI Relay 2 in Figure B.2. In this Case, the point of inflation (for Δ) is very

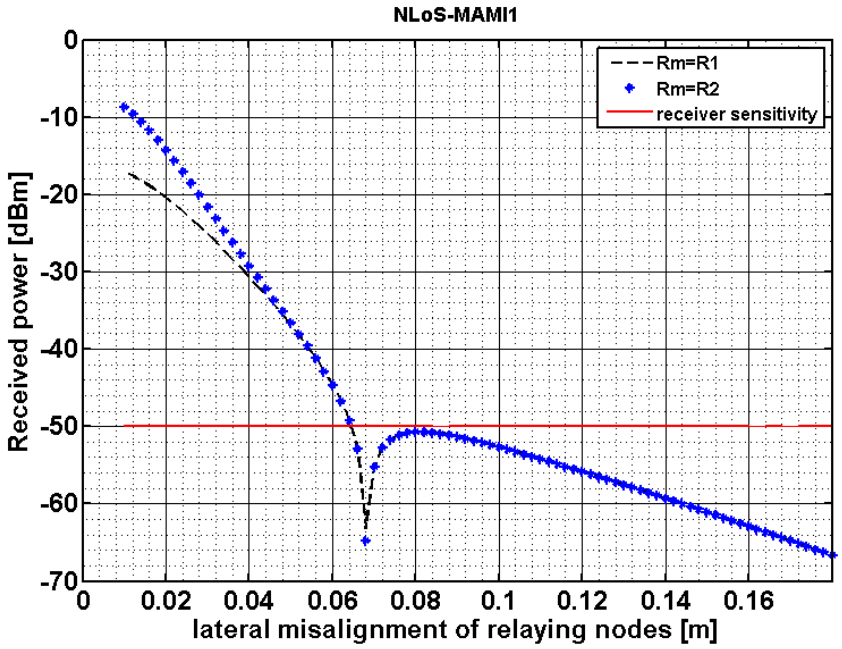

Figure B.1 NLoS MAMI Relay1: achieved received signal against the relaying nodes lateral misalignment

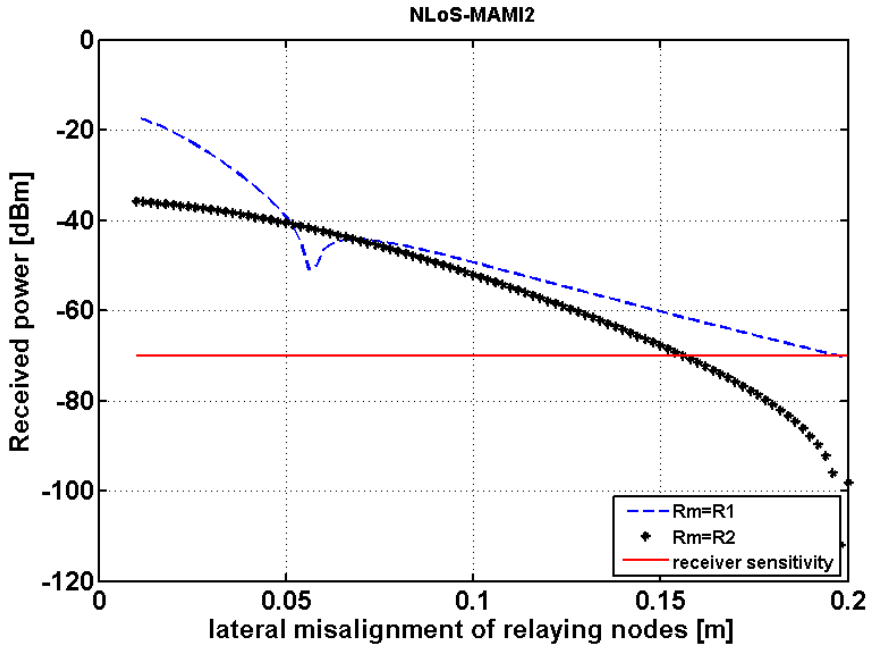

Figure B.2 NLoS MAMI Relay2: achieved received signal against the relaying nodes lateral misalignment

different for different selection of the M/A nodes.

In LoS- MAMI Relay 1 and 2, although the fluctuation does not occur within the defined range (the range of Δ is selected, in which the nodes are in the communication range of the transmitter), the received signal strength experiences very sharp decline compared to the NLoS case (Figure B.3 and B.4).

It is concluded from the theoretical and the above discussion that the angle displacement alone is not a proper metric for relay selection, since even with small angle displacement, the received signal can be extremely low, when a large lateral misalignment exists.

Figure B.5 to B.8 show the system performance for MAMI Relay1 and 2, for both LoS and NLos cases, when the relay selection is performed according to the relaying nodes lateral misalignment. In this scenario, R1 has smaller lateral displacement compared to R2 ($\Delta_{R1} = 2$ cm and $\Delta_{R2} = 7$ cm). However, the orientation of both

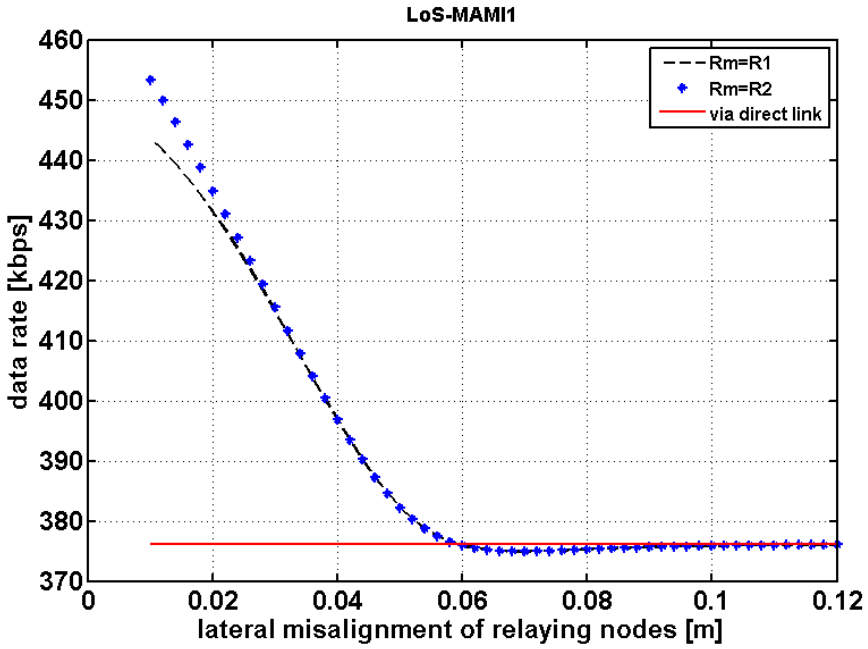

Figure B.3 LoS MAMI Relay1: achieved data rates against the relaying nodes lateral misalignment

relaying nodes are changed in order to observe the impact of the angle misalignment on the system. As can be seen from the figures, although the nodes are still in direct communication range of the transmitter, they cannot receive the signal when their angle displacement approaches $\pi/2$ in all cases. This implies that angle misalignment alone as well cannot be an optimum metric. Therefore, there is a need to determine a proper relaying metric that takes into account not only the location of the relaying nodes but also the angular orientation of them in respect to both the transmitter and receiver. This concept is discussed in detail in Chapter 5.

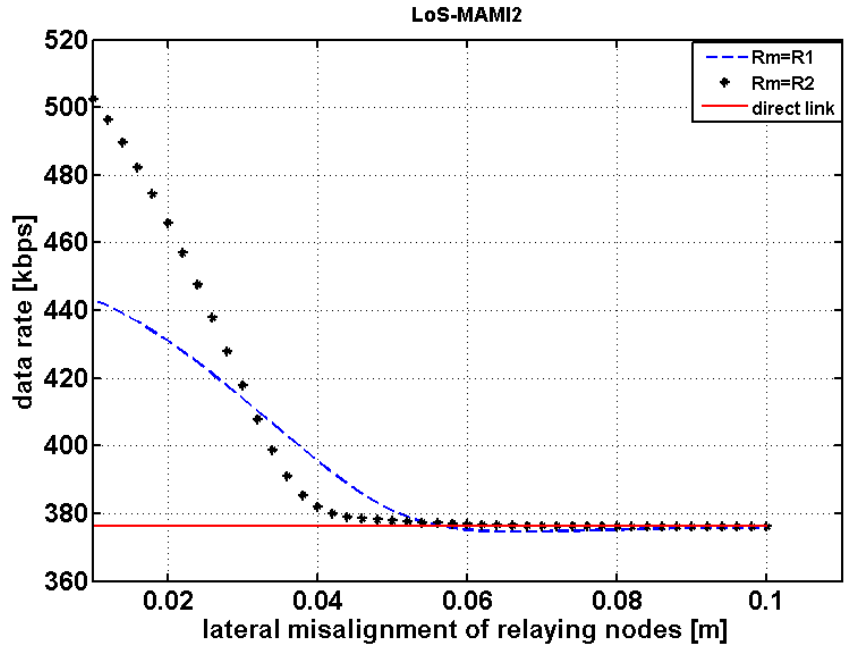

Figure B.4 LoS MAMI Relay2: achieved data rates against the relaying nodes lateral misalignment

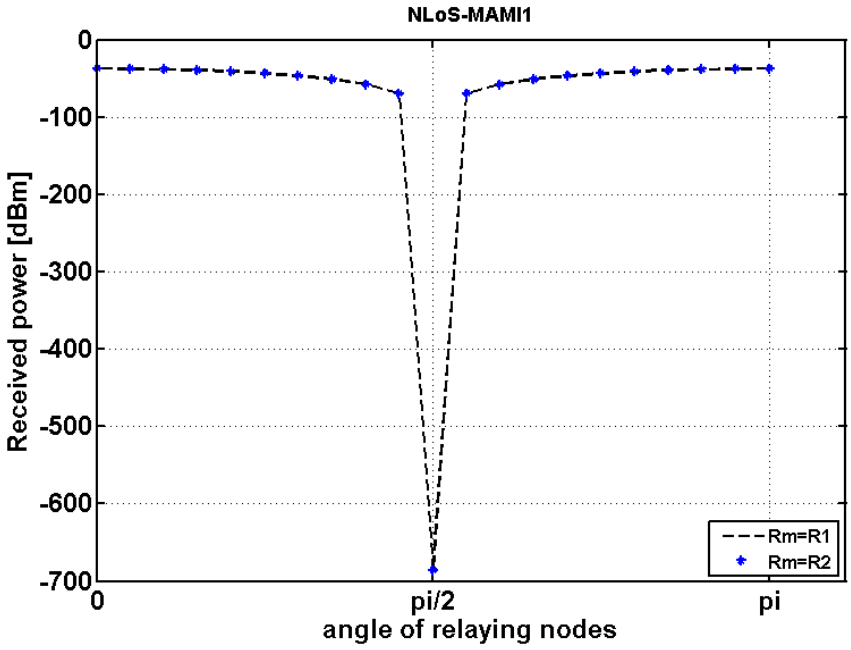

Figure B.5 NLoS MAMI Relay1: achieved received signal against the relaying nodes angle misalignment

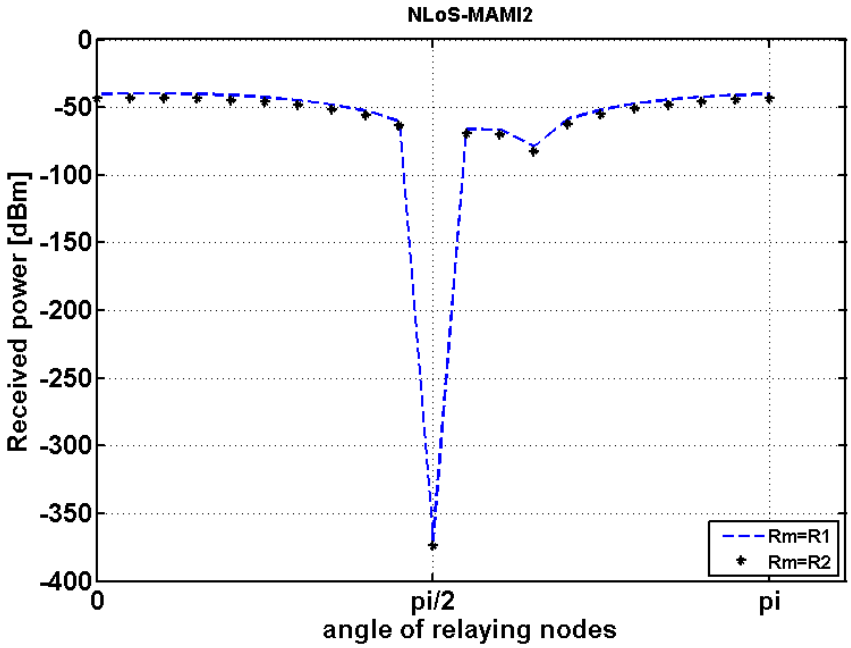

Figure B.6 NLoS MAMI Relay2: achieved received signal against the relaying nodes angle misalignment

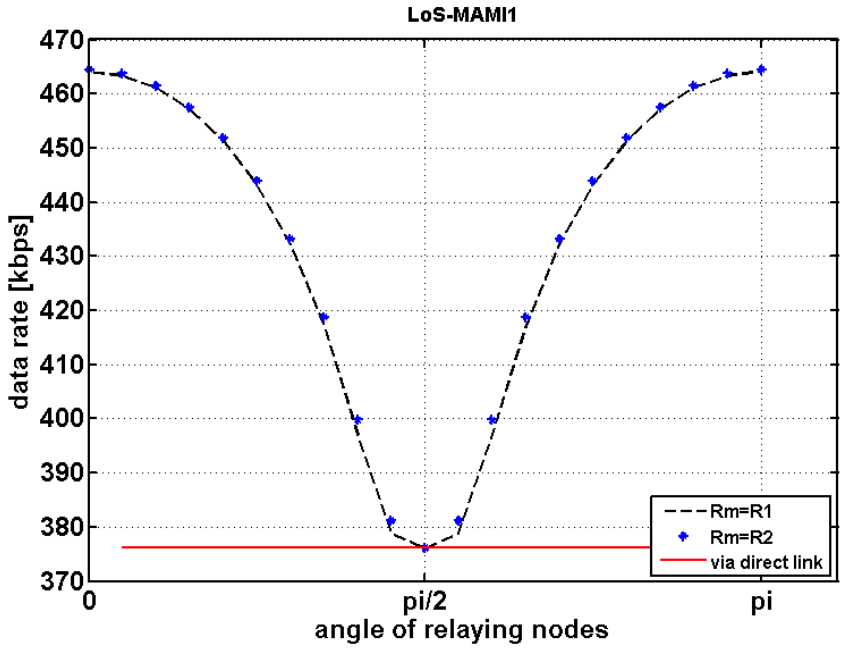

Figure B.7 LoS MAMI Relay1: achieved data rates against the relaying nodes angle misalignment

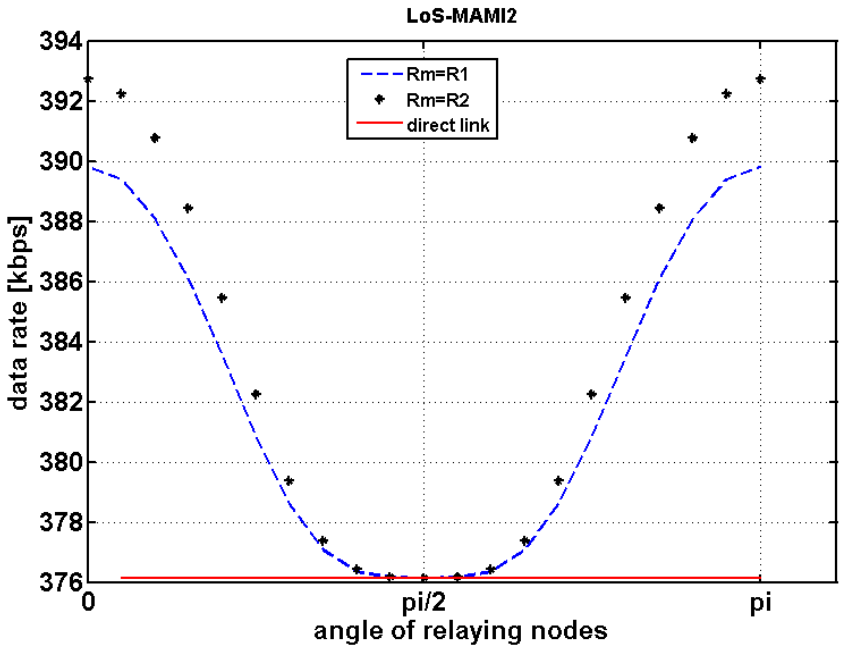

Figure B.8 LoS MAMI Relay2: achieved data rates against the relaying nodes angle misalignment

Appendix C

NFMIC Realistic Range and Interference Test

C.1 Chapter Overview

Recently FreeLinc [10] released to market MI radios with very short range but capable of producing voice signals that die out within very short distances. To test the theory of NFMIC, it was decided to use FreeLinc's systems and to check the power decay properties and hence the size of the magnetic bubble around each radio. This chapter provides the test results for effective range detection of the FreeLinc's devices, as well as interference with different objects.

C.2 Realistic Range of Magnetic Induction Communication Hardware

Currently finding products that use similar technology for personal area network system is hard to come by. FreeLinc is a privately held corporation in secure, wireless capabilities. It was founded in 2003 [10]. Several products that can be used for testing the operability of MI technology developed by FreeLinc were acquired. The specific product is the speaker microphone and radio adapter that attaches to a personal radio [10]. The images of radio adapter and speaker microphone are shown in

Figure C.1 Radio Adaptor [10]

Figure C.2 Speaker Microphone [10]

Figures C.1 and C.2 respectively.

The communication link between the speaker microphone and the radio adapter uses magnetic induction in the near field range. The adapter acts as transmitter and the speaker microphone acts as receiver. This may be seen in Figure C.3. However, this technology can be used to implement a body area network. A general case is shown in Figure C.4, in which the MI devices are placed around the person's body and they communicate with each other. For instance, using MI equipments in biomedical monitoring, reliable, secure and low power communication between the devices may be achieved. In Figure C.4, the largest distance to the hub located in the middle of the body is about a meter. These devices form a wireless body area mesh network. The hub aggregates data from the other body area nodes and forwards a packet through to a wide area networks, which could be a cellular network or the Internet.

Figure C.3 Near Field Magnetic Induction Communication

The equipment is used to test the effective range detection for the communication as well to find out if it is possible to introduce interference and study its effect on communication. Several obstacles were placed in and near the propagation path to observe if the range of communication was affected by these obstacles. By performing these tests a better understanding of how MI technology works is obtained as well as a better understating of the properties of NFMI communication.

C.2.1 Hardware Experiments

This section presents the results for several tests that were conducted in UTS laboratory in order to gain familiarity with the technology as well as to find out if noise and interference can be introduced in the propagation path. The intention is to validate if NFMIC is much more effective than RF communication in terms of interference. The simple test results shown in this section will provide some verification on what was uncovered in current literature with respect to MI communication.

C.2.2 Detection Range

In this test the speaker microphone was placed at some distance away from the transmitter to see what the effective range of communication is. The maximum range can be determined because the speaker microphone produces a beeping sound once the

communication link is lost meaning it is out of range. By using these techniques it can be approximated the maximum and most effective range at which the devices operate. The microphone is placed in different positions to ensure that the same range is achieved in all directions and to verify that the power is transmitted omni-directionally. This includes moving the speaker microphone to the left, right, up and down from the transmitter to ensure that the full range is covered as shown in Figure C.5.

C.2.3 Detection Range Results

The most effective rage found, which provides greatest reliability in all the direction before the speaker microphone looses the communication and produces the beeping sounds, is approximately about 1.5 m. As this was the case, it was found that the most reliable distance was at 1.45 m as at that distance the link was never lost, where as at some instances the link was lost at 1.5 m. The receiver was rotated in different directions from the transmitter in order to verify when range is lost depending on the position of the antenna. On occasions the speaker microphone still had communication at greater distances up to 1.7 m, but was very unreliable as these results could not be achieved when tests were repeated or when the speaker microphone was placed in a different location away from the transmitter. The distance of 1.45 m provided to be the most reliable distance as the reliability was 100 percent since signal was not lost once. These results also match with simulation when the power behavior in the NFMI is examined. The power decays at approximately $1/d^6$ and it is know from previous sections that NFMI communication is suitable for a short range communication of a few meters.

C.2.4 Interference Tests

This section presents the results from the attempt to introduce interferences in the communication paths. The test focused on trying to degrade signal and reduce the communication range by placing several objects in or near the propagation path to observe if the detecting range can be reduced. It is known that cross-coupling noise

Figure C.4 Body Area Network (adapted from [11])

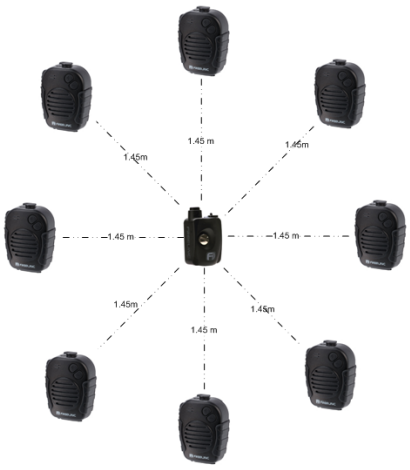

Figure C.5 Effective Detection Range

exists when there are multiple MI receivers and transmitters near each other. In this section the noise is introduced using one transmitter and a receiver. Interfering objects were placed one at a time and repeated several times. The obstacles include:

- Plaster Wall: The receiver is placed on the other side of the plaster wall from the transmitter to observe if the communication range is degraded and interfered with.

- Laptop Computers: Since a laptop computer contains many electrical components which are magnetic, this may cause interference.

- Human Body: The receiver is placed behind the body to observe if the signal is absorbed by the human body. Since the human specific absorption rate (SAR) is lower at low frequencies, it should be expected that the signal will not be degraded.

- Large aluminium box and near a laptop computer

- Transmitter is placed inside a large aluminium box

C.2.5 Interference Tests Results

Plaster Wall: When the receiver is placed on the other side of the plaster wall from the transmitter, it seems to have no effect in terms of interference. The signal is still received at approximately the same strength with distance as tested in the earlier sections without any obstacles. Therefore, plaster walls have no significant effect on the signal and not a strong interference source.

Laptop Computer: When the receiver is placed near a laptop, there is a minimal loss of the communication range. The signal is still received at approximately the

same distance of 1.45 m, but occasionally the signal drops at 1.40 m. This could be due to the components that laptops contain which may interfere with the MI signals.

Body: When the receiver is placed behind an average human body (a young student) to mimic a body area network system, the signal does not seem to be affected by the presence of biological tissues. The magnetic signal seems to penetrate human body without any signal loss as expected.

Large aluminium box and near a laptop: When the receiver was placed near a laptop and in front of a large aluminium box the signal strength was reduced, and the detection range was also reduced. The signal was detected by the receiver at about 1.15 m. This is much smaller than the case when the laptop and the aluminium box were not present in the signal path, at which the detection range was approximately 1.45 m.

Large aluminium box: The transmitter was placed inside a large aluminium box and the signal range was reduced significantly. At times the signal could be detected only at approximately 1.20 m. Depending on the setup of the transmitter antenna, it is known from earlier analysis that at some positions maximum coupling is achieved. On the rotation of receiver in different directions, at times only 80 cm range could be achieved. It seems that the aluminium box has a significant effect on the coupling between the transmitters and receiver by introducing interference in the communication system.

C.3 Summary

This chapter provides the test result of effective communication range and interference of NFMIC transceivers' (produced by FreeLink). It is concluded that the effective communication range of the transceivers is 1.45 m, and the interference test result shows that objects such as human body and plaster wall has minimal impact on the transmitted signal; however, result has shown that the electronic devices inside a

laptop computer and metals such as aluminium can effect the transmitted signal and contribute to higher signal attenuation.